UNCLASSIFIED

AD 401 770

Reproduced
by the

ARMED SERVICES TECHNICAL INFORMATION AGENCY
ARLINGTON HALL STATION
ARLINGTON 12, VIRGINIA

UNCLASSIFIED

NOTICE: When government or other drawings, specifications or other data are used for any purpose other than in connection with a definitely related government procurement operation, the U. S. Government thereby incurs no responsibility, nor any obligation whatsoever; and the fact that the Government may have formulated, furnished, or in any way supplied the said drawings, specifications, or other data is not to be regarded by implication or otherwise as in any manner licensing the holder or any other person or corporation, or conveying any rights or permission to manufacture, use or sell any patented invention that may in any way be related thereto.

401770
CATALOGED BY ASTIA
AS AD No. 401770

NOT SUITABLE FOR RELEASE TO OTS

FINAL REPORT NO. 63-94
This report covers the period
August 1, 1961 to July 31, 1962

STUDY OF ELECTRICAL BREAKDOWN CONDITIONS IN THE AERODYNAMIC FLOW FIELD OF A HYPERSONIC VEHICLE

by
Morton Rudin
Boris Ragent
Charles E. Noble, Jr.

prepared for
OFFICE OF NAVAL RESEARCH, WASHINGTON, D.C.
and
ADVANCED RESEARCH PROJECTS AGENCY, WASHINGTON, D.C.

Contract No. Nonr 3581(00)
Under ARPA Order No. 207-62
Project Code No. 7400
"Microwaves in Hot Gases"

January 30, 1963
Vidya Project No. 64/C

ASTIA
RECEIVED
APR 10 1963
TISIA A

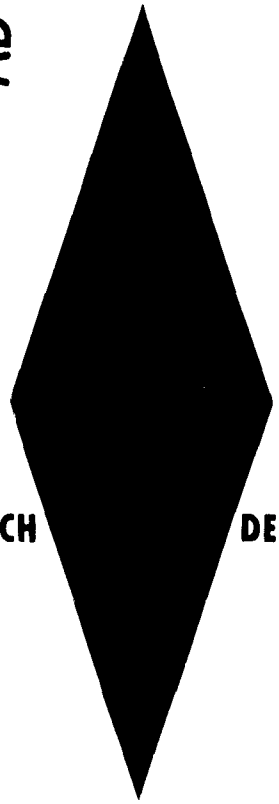

RESEARCH DEVELOPMENT

A DIVISION OF Itek CORPORATION

व VIDYA

The word Vidya, taken from the Vedanta philosophy of the Hindus, means knowledge. The symbol used to denote the Vidya organization is the letter "V" from Sanskrit, the ancient language of India.

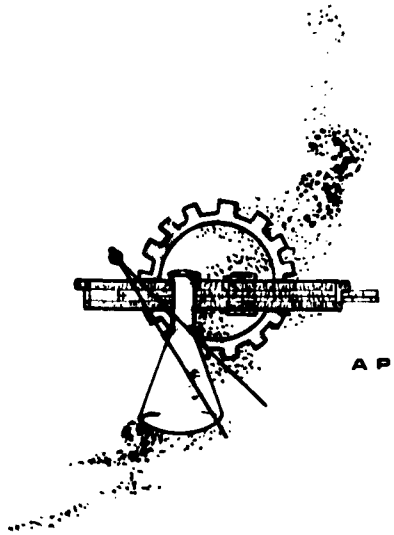

APPLIED MECHANICS . . . . PHYSICS . . . . ANALYSES

VIDYA COPY NO. 6

FINAL REPORT NO. 63-94
This report covers the period
August 1, 1961 to July 31, 1962

STUDY OF ELECTRICAL BREAKDOWN CONDITIONS IN THE AERODYNAMIC FLOW FIELD OF A HYPERSONIC VEHICLE

by
Morton Rudin
Boris Ragent
Charles E. Noble, Jr.

prepared for
OFFICE OF NAVAL RESEARCH, WASHINGTON, D. C.
and
ADVANCED RESEARCH PROJECTS AGENCY, WASHINGTON, D. C.

Contract No. Nonr 3581(00)
Under ARPA Order No. 207-62
Project Code No. 7400
"Microwaves in Hot Gases"

January 30, 1963
Vidya Project No. 64/C

This research is a part of Project DEFENDER sponsored by the Advanced Research Projects Agency, Department of Defense, and technically administered by the Fluid Dynamics Branch of the Office of Naval Research.

Reproduction in whole or in part is permitted for any purpose of The United States Government

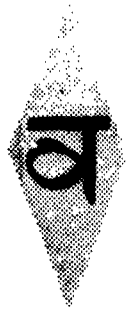

VIDYA
A DIVISION OF Itek CORPORATION

1450 PAGE MILL ROAD • PALO ALTO, CALIFORNIA
TEL: DAVENPORT 1-2455 TWX: 415 492-9270

ABSTRACT

A numerical technique has been formulated for solving the antenna breakdown equation in the presence of gaseous flow for typical antenna electric field and aerodynamic flow-field configurations. The results of computations for nonflow conditions agree well with existing data. Breakdown conditions were computed for sample cases of antenna type, vehicle shape, and velocity-altitude combinations. The results in air show that once ambipolar diffusion has been established increasing the vehicle velocity at a fixed altitude usually increases the breakdown field strength. This increase is found to be caused principally by the increase of gas density near the antenna and, to a much lesser degree, by the effect of the boundary-layer flow velocity in sweeping electrons out of the high electric field regions.

The kinetic theory concepts involved in the above calculations have been critically examined and the gaseous material properties necessary for these calculations have been estimated. The inviscid and viscous flow fields in which the test antenna is immersed were calculated for wedges and cones, using equilibrium real-gas theory, and the results of these calculations were used as inputs for the previously discussed calculations.

Finally, the results of these calculations are summarized and conclusions and recommendations for future work are given.

ACKNOWLEDGMENTS

The aid of Mr. Frederick K. Goodwin for programing the equations and supervising many of the numerical computations, Miss Cirel Menkes for aid in checking equations, Mr. E. Glenn Tickner for his efforts in setting up the flow-field calculations, and Dr. Grove C. Nooney for helpful discussions is gratefully acknowledged.

TABLE OF CONTENTS

TABLE OF CONTENTS (continued)

TABLE OF CONTENTS (continued)

TABLE OF CONTENTS (concluded)

LIST OF TABLES

LIST OF FIGURES

LIST OF FIGURES (continued)

LIST OF FIGURES (continued)

LIST OF FIGURES (concluded)

LIST OF SYMBOLS

a_i, a_{ijk}	parameters used in describing ζ in two dimensions and three dimensions, respectively (see Eqs. (5.3) and (5.29))
$A_{m,n}$ or $A_{l,m,n}$	coefficients used in the trial function for ψ in two dimensions and three dimensions, respectively
b	parameter used in specifying the flow field (see Eq. (4.5))
$B_{m,n}$ or $B_{l,m,n}$	coefficients used in the trial function for $\tilde{\psi}$ in two dimensions and three dimensions, respectively
B_o	$= V_o/D$
$\vec{B}$	$= \vec{V}/D$
C_{ijk}	parameters used in specifying $B = V/D$ (see Eq. (5.28))
$\vec{c}$	$= \vec{v} - \vec{V}$, the random electron velocity
d	gap width of a gap antenna (the shorter dimension)
D	diffusion coefficient
D_a	electron ambipolar-diffusion coefficient
D_e	electron free-diffusion coefficient
d_i	parameters used in describing ζ (see Eqs. (5.3) and (5.29))
D_I	heavy ion diffusion coefficient
D_o	electron diffusion coefficient in the absence of an applied field
D_t	total effective electron diffusion coefficient

e	the electronic charge
E_D	the diffusion field caused by electron and ion diffusion
E_e	effective electric field intensity for an a-c field
$E_{e'}$	effective electric field intensity for an a-c field at a specific point in space (see Eq. (6))
E_{rms}	the root-mean-square electric field intensity
$\vec{E}$	the electric field intensity
f	the random velocity distribution function (RVDF) (Eq. (3.10))
F	function defining the electric field spacial dependence (Eq. (2.11))
F_e	the electron density in phase space (velocity and position space)
F_o^o	a reduced electron density function defined by Equations (3.1) and (3.3)
G	quantity defined by Equation (2.12) for continuous wave and (2.18b) for pulsed waves
g_i	parameters used in describing G (see Eqs. (5.4a) and (5.5))
H_n^γ	Hermite polynomials defined by Equation (5.10b)
h_1, h_2	enthalpy per unit mass before and after the shock wave
$I_{m,n}^{\gamma,\eta}$	integrals defined by Equation (5.15)
j	$\sqrt{-1}$
$\vec{J}$	electrical current density (flux)
$J_{m,n}^{\alpha,\eta}$	integrals defined by Equation (5.16)
k	(not squared) Boltzmann's constant
k^2	(always squared) eigenvalue related to physical quantities by Equation (2.10)

k^{*2}	eigenvalue for pulsed breakdown (Eq. (2.18a))
L_E	length of the field containing region
$L_m^{\alpha,2}$	Laguerre polynomial defined in Equation (5.10a)
m	the electron mass
M	average mass of the neutral particles
$M_{m',n'}^{m,n}$ or $M_{l',m',n'}^{l,m,n}$	expressions defined by Equations (5.14a) and (5.14b) or (5.27a) and (5.27b), respectively
M_1	reentry Mach number
M*	effective mass of the neutral particles with moderately high ionization (see Eq. (3.9a))
n	(when not used as an indice) number of electrons per unit volume
N	number of neutrals per unit volume
N_I	number of ions per unit volume
$N_{m',n'}^{m,n}$ or $N_{l',m',n'}^{l,m,n}$	expressions defined by Equations (5.13) or (5.26), respectively
n_p	number of electrons per unit volume at the condition $\omega = \omega_p$ (Eq. (2.30b))
p	gas pressure
P	= p*'/E'; except in Section 2.2 where it is used for the time dependence of the repeated pulse (Eq. (2.15))
p_1, p_2	free-stream atmospheric pressure and pressure after the shock wave, respectively
p*	= $\rho ZRT = (\rho/\rho_o)Z(760)$ mm

q	the electron appearance or reappearance rate after inelastic collisions per electron per unit volume
$Q^{m,n}_{m',n'}$ or $Q^{l,m,n}_{l',m',n'}$	expressions defined by Equations (5.12) and (5.25), respectively
R	gas constant per unit mass for cold air
RVDF	the random velocity distribution function (f)
s_o, s_1	approximate production and attenuation constants, respectively (Eqs. (2.24a) and (2.24b))
t	time
T	gas temperature (heavy particles) or, in Section 2.2, pulse spacing in time
T_e	$= (1/2)\overline{mc^2}/(3k/2)$ the electron "temperature"
T^*	effective gas temperature at moderately high ionization (Eq. (3.9b))
u	$= (1/2)mc^2$ the electron energy variable
u_c	defined by Equation (3.13b)
u_o	the average value of u at which electrons undergo inelastic collisions
u_r	$= u_2/u_1$
u_x	the lowest energy level of the neutrals, above the ground state, readily excited by electron impact
u_1	free-stream velocity component normal to shock wave
u_2	velocity component normal to shock wave after the wave
V_o	flow velocity just outside of the boundary layer
V_1	free-stream flow velocity before the shock wave or vehicle velocity

$\vec{V}$	flow velocity
x	coordinate across flow parallel to surface
y	coordinate away from surface
z	coordinate in the flow direction
Z	particles per cold air gas particle in hot air
Z_{av}	the average ionic charge divided by the charge per electron
α	scale parameter for the Laguerre polynomials
α_T	Townsend ionization coefficient - the number of electrons produced by an electron while drifting 1 centimeter
β	scale parameter for the x-dependent Hermite polynomials
γ	scale parameter for the z-dependent Hermite polynomials
δ_l^m	Kronecker delta (= 1 if $l = m$; = 0 if $l \neq m$)
$\epsilon(t)$	unit step function
$\epsilon_1, \epsilon_2, \epsilon_s$	parameters used in describing the electric field spacial dependence (see Eqs. (5.7) and (5.21))
ζ	ionization coefficient - net number of electrons produced by an electron in falling through 1 volt ($= \nu/DE^2$)
ζ'	value of ζ at that spacial point where $E = E'$
η	number of attachments per electron per unit drift length
θ	deflection angle of flow
λ	wavelength of transmitted electric field
Λ	"diffusion length" $\Lambda^{-2} = \nabla^2(nD)/(nD)$, except in Section 4 where it is the wedge or cone half angle
λ_D	the Debye "screening distance" (Eq. (3.42))
μ_e	free electron mobility

μ_I	heavy ion mobility
ν	$(= \nu_I - \nu_A - \nu_R)$ effective net rate of production of electrons
ν_A	number of electrons removed by attachment per electron per second
ν_{en}, ν_{ee}	elastic momentum transfer collision frequency for an electron with neutrals and with other electrons, respectively
ν_I	number of electrons produced per second per electron by electron impact
ν_{In}	elastic momentum transfer collision frequency for a heavy ion with neutrals
ν_R	number of electrons removed by recombination per electron per second
ρ	gas density
ρ_o	air density at the earth's surface
ρ_1	free-stream gas density at altitude in question
σ_I	the imaginary electrical conductivity (see Eq. (3.37))
σ_R	the real electrical conductivity (see Eq. (3.37))
τ	the duration of an individual pulse, "pulse width"
Φ	diffusion parameter defined by Equation (3.22)
$\vec{\phi}$	diffusion parameter defined by Equation (3.13c)
χ	degree of ionization $(= n/N)$
ψ	$= nD$
$\psi_{m,n}$ or $\psi_{l,m,n}$	defined by Equations (5.9) and (5.23), respectively

$\tilde{\psi}$	the adjoint function of ψ
ω	the (angular) frequency of the applied E field
ω_p	the plasma frequency (see Eq. (2.30))
$\langle\ \rangle$	as used in Section 2.2.2, the time average over a time $\Delta t = T$ after transients have died out (see Eqs. (2.20) and (2.21)); as used elsewhere, the time average over a time $\Delta t = 2\pi/\omega$
$\bar{}$	the bar is used to indicate a Laplace transform in Section 2.2.2; elsewhere it indicates an average over the RVDF
$'$	prime used on p^*, ρ, and E means quantity evaluated at the center of the antenna aperture

STUDY OF ELECTRICAL BREAKDOWN CONDITIONS IN THE AERODYNAMIC FLOW FIELD OF A HYPERSONIC VEHICLE

1. INTRODUCTION

This report covers work done on Contract Nonr 3581(00), Project No. 061124, during the period 1 August 1961 to 1 August 1962. The purpose of this project is to perform a "Study of Electrical Breakdown in the Hypersonic Flow Field of a Hypersonic Vehicle."

The difficulties of propagating electromagnetic energy through highly ionized gases, such as may occur in a plasma sheath surrounding hypersonic vehicles, have been much discussed. The attenuation of weak signals in such plasmas is fairly well understood theoretically, and for such a situation the electron random-energy distribution or random-velocity distribution is very little disturbed by the presence of the electromagnetic field, and calculations based upon an unperturbed distribution function usually suffice. Contrasted with this case is that when a strong electromagnetic field is present in the gas, such as occurs near an antenna surface. In this case the presence of the field strongly perturbs the initial electron random-velocity distribution function by adding energy to the electrons and may, under certain conditions, lead to very high ionization rates, a condition known as "breakdown." This high ionization surrounding an antenna may change the radiation characteristics of the antenna and drastically impair propagation of energy from the antenna.

For electrical breakdown in the flow field of a hypersonic vehicle, we are interested in the breakdown condition for both pulsed and c-w electromagnetic waves in hot air (possibly not in thermodynamic equilibrium and with ablation additives) and with the gas flowing in an open geometry over a surface containing the source of the electromagnetic field. The flow field is not uniform and the alternating electric field is not of uniform amplitude. All of these conditions, as examination in this report shows, can and do have some effect upon the breakdown conditions.

Experimental studies of the breakdown condition in the past include c-w breakdown of a gas in a closed container (data and experiments reviewed in Refs. 1, 2, and 5), pulsed a-c breakdown in a closed-container (Ref. 3), no-flow pulsed a-c breakdown in an open region over a surface containing the antenna (Ref. 4), and breakdown with flow between plates or within tubes (Ref. 6). All of these were for relatively cold gases (approximately 300° K). In addition, there have been measurements of breakdown field strengths in flames of uncertain composition (Refs. 7a and 7b) and in a plasma-filled cold-air region (Ref. 7c).

Theoretical breakdown studies in the past include those for closed containers with c-w (Refs. 1, 3, and 5) or pulsed (Ref. 3) uniform or nonuniform electric fields. There is also a closed solution for breakdown in a gas flowing with constant velocity in a tube or between plates with an applied electric field constant in a finite region and zero elsewhere (Ref. 8).

All of these studies were not concerned with the effects of hot (rather than cold) air. Also, of all the papers cited above, only one (Ref. 4) has a surface geometry and electric field geometry pertinent to the problem with a reentry vehicle. In addition to all the papers mentioned above, there are some cursory attempts to compute breakdown conditions for reentry problems (Refs. 9, 10, and 11). In Reference 9, the breakdown field strength is estimated for air (not flowing) in a field-containing region which is assumed to be $\lambda/2$ long. The problem is first treated as diffusion-controlled breakdown with diffusion length $\lambda/2$. Subsequently, the problem is treated as ionization growth in a uniform field for finite time, without diffusion and with all electrons produced in previous pulses swept out. In Reference 10 these estimates are modified to include ambipolar phenomena and "initial ionization level."

We find (as will be shown) that this last analysis is not applicable to our problem for the following reasons - in addition

to the unqualified use of ionization rates for cold air. First, we find that diffusion into the antenna containing wall contributes appreciably and may even predominate over the diffusion across the field. Second, we find that no initial ionization-level correction is necessary for the multiple pulse, diffusion-pulse-width controlled case and that such a correction only has meaning when one is trying to inhibit breakdown by use of short pulse width alone. Third, it is difficult to be sure that the electrons from one pulse are completely swept out before the advent of the next pulse, since the boundary-layer velocity is zero at the wall. One must treat the problem in a completely coupled manner.

In Reference 11, the reentry problem is again treated as ionization growth in a uniform field during a finite time. The only major modification over References 9 and 10 is that the time concerned is taken as the smaller of $\lambda/2V$ and τ, where $\lambda/2V$ is the time to traverse the assumed width of the field when flow is at velocity V, and τ is the pulse width. Diffusion and multiple pulses are not considered. Also, the data used are again for cold air.

We treat the problem in a completely coupled manner and formulate a procedure by which any velocity variation and any nonuniform field may be considered in the breakdown computations for the desired geometry. These concepts are discussed generally in Section 2, but are not fully formulated for the problem at hand until Section 5.

In Section 3, restrictions on the applicability of experimental data obtained in various laboratory situations are analyzed and computed. The point is that such data are not always applicable to pulsed or flowing problems, even in cold air. Since the microscopic processes governing ionization growth and breakdown phenomena are dependent on the velocities of the electrons involved (by collision) in these processes, it became necessary to study the random-velocity distribution functions for the electrons and their rates of relaxation under the physical conditions imposed by the

environment. In particular, the macroscopic quantities which must enter into the evaluation of breakdown conditions, such as electron production and loss rates, are those values for these quantities which have been averaged over the pertinent distribution function. All the available data on these macroscopic quantities are from measurements made under conditions which involved one particular type of electron random-velocity distribution function; therefore, caution must be exercised in utilizing these data under physical conditions which are vastly different from those under which they were determined or in which transient effects are present.

In Section 4, the velocity profiles in reentry boundary layers are determined for two sample body shapes and typical flight conditions and matched with a function for computation. Other pertinent boundary-layer properties are also deduced.

To test the breakdown computation procedure, computations are made in Section 6 at zero velocity to compare with an analogous experiment in the proper geometry. In Section 7, computations with a velocity profile similar to the reentry boundary layer for cones and wedges are conducted. Section 8 contains a summary of the work accomplished in this report, conclusions reached, and recommendations for future work.

2. THE ELECTRON CONSERVATION EQUATION AND THE CONCEPT OF BREAKDOWN

2.1 The Electron Conservation Equation

The purpose of this study is the determination of the electric field strength necessary to cause breakdown in a gas steadily flowing along a surface and through an applied electric field. The flow velocity is assumed to be in a uniform direction parallel to the surface and its magnitude to vary with distance away from the surface. The electric field is also a function of the coordinates and should resemble the pattern of an antenna positioned within the surface. Take coordinates (see Fig. 2.1) such that the flow velocity $\vec{V}$ is in the direction of the z-axis, the surface S is in the x-z plane, and y is distance above the surface S.

The equation governing the electron density $n(\vec{r},t)$ is then

$$\frac{\partial n}{\partial t} = - \vec{V} \cdot \vec{\nabla} n + \nabla^2 (Dn) + \left(\bar{\nu}_I - \bar{\nu}_A - \bar{\nu}_R \right) n \qquad (2.1)$$

where D is the diffusion coefficient, $\vec{V}$ is the flow velocity, and $(\bar{\nu}_I - \bar{\nu}_A - \bar{\nu}_R)$ is the net ionization frequency defined in the list of terminology. The origin of this equation is discussed in References 12, 13, and 1; it is also discussed in Section 3 with Appendix A. Discussed immediately below are some of the more pertinent assumptions involved in the form of this equation.

2.1.1 The linear electron production term and boundary conditions

A common argument for the linearity of the electron production term, $\bar{\nu}_I n$, where $\bar{\nu}_I$ is the ionization frequency averaged over the velocity distribution function, may be made as follows:

The electron production is proportional to n only if ionization produced by collisions among the heavier ions and neutrals is negligible compared to ionization produced by electron collisions with heavier particles. Since we will be interested in determination of the "breakdown conditions," since the probability of ionization by electron impact is several orders of magnitude greater than by heavy particle impact, and since, in addition, the

electrons will be more energetic than the heavier particles once they are in the applied field, the ionization induced by heavy particle impacts may usually be neglected so long as some electrons are on hand initially.

The above argument is unnecessary since the ionization due to collisions among the heavy particles is actually not neglected by use of Equation (2.1) for breakdown studies. To demonstrate this fact, let us consider the steady-state equation since it will be shown in Section 2.2 that the determination of breakdown conditions involves the steady-state solutions to Equation (2.1). Let Q be the ionization rate due to collisions among the neutral particles. Then the complete electron conservation equation in steady state becomes

$$- \vec{V} \cdot \vec{\nabla} n_1 + \nabla^2 (D n_1) + \nu n_1 + Q = 0 \qquad (2.2)$$

where we have used the abbreviation $\nu = (\bar{\nu}_I - \bar{\nu}_A - \bar{\nu}_R)$ and n_1 is the electron density.

Consider now the electron conservation equation in the absence of the applied electric field - for example, that which could apply far upstream of the electric field, namely,

$$- (V \cdot \nabla) n_o + \nabla^2 \left(D_o n_o \right) + \left(\bar{\nu}_I - \bar{\nu}_A - \bar{\nu}_R \right)_o n_o + Q = 0 \qquad (2.3)$$

The terms Q in these two equations are assumed equal because each depends on the energy of the heavy particles, an energy which is assumed unaffected by the presence of the field. The applied field heats the electrons largely, not the ions, and the electrons cannot readily transfer their energy to the heavy particles (Refs. 1, 12, and 13). If Equation (2.3) is subtracted from Equation (2.2), one obtains

$$- (V \cdot \nabla) n + \nabla^2 \left[D n + \left(D - D_o \right) n_o \right] + \nu n + \left(\nu - \nu_o \right) n_o = 0$$

where $n \equiv n_1 - n_o$.

Within the applied field, the solution we seek (the unique solution between breakdown and squelching discussed in Section 2.2) will generally have[1] $n >> n_o$. On the other hand, just outside the applied field we have $\nu >> \nu - \nu_o$, $D >> (D - D_o)$, with $n \geq n_o$. Therefore, in all regions of interest, the last equation may be written to sufficient accuracy.

$$- (V \cdot \nabla)n + \nabla^2(Dn) + \nu n = 0 \qquad (2.4)$$

This is the same as Equation (2.1) in the steady state. In addition, we see that since the boundary conditions for Equation (2.2) are $n_1 = n_o$ at $x = \pm \infty$ or $z = \pm \infty$; the boundary conditions for Equation (2.4) are $n = 0$ at $x = \pm \infty$ or $z = \pm \infty$. As is common in breakdown studies, the surface is assumed to absorb (or annihilate by acting as a third body in recombination) all electrons striking it. Thus, we take $n_1 = 0$, $n_o = 0$, and $n = 0$ at $y = 0$ as well as at $y = \infty$.

2.1.2 The linear electron loss term

The electron attachment is linear in n if either dissociative attachment predominates over three-body processes or if the degree of ionization is so low that heavy particles predominate over electrons as third bodies during attachments. This will be true when $\chi = n/N < \sim 10^{-4}$, where N is the heavy particle density. The recombination, however, will be proportional to n^2 and even n^3 for very large χ.

Experimentally measured values of attachment coefficients in cold air indicate[2] (Ref. 2b, p. 150)

$$\left(\frac{1}{n}\frac{dn}{dt}\right)_{attach} \sim 2\times10^4 \; p \left(\frac{E_e}{p} + 1\right) \; sec^{-1}$$

---

[1] See Reference 8 for a typical solution.

[2] Here E_e is the "effective" field strength discussed in Section 3.1.3

where E_e is in volts per centimeter and p is in mm Hg, whereas experimental values of recombination coefficients in cold air give approximately (Ref. 2b, p. 159)

$$\left(\frac{1}{n}\frac{dn}{dt}\right)_{recomb} \sim \left(\frac{100}{p} + \frac{1}{2.3}\right)^{-1} \times 10^{-6} \text{ n sec}^{-1}$$

with n in cm^{-3}. Thus, when p is of the order of 1 mm Hg and E is greater than 10 volts per centimeter, the ratio gives

$$\frac{\text{Attachments}}{\text{Recombinations}} \approx 2\times10^{12} \frac{E_e(\text{volts/cm})}{p(\text{mm})\,n(cm^{-3})}$$

In the other extreme, for E_e/p small with p large, the ratio gives

$$\frac{\text{Attachments}}{\text{Recombinations}} \approx 10^{10} \frac{p(\text{mm})}{n(cm^{-3})}$$

Thus, at least for cold air, recombinations are negligible compared with attachments except when the degree of ionization is very high.

In addition, for the reentry problem, we are largely interested in cases where diffusion loss predominates so that the effects of both $\bar{\nu}_A$ and $\bar{\nu}_R$ on electron loss will be small compared with diffusion losses.

2.1.3 The form of the diffusion term

The diffusion term in Equation (2.1) is $\nabla^2(Dn)$ rather than $\vec{\nabla}\cdot(D\vec{\nabla}n)$ as commonly encountered in gas kinetics. It is shown in Sections 3.2.1 and 3.2.2 that, when (1) the collision frequency between electrons and neutral particles is much greater than the collision frequency between electrons, that is, $\nu_{en} \gg \nu_{ee}$ and when (2) the average momentum transfer collision frequency changes slowly with position in the region of interest, the form of the diffusion term is indeed $\nabla^2(Dn)$ and that this term includes

thermal diffusion. (The main physical reason for the difference between the structure of the electron diffusion term and the usual gas kinetic diffusion term is that the electron mass is so extremely small that it does not contribute appreciably to the average mass-flow velocity.)

Let us now examine whether the restrictions just mentioned are fulfilled in the reentry application. The usual estimate for $\bar{\nu}_{ee}$ (Ref. 14) gives

$$\bar{\nu}_{ee} = 2\pi n \frac{e^4}{m^2c^3} \ln\left[1 + \frac{m^2c^4}{e^4}\left(\frac{kT_e}{4\pi ne^2}\right)\right] \sec^{-1} \tag{2.5}$$

where all of the symbols are defined in the list of notations. If we take a cross section of 10^{-15} cm^2 for electron-neutral collisions, then

$$\bar{\nu}_{en} \simeq N(10^{-15}) \sqrt{8kT_e/\pi m}$$

and, noting that $c \propto \sqrt{T_e}$,

$$\frac{\bar{\nu}_{ee}}{\bar{\nu}_{en}} \sim \frac{10^{10}\chi}{T_e^{\,2}(^{\circ}K)} \tag{2.6}$$

where $\chi = n/N$. Thus, $\bar{\nu}_{ee} \ll \bar{\nu}_{en}$ is achieved if $\chi/T_e^{\,2} \ll 10^{-10}$. This is easily fulfilled for temperatures of thousands of degrees, such as are common in reentry.

From Equation (3.31) it will be seen that the second requirement mentioned above is approximately equivalent to

$$\frac{\nabla\bar{\nu}_{en}}{\bar{\nu}_{en}} \ll \left(\text{the larger of } \frac{\nabla n}{n}, \text{ or } \frac{\nabla\overline{c^2}}{\overline{c^2}}\right) \tag{2.7a}$$

The data and estimates of Reference 15 indicate that ν_{en} is fairly independent of energy. Thus, the condition of Equation (2.7) is largely density dependent and may be written

$$\frac{\nabla\rho}{\rho} \ll \left(\text{larger of } \frac{\nabla n}{n} \text{ or } \frac{\nabla\overline{c^2}}{\overline{c^2}}\right) \qquad (2.7b)$$

It is quite possible that this condition is not always satisfied in a hypersonic boundary layer and thus the term omitted from Equation (3.31) to obtain the form $\nabla^2 Dn$ in Equation (2.1) should be included. However, the data and estimates available for D, ν_{en}, and $\overline{c^2}$ are so poor under conditions obtained in a reentry boundary layer that such a correction to our breakdown calculations would have little meaning. Since the omitted term is linear in n, there would be no problem in including such a term in the procedure developed in Section 5 for the computation of breakdown field strength, that is, if the needed data were available.

For the reentry problem, the diffusion will quite often be fully ambipolar. For, as shown in Section 3.2.3, if n is greater than 3×10^3 cm^{-3}, the ambipolar diffusion is fully established. Such a minute electron density is certainly attained in many reentry boundary layers. However, to check our computational methods with experiment, it was necessary in Section 6 to make a few computations using the free-diffusion coefficient, since the only experiments involving the geometries of concern here were for cold un-ionized air under no-flow conditions (Ref. 4).

2.2 The Breakdown Concept

2.2.1 Continuous-wave breakdown

We shall first discuss breakdown due to continuous-wave operation of the transmitting antenna. In Equation (2.1), both macroscopic parameters D, the diffusion coefficient, and $\nu \equiv \bar{\nu}_I - \bar{\nu}_A - \bar{\nu}_R$, the net ionization coefficient, are functions of the average electron energy. We will assume that the electron random-velocity distribution is "relaxed" or "stationary" so that the average electron energy is a function only of the "effective" electric field strength and species concentrations at any position in question. The discussion of Section 3.1.2 examines the conditions

under which this assumption is valid. It is found that a large portion of the reentry regime fulfills this condition. We also assume that the mixture of heavy particles is not appreciably changed by the applied field and resulting ionization. Thus, all coefficient functions in Equation (2.1) are functions only of position and the effective electric field strength.

At a fixed position, Equation (2.1) behaves in a manner similar to the expression

$$\frac{\partial n}{\partial t} = sn$$

where s is negative for weak electric fields and positive for strong electric fields. Thus, there are only three types of steady-state solutions: $n = 0$, corresponding to s negative and no breakdown; $n = 0$, corresponding to s positive and giving breakdown; and a unique condition at which $s = 0$, or, from Equation (2.1)

$$\nabla^2 (Dn) - \vec{v} \cdot \vec{\nabla} n = - \nu n \qquad (2.8)$$

This equation determines the electric field strength above which breakdown will occur. Once ionization growth sets in at a rate above that occurring in the solution to this equation, the gas cannot, in steady state, flow through the applied field fast enough to limit the ionization to a finite value. Ionization would remain finite, but the gas would become completely ionized, if in ν we had accounted for the depletion of the number of ionizable particles. The ionization becomes infinite everywhere due to the action of the diffusion term coupled with the unrealistically unlimited supply of ionizable particles.

Let us put Equation (2.4) or (2.8) in a form that will make use of tabulated data (for cold air) more convenient. Take $\psi = nD$, then, since in the problem considered here, $\vec{\nabla} \cdot \vec{v} = 0$, the equation may be rewritten as

$$\nabla^2\psi - \nabla \cdot \left(\frac{\vec{V}}{D}\psi\right) = -\frac{\nu}{D}\psi \equiv -\zeta E_e^2\psi \equiv -k^2\left(\frac{\zeta}{\zeta'}\right)\left(\frac{E_e}{E_e'}\right)^2\psi \quad (2.9)$$

where $\zeta \equiv \nu/DE_e^2$ is the high-frequency ionization coefficient for the mixture in question, and

$$k^2 = \zeta' E_e'^2 \quad (2.10)$$

Here the effective electric field is given by

$$E_e = E_e' F(x,y,z) \quad (2.11)$$

where E_e' is the effective field at some specified point in the region of interest and ζ' is the value of ζ at this point. Determination of the field strength above which breakdown occurs then involves determining the lowest eigenvalue k^2 of Equation (2.9) and thus, E_e through Equations (2.10) and (2.11). In the case of a high-frequency alternating electric field, E_e is the effective d-c field strength defined in Section 3.1.3.

Let us use the abbreviations

$$G = (\zeta/\zeta')(E_e/E_e')^2 \quad \text{and} \quad \vec{B} = \vec{V}/D \quad (2.12)$$

so that Equation (2.9) is simplified to

$$\nabla^2\psi - \nabla \cdot (\vec{B}\psi) = -k^2 G\psi \quad (2.13)$$

2.2.2 Multiple-pulse breakdown

As in the c-w case we are again concerned with the condition that ionization does not exhibit unlimited growth as time increases. Let the discussion for the moment be restricted such that D is assumed constant in time. The discussion with nonconstant D will follow.

Suppose we assume, as in Sections 2.2.1 and 2.2.2, that ν is a function only of the effective local electric field and the local mixture. As stated earlier, this necessitates the assumption of a stationary or relaxed random-velocity distribution function (RVDF). The discussion in Section 3.1 will show that for pulses this assumption places certain restrictions on the pulse width and on the field strength. Let us expand ν in a series

$$\nu = \sum_i \Gamma_i(\vec{r}) E_e^{\gamma_i} \tag{2.14}$$

and let the effective electric d-c field (defined in Sections 3.1.3 and 3.2.4) be

$$E_e = E_e' F(\vec{r}) P(t) \tag{2.15}$$

where E_e' is the value of E_e at some point $\vec{r}'$ and $P(t)$ gives the repeated pulse shape. For a square pulse, if $\epsilon(t)$ is a unit step function, the function $P(t)$ is

$$P(t) = \Big[\epsilon(t) - \epsilon(t-\tau) + \epsilon(t-T) - \epsilon(t-T-\tau) + \cdots + \epsilon(t-qT) - \epsilon(t-qT-\tau) + \cdots\Big] \tag{2.16}$$

where q is an integer, τ is the pulse width, and T is the pulse spacing. Note that if P is raised to any power, then

$$P^\gamma = P$$

because of the nature of step functions.

Equation (2.1) may be rewritten as (D is assumed constant)

$$\frac{\partial n}{\partial t} + V \cdot \nabla n - D\nabla^2 n = (k^*)^2 G(\vec{r},\vec{r}') P(t) n \tag{2.17}$$

where

$$(k^*)^2 = \sum_i \Gamma_i(\vec{r}') \left(E_e'\right)^{\gamma_i} \tag{2.18a}$$

and

$$G(\vec{r},\vec{r}') = \frac{\sum \Gamma_i(\vec{r}) \left[E_e' F(\vec{r})\right]^{\gamma_i}}{\sum \Gamma_i(\vec{r}') \left(E_e'\right)^{\gamma_i}} \tag{2.18b}$$

Consider now the Laplace transform $\bar{f}$ of any function $f(t)$ that is either periodic, or constant and finite, or diverges more slowly than $e^{\alpha t}$ for large time. Then

$$\bar{f} = \int_0^\infty e^{-st} f(t)dt \quad , \quad \mathrm{Re}(s) > 0 \tag{2.19}$$

This definition may be used even for f diverging as fast or faster than $e^{\alpha t}$ for large t, so long as we do not attempt to invert the transform. Then, of course, $\bar{f} = \infty$. For such a function, the following theorem may be proved:

$$\lim_{s \to 0} \left[s\bar{f}(s)\right] = \lim_{t \to \infty} \begin{cases} \frac{1}{T}\int_t^{t+T} f(t)dt & \text{if } f(t) \text{ goes to a constant, is periodic with period } T, \text{ or diverges more slowly than } e^{\alpha t} \text{ for large } t \\ \infty & \text{if } f(t) \text{ diverges as fast or faster than } e^{\alpha t} \end{cases} \tag{2.20}$$

Let us call

$$\lim_{s \to 0} \left[s\bar{f}(s)\right] \equiv \left\langle f \right\rangle \tag{2.21}$$

Take the Laplace transform of Equation (2.17), obtaining

$$s\bar{n} - n_{t=o} + \vec{V} \cdot \vec{\nabla}\bar{n} - D\nabla^2\bar{n} = k^{*2}G\ \overline{P(t)n}$$

Multiply through by s and take the limit as $s \to 0$. Then if f does not diverge exponentially, using Equations (2.20) and (2.21), one obtains

$$\vec{V} \cdot \vec{\nabla} \left\langle n \right\rangle - D\nabla^2 \left\langle n \right\rangle = k^{*2}G\ \ n\ \frac{\left\langle Pn \right\rangle}{\left\langle n \right\rangle} \tag{2.22}$$

If n is periodic at large t, it must have the same period as P, namely, T, such that

$$\left\langle n \right\rangle = \lim_{q \to \infty} \frac{1}{T} \int_{qT}^{(q+1)T} n(t)dt \tag{2.23a}$$

and

$$\left\langle Pn \right\rangle = \lim_{q \to \infty} \frac{1}{T} \int_{qT}^{qT+\tau} n(t)dt \tag{2.23b}$$

since $P(t)$ vanishes for $qT + \tau < t < (q + 1)T$. At fixed $\vec{r}$ within the field, while the field is on, n behaves something like

$$n \sim n_o e^{s_o(t-qT)}, \quad qT \leq t \leq (qt + \tau) \tag{2.24a}$$

and while the field is off, it behaves like

$$n \sim n_{(t=\tau)} e^{-s_1(t-qT-\tau)}, \quad (qT + \tau) \leq t \leq (q + 1)T \tag{2.24b}$$

But at critical conditions between breakdown and no breakdown, one must have

$$n_{(t=qT)} = n_{t=(q+1)T} \tag{2.24c}$$

as depicted schematically in Figure 2.2. Then from these last three relations, one obtains

$$e^{s_o \tau} \; e^{-s_1 (T-\tau)} = 1$$

or

$$s_o = \frac{T - \tau}{\tau} s_1 \tag{2.24d}$$

Then using (2.24a) and (2.24b) and (2.23a) and (2.23b), one finds

$$\langle n \rangle \sim \frac{1}{T} \left\{ \frac{1}{s_o} n_o \left(e^{-s_o \tau} - 1 \right) + \frac{1}{s_1} n_o \, e^{-s_o \tau} \left[1 - e^{-s_1 (T-\tau)} \right] \right\}$$

$$\langle Pn \rangle \sim \frac{1}{T} \left[\frac{1}{s_o} n_o \left(e^{s_o T} - 1 \right) \right]$$

Then with these relations and Equation (2.24d), one finds

$$\frac{\langle Pn \rangle}{\langle n \rangle} = \frac{1/s_o}{\frac{1}{s_o} + \frac{1}{s_1}} = \frac{1}{\frac{T - \tau}{\tau} + 1} = \frac{\tau}{T}$$

Substitution of this into Equation (2.22) gives

$$(\vec{V} \cdot \nabla) \langle n \rangle - D \nabla^2 \langle n \rangle = k^{*2} \frac{\tau}{T} G \langle n \rangle \tag{2.25}$$

The eigenvalues of this equation give the breakdown field strength just as they do for Equation (2.8) or (2.13) in the c-w case. In addition, for constant D, the equations are identical except for the factor τ/T on the right-hand side. Notice that k^{*2} defined above is Dk^2. Thus the multiple-pulse case is identical to a c-w breakdown problem with $k^{*2}G = \nu$ reduced by the factor τ/T.

For the case of nonconstant D, the treatment is very similar. The transformed conservation equation, multiplied by s, becomes in the limit as $s \to 0$

$$(\vec{V} \cdot \vec{\nabla}) \langle n \rangle - \nabla^2 \left(\langle n \rangle \frac{\langle Dn \rangle}{\langle n \rangle} \right) = k^{*2} G \langle n \rangle \frac{\langle Pn \rangle}{\langle n \rangle} \qquad (2.26)$$

where $\langle Pn \rangle / \langle n \rangle$ is again τ/T. The new effective diffusion constant

$$D_{eff} = \frac{\langle Dn \rangle}{\langle n \rangle} \qquad (2.27)$$

may be evaluated in a manner similar to $\langle Pn \rangle / \langle n \rangle$. For the relaxed RVDF (Section 3.1), D is a function only of the average electron energy, and the average electron energy is determined solely by the effective applied field strength. Therefore, for a square pulse at a fixed position in space, D is discontinuous in time; it has one value when the field is on and another when the field is off. The size of the discontinuity depends upon position because of the antenna pattern. Such an evaluation is then straightforward but cannot be carried out very precisely since the dependence of the average electron energy on E is not very well known. In addition, there is the problem that, when the field is off, the electrons do not cool very readily back to the average field-off energy; the cooling time is approximately

$$(M/2m)(1/3\nu_{en}) \qquad (2.28)$$

where M is the heavy particle mass, m is the electron mass, and ν_{en} is the electron-neutral collision frequency. For intervals between pulses shorter than this time, the value of D with the field on and constant in time would probably be a reasonable approximation. Then one can take

$$\frac{\langle Dn \rangle}{\langle n \rangle} \simeq D \text{ (field on)} \qquad (2.29)$$

and again we have the result that the multiple-pulse problem is identical to a c-w eigenvalue breakdown problem with an effective net ionization frequency of $(\tau/T)\nu$. This result was obtained in Reference 3 with what appears to be a much simpler argument; however, it is believed that the present treatment brings out the validity of the corrected eigenvalue approach more clearly.

It then appears that, as the pulse interval goes to infinity ($T \rightarrow \infty$), the eigenvalue and the electric field for breakdown goes to infinity. In such a case, however, one must consider that the problem has gone over into single-pulse breakdown and thus the breakdown field strength is limited to the value determined there (see the next section). There would have been no need for special treatment of the single-pulse case, that is, it could be treated naturally in the limit as T becomes large, if in the treatment of the random-velocity distribution function (Section 3), and thus in ν, we were to include the effect of plasma resonance in the rate of heating. However, to include plasma resonance in an accurate way in the kinetic equation introduces a considerably more complex kinetic equation (see, e.g., Appendix A).

2.2.3 Single-pulse breakdown

Since it is difficult to include plasma resonance in the kinetic equation for evaluation of the rate of heating, because of the nonlinearity introduced, the concept of single-pulse breakdown has been used in the literature (Refs. 3, 9, and 11). Here one is no longer concerned with an eigenvalue problem, but rather with limitations imposed by the condition that resonant plasma oscillations do not occur. If such oscillations were to occur, resonant absorption of the applied energy by the electrons would result (Ref. 16, p. 50), and thus the ionization growth rate would be greatly increased.

The condition that such resonance does not occur is that the applied frequency be greater than the plasma frequency

$$\frac{\omega}{2\pi} \gg \frac{\omega_p}{2\pi} \tag{2.30a}$$

where

$$\frac{\omega_p}{2\pi} = \left(\frac{n_p e^2}{\pi m}\right)^{1/2} = 8.97\times10^3\ n_p^{1/2}\ \text{sec}^{-1} \qquad (2.30b)$$

Here n_p is the density of electrons (in cm^{-3}) giving rise to the plasma frequency ω_p.

The breakdown field strength is evaluated from this condition by using Equation (2.1) in a coordinate system with zero velocity, that is, moving with the flow. The condition that no parcel of air should attain the electron density n_p during the period τ of the applied field becomes, by integration of Equation (2.1) without the velocity term,

$$\ln\left(\frac{n_p}{n_o}\right) \geq \int_o^\tau \left[\nu(E_e) + \frac{\nabla^2(Dn)}{n}\right] dt \qquad (2.31)$$

where n_o is the initial electron density. To evaluate this relation, one takes $\nabla^2(Dn)/(Dn) = 1/\Lambda^2$, where Λ is the diffusion length which may be evaluated from solution of the steady-state problem (Eq. (2.8)), or approximated by the length over which escaping electrons must diffuse to get out of the applied field.

To compensate for the neglect of resonant plasma oscillations in the multiple-pulse problem, the value of E_e determined from Equation (2.31) is used as an upper limit for large spacing between pulses. Typical multiple-pulse results using this upper limit, computed in Reference 3, are shown in Figure 2.3. These data have been obtained from breakdown measurements and theory in a closed cavity.

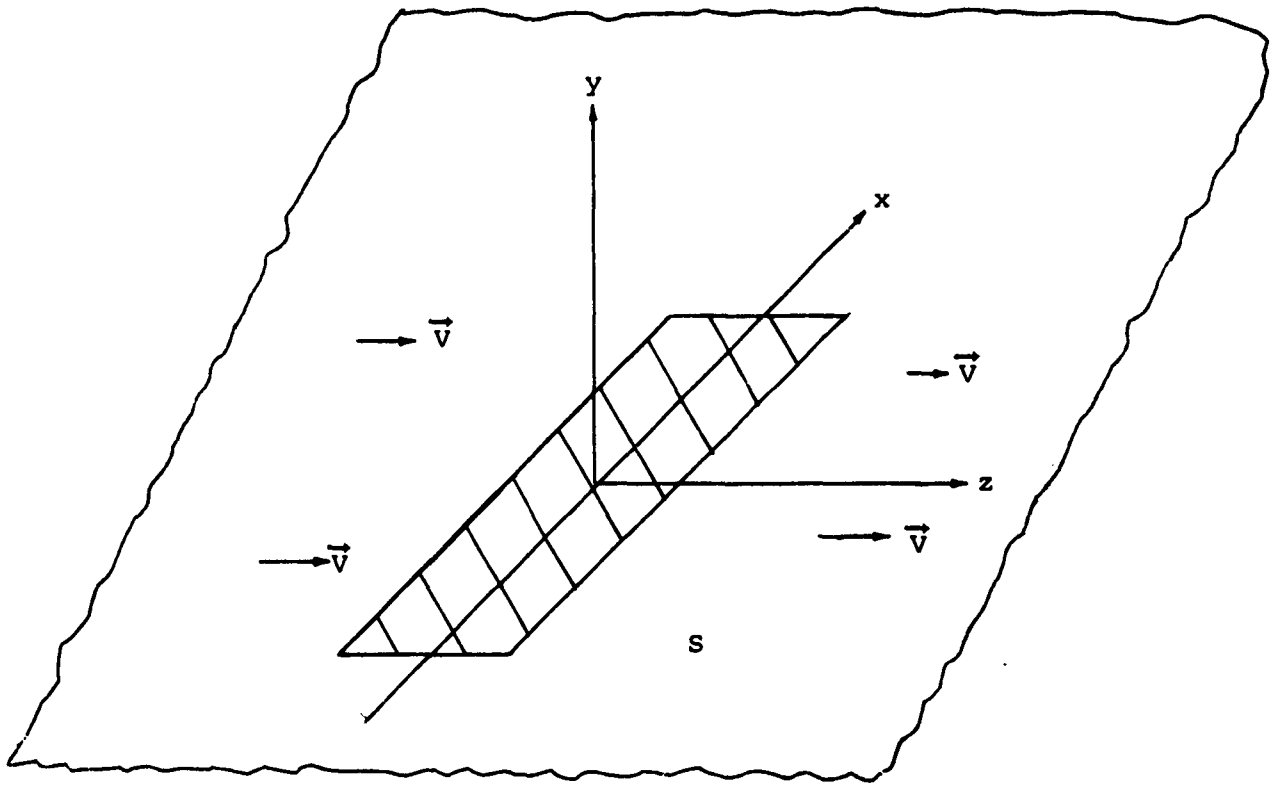

Figure 2.1.- Coordinates and geometry.

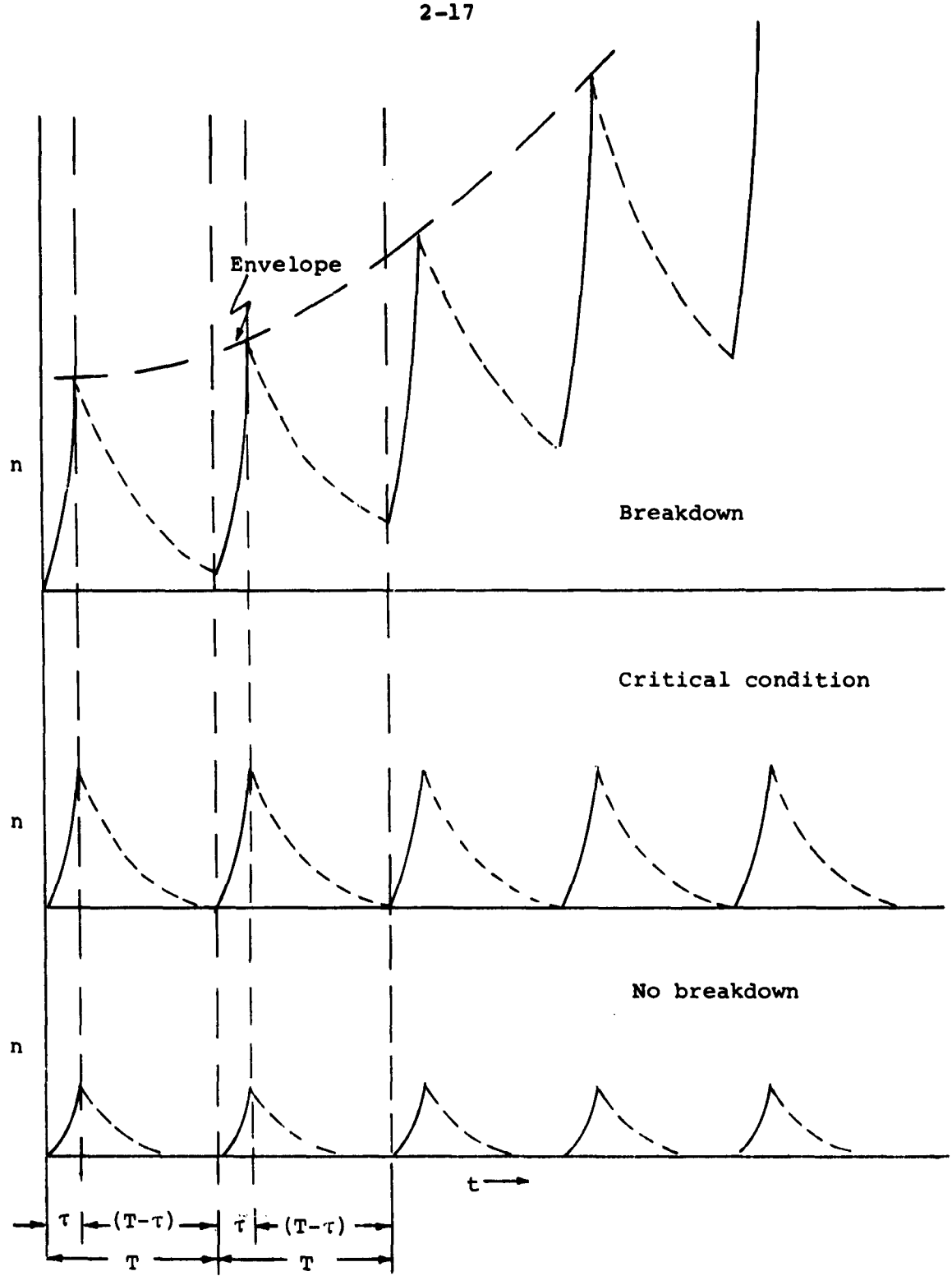

Figure 2.2.- Multiple-pulse breakdown schematic.

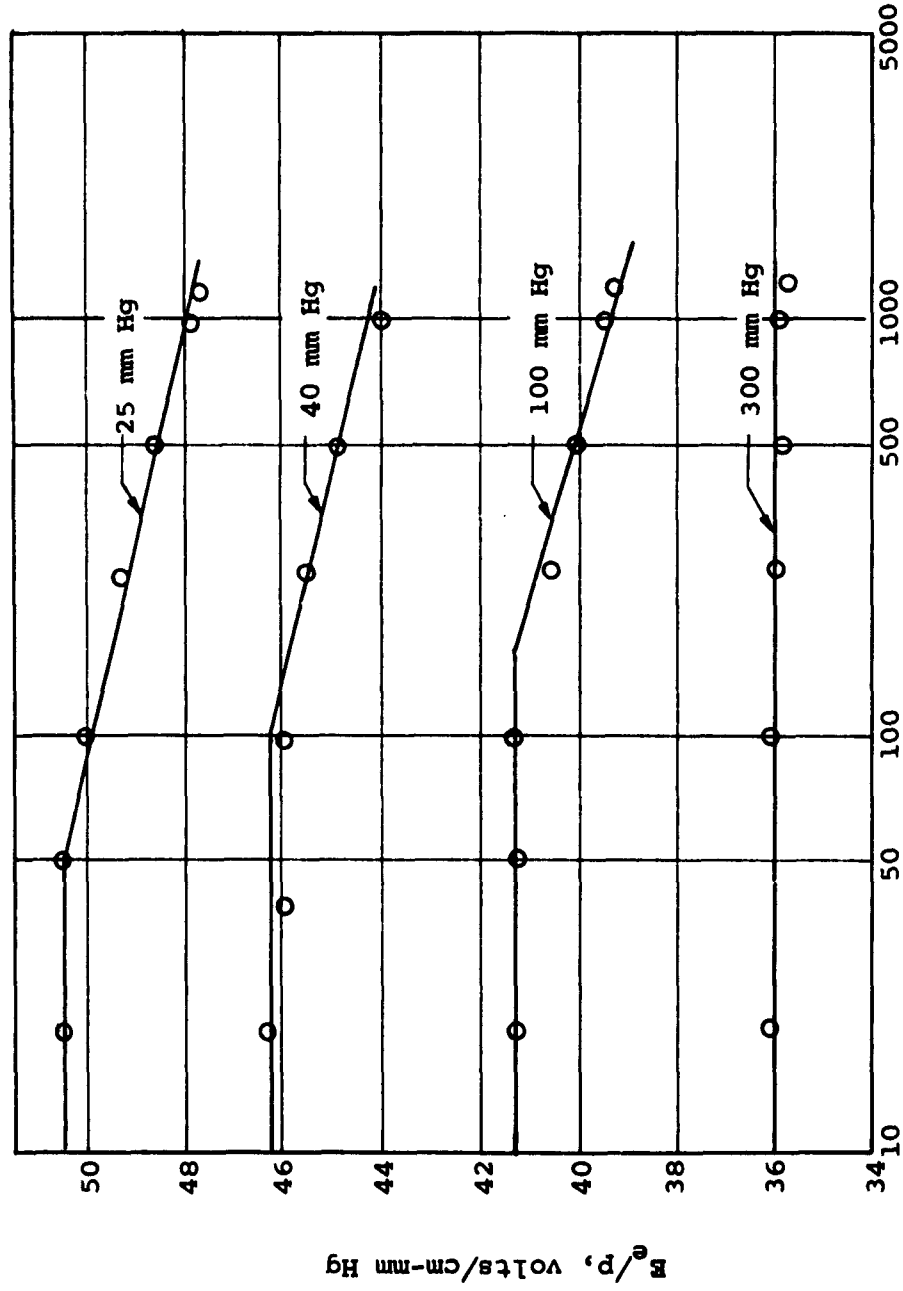

Figure 2.3.- Breakdown field as a function of repetition rate for various pressures from Reference 3. The indicated points are experimental. The parts of the curves that are horizontal lines are due to the single-pulse breakdown cutoff as described in Sections 2.2 and 2.3. These data are for a large cavity with one short dimension of 0.635 centimeters.

3. ESTIMATES OF MACROSCOPIC PROPERTY INPUTS FROM THEORY AND EXPERIMENT

In this section, the theoretical relationships between microscopic collisions and macroscopic properties is reviewed and used to help in estimating macroscopic properties. It is also used to determine restrictions on the applicability of experimental data obtained with various laboratory experiments and environments. In particular, it is pointed out that the usual d-c laboratory data have all been obtained under conditions of a relaxed electron random-velocity distribution function (RVDF) and are applicable only under conditions of a relaxed RVDF. Also pointed out is the importance of using data for the precise (or nearly precise) mixture in question.

The criteria for this relaxed RVDF are analyzed, and it is demonstrated that many, although not all, of the reentry situations involve relaxed distributions. For the case of unrelaxed distributions, it is pointed out that the breakdown problem is still completely tractable with the use of reasonable functions for the microscopic ionization frequency, excitation collision frequency and attachment frequency, as well as the microscopic momentum transfer collision frequency. These microscopic quantities are functions of the individual electron velocity; that is, they are not yet averaged over a velocity distribution. It is demonstrated that the unrelaxed breakdown problem may be handled with a variational principle similar to that used in this report.

It is believed that the above points have not been previously discussed in the literature. In addition, some theoretical relations have been misinterpreted or misused in portions of the literature. For clarity, therefore, results have been rederived here. In particular, one misconception is that the electron RVDF is either "Maxwellian" or "Druyvestein" or somewhere in between these. Another misconception is that in the relationship $D = 2/3\ \mu\bar{u}$, between the diffusion constant, the mobility, and

the average particle kinetic energy, the factor of two-thirds is exact only for a Maxwellian distribution.

3.1 Kinetic Equations and Velocity Distribution and Density Functions

3.1.1 The reduced kinetic equation and the random-velocity function (RVDF)

For prediction of macroscopic properties from microscopic collision phenomena, one must know the velocity distribution of the electrons. The form of the velocity distribution must be determined from the kinetic equation. In Reference 1, 12, 13, 14, 17, 18, or 19, it is shown[3] from the kinetic equation that, under certain conditions, the electron density function in velocity and position space is given approximately by

$$F_e(t,\omega,\vec{c},\vec{r}) \simeq F_o^{\,o}(t,\omega,|\vec{c}|,\vec{r}) \frac{\vec{c}\cdot\nabla F_o^{\,o}}{\nu_{en}} + \mathrm{Re}\left[\frac{e^{j\omega t}}{\nu_{en}+j\omega}\frac{\sqrt{2}\,e\vec{c}\cdot\vec{E}_{rms}}{mc}\frac{\partial}{\partial c}F_o^{\,o}\right] \qquad (3.1)$$

where $\vec{c}$ is not the actual electron velocity, but rather the random velocity defined in terms of the actual electron velocity $\vec{v}$ and the macroscopic flow velocity $\vec{V}$ by

$$\vec{c} = \vec{v} - \vec{V} \qquad (3.2)$$

and the electric field is assumed to be $E_o e^{j\omega t}$. The function $F_o^{\,o}$ satisfies the reduced kinetic equation (assuming $\vec{V} = V\vec{k}$)

$$\frac{\partial F_o^{\,o}}{\partial t} + \vec{V}\cdot\nabla F_o^{\,o} - \frac{c^2}{3}\vec{\nabla}\cdot\frac{1}{\nu_{en}}\vec{\nabla}F_o^{\,o} - \frac{1}{3}\left(\frac{e}{mc}\right)^2\frac{\partial}{\partial c}\left(\frac{E_{rms}^{\,2}\nu_{en}}{\nu_{en}^{\,2}+\omega^2}c^2\frac{\partial}{\partial c}F_o^{\,o}\right)$$
$$= \frac{1}{c^2}\frac{\partial}{\partial c}\left[c^3\frac{m\nu_{en}}{M}\left(F_o^{\,o}+\frac{kT}{mc}\frac{\partial}{\partial c}F_o^{\,o}\right)\right] - \left(\nu_I+\nu_X+\nu_R+\nu_A-q\right)F_o^{\,o} \qquad (3.3)$$

---

[3] In Appendix A, some of the special restrictions and considerations imposed on this kinetic development by the flow and geometry in the present application are considered, as well as a review of the development.

The terms on the right are due to collisions; the first is due to elastic collisions and the second is due to all inelastic collisions (and reappearance after an inelastic collision). Here ν_I, ν_A, ν_R, and ν_{en} are the ionization frequency, etc., for an individual electron of velocity c, as opposed to the average frequencies (with the bars) used earlier. The function $q(c)$ is the appearance or reappearance rate for electrons that have been produced or lost energy in an inelastic collision. The density function F_o^o is normalized such that

$$\iiint F_o^o \, dc_x \, dc_y \, dc_z = n(\vec{r},\omega,t) \tag{3.4}$$

The most restricting of the conditions[3] under which Equations (3.1) and (3.3) are valid are (i) the requirement of low ionization density such that electron-electron collisions are neglected, and thus

$$\bar{\nu}_{ee} \ll \frac{2m}{M} \bar{\nu}_{en} \tag{3.5}$$

and (ii) a high-frequency electric field such that relaxation is negligible within a cycle, so that

$$\omega \gg \frac{m}{M} \bar{\nu}_e \simeq \frac{m}{M} \bar{\nu}_{en}, \quad \text{where } \left(\bar{\nu}_e = \bar{\nu}_{en} + \bar{\nu}_{ei}\right) \tag{3.6}$$

The restrictions imposed by Equation (3.5), when evaluated in the same manner as (2.6) with (2.5), give approximately

$$\chi \ll 10^{-14} \, T_e^{\,2}(^oK) \tag{3.7}$$

where T_e is representative of the average electron random energy such that $(1/2)\overline{mc^2} \equiv 3kT_e/2$. Since T_e will usually be between about $2{,}000^o$ and $15{,}000^o$ K (as will be discussed later), this

---

[3]See footnote 3 on page 3-2.

restricts the model to a degree of ionization significantly below 10^{-5} to 10^{-6}. Such a restriction is probably fulfilled in reentry along the sides of the body, that is, if the electrons are not "frozen in" at a level corresponding to stagnation temperature. At stagnation conditions the reentry degree of ionization may reach and even slightly exceed these values. If this happens, but the ionization is still low enough to satisfy $\bar{\nu}_{ee} \ll \bar{\nu}_{en}$ such that

$$10^{-10}\ T_e^{\,2}(^{\circ}K) \gg \chi \sim 10^{-14}\ T_e^{\,2}(^{\circ}K) \tag{3.8}$$

then, one obtains to sufficiently good approximation (Refs. 17 and 18) an equation identical to Equation (3.3) except that the mass of the heavy particles is replaced by

$$M^* = \left[\frac{1}{M} + \frac{1}{m}\left(\frac{\nu_{ee}}{\nu_{en}}\right)\Omega\left(\frac{mc^2/2}{kT_e}\right)\right]^{-1} \tag{3.9a}$$

and the temperature of the heavy particles is replaced by

$$T^* = T + T_e\,\frac{M}{m}\left(\frac{\nu_{ee}}{\nu_{en}}\right)\Omega\left(\frac{mc^2/2}{kT_e}\right) \tag{3.9b}$$

where

$$\Omega(\xi) = \operatorname{erf}\xi - \frac{2\xi}{\sqrt{\pi}}\exp(-\xi^2) \tag{3.9c}$$

and

$$\nu_{ee} = 2\pi n\,\frac{e^4}{mc^3}\ln\left[1 + \frac{m^2c^4}{e^4}\left(\frac{kT_e}{4\pi ne^2}\right)\right] \tag{3.9d}$$

Here, as before, $3kT_e \equiv \overline{mc^2}$. The equation is actually nonlinear, since one must use F_o to evaluate $\overline{c^2}$; however, one can approximate the $\overline{c^2}$ expected, solve, and, if necessary, iterate.

The function $\Omega(\xi)$ is very small for $\xi < 1$ and grows to a maximum of unity when ξ is very large. The effect of the electron-electron collisions is, therefore, to make the average- and faster-than-average-velocity electrons act as if they see lighter but hotter neutrals. Since an electron could transfer energy more easily to lighter and with more difficulty to hotter particles by collision, these two effects tend to compensate one another. This possibly helps to explain why breakdown predictions have been so accurate even with neglect of electron-electron collisions in the analysis; however, the reduction in mass effect surely predominates.

In solving these equations it has become common to define a random-velocity distribution, f, given by

$$F_o^{\circ} = fn(\vec{r},t) \tag{3.10}$$

If η is any function of the magnitude $\left|\vec{c}\right| \equiv c$, then the average $\bar{\eta}$ is given by

$$n\bar{\eta} = \iiint \eta(c) F_o^{\circ}(c)\, dc_x\, dc_y\, dc_z = \int \eta(c) F_o^{\circ}(c) 4\pi c^2 dc$$

$$= n \int \eta(c) f(c) 4\pi c^2 dc \tag{3.11}$$

Multiply Equation (3.3) by $4\pi c^2 dc$ and integrate from zero to ∞. Then with use of Equations (3.4) and (3.11) integration by parts gives

$$\frac{\partial n(\vec{r},t)}{\partial t} + \vec{v} \cdot \vec{\nabla} n - \nabla^2 \left[\left(\overline{\frac{c^2}{3\nu_{en}}} \right) n \right] + \vec{\nabla} \cdot \left[n \left(\overline{\frac{c^2}{3} \nabla \frac{1}{\nu_{en}}} \right) \right]$$

$$= \left(\bar{\nu}_I - \bar{\nu}_A - \bar{\nu}_R \right) n \tag{3.12}$$

since $\bar{q} = 2\bar{\nu}_I + \bar{\nu}_X$, due to the fact that for each fast electron lost in ionization there reappear two slow electrons, whereas for each fast electron lost by excitation there reappears one slow electron. The terms involving $\partial/\partial c$ vanished at the limits of integration because at $c = \infty$, $F_o^o(\infty) = 0$. Thus, we have derived the electron conservation equation except for one extra term which will be discussed in Section 3.2.2.

Now, substituting Equation (3.10) into Equation (3.3), one obtains with use of Equation (3.12),

$$\frac{\partial f}{\partial t} + \mathbf{V}\cdot\nabla f + \frac{1}{n}\nabla\cdot(\vec{\phi} n f) + \left(\nu_I + \nu_A + \nu_R + \nu_X + \bar{\nu}_I - \bar{\nu}_A - \bar{\nu}_R - q\right) f = \frac{2}{3\sqrt{u}}\frac{d}{du}\left[\nu_{en} u^{3/2}\left(u_c\frac{df}{du} + \frac{3m}{M} f\right)\right] \quad (3.13a)$$

where

$$u \equiv \frac{mc^2}{2} \quad , \quad u_c \equiv \frac{e^2 E_{rms}^{\ 2}}{m}\left(\frac{1}{\nu_{en}^{\ 2} + \omega^2}\right) + \frac{3mkT}{M} \quad (3.13b)$$

and

$$\vec{\phi} \equiv \frac{c^2}{3\nu_{en}}\frac{\vec{\nabla}(fn)}{fn} - \frac{\vec{\nabla}\left[\left(\overline{c^2/3\nu_{en}}\right) n\right]}{n} + \left(\overline{\frac{c^2}{3}\vec{\nabla}\frac{1}{\nu_{en}}}\right) \quad (3.13c)$$

Equation (3.13a) must be solved in order to determine the random-velocity distribution function.

3.1.2 Criteria for a relaxed or stationary RVDF and difficulties introduced if not applicable

Virtually all work on breakdown in gases which has utilized a velocity-distribution function for electrons to compute macroscopic parameters has been concerned with the breakdown condition under nontransient, nonflow conditions. Previous work has therefore not considered velocity-distribution transients either in time or position space (such as would arise from flow into a field).

The RVDF was determined solely by the balance between energy input from the electromagnetic field and energy losses due to elastic and inelastic collisions and diffusion (the more energetic particles diffusing faster). The equation satisfied by such an RVDF is Equation (3.13a) without the $\partial/\partial t$ and the $\vec{v} \cdot \nabla$ terms, namely,

$$\frac{1}{n} \nabla \cdot (\vec{\phi} n f) + \left(\nu_I + \nu_A + \nu_R + \nu_X + \bar{\nu}_I - \bar{\nu}_A - \bar{\nu}_R - q \right) f = \frac{2}{3\sqrt{u}} \frac{d}{du} \left[\nu_{en} u^{3/2} \left(u_c \frac{df}{du} + \frac{3m}{M} f \right) \right] \quad (3.13d)$$

Before attempting to estimate under what conditions such a simplification is possible, let us consider the complications introduced when this simplification is not possible. With a nonstationary RVDF, one might as well go back to Equation (3.3) for breakdown studies. In the c-w case, the $\partial F_o^{\circ}/\partial t$ term may be omitted for determination of the breakdown condition for the same reasons as discussed in Section 2.2 ($\partial n/\partial t = 0$ condition). In the multiple-pulse case, one may use the time transform technique, as in Section 2.2.2, to obtain an equation for $\langle F_o^{\circ} \rangle$ without the $\partial/\partial t$ term. For the nonstationary RVDF the breakdown problem again reduces to an eigenvalue problem, but now it is further complicated by the presence of an additional dimension or independent variable, the quantity c, and differential operators involving this additional variable that are not self-adjoint. This problem, however, is still quite tractable and may be handled by the variational technique described in Appendix B. The main difference between this and the treatment of Section 5.2, which will be used in the present study, is that the computations involved in such a problem would require the machine storage of at least $2s^{n+1}$ pieces of information if there were s^n pieces stored for the relaxed n-dimensional self-adjoint RVDF problem, and if about the same accuracy were desired.

Although this extra difficulty is far from prohibitive, it is entirely unwarranted under the present state of our information (especially if the criteria for a stationary RVDF are met). This is because of the very poor information presently available for $\nu_I(c)$, $\nu_A(c)$, $\nu_R(c)$, and even $\nu_{en}(c)$. Also, data for the relaxed problem are more readily available since any measurements of macroscopic properties under stationary conditions may be used again for macroscopic properties under similar stationary conditions (but not under transient RVDF conditions). In addition, fairly good values of the macroscopic parameters D and ν can sometimes be estimated without precise knowledge of the RVDF.

Let us now attempt to estimate under what conditions this stationary assumption is possible. This criterion must require that the balance between energy input from the field and energy lost must be established during flow through the field in a negligible distance compared to externally applied field width (in the flow direction) and in a time short compared to the pulse width (when there is one).

If we assume that the initial distribution, upon entering the field, is Maxwellian at temperature, T, and if this is substituted into Equation (3.13a), there results

$$v\left(\frac{\partial f}{\partial z}\right)_{initial} = \left(\frac{1}{2mkT}\right)\left(-1 + \frac{mc^2}{3kT}\right)\frac{2E_{rms}^2 e^2}{\nu_{en}\left(1 + \frac{\omega^2}{\nu_{en}^2}\right)}(f)_{initial}$$

Here we have neglected inelastic collisions for we are interested in evaluating this expression at energies less than the threshold energy of the lowest excited state. Also, diffusion loss was neglected, for there will be little such loss, initially.

This may be also rewritten as

$$\left(\frac{d \ln f}{dz}\right)_{initial} = \frac{1}{nkTV}\sigma_R E_{rms}^2\left(-1 + \frac{1}{3}\frac{mc^2}{kT}\right) \equiv \frac{1}{H} \qquad (3.14)$$

defining H and σ_R (later shown to be the electrical conductivity) so that, initially,

$$f = f_{z=o}(c)e^{z/H(c)}$$

where H is the initial relaxation length and we have taken the field to start at $z = 0$. For the pulsed nonflow case, we would have obtained

$$\frac{d \ln f}{dt} = \frac{V}{H} \quad \text{or} \quad f = f_{t=o}(c)e^{Vt/H(c)}$$

We see that, initially, from the behavior of H, the distribution function is "pivoting" about the average energy; it is decreasing below and increasing above the average with time or length of flow into the field. In the region of $(1/2)mc^2 = u_x$, the lowest inelastic energy level, the requirement that $|H| \ll L_E$, where L_E is the length of the field-containing region, gives

$$\frac{nu_x}{\sigma_R E_{rms}^2} \ll \frac{L_E}{V}\left(\frac{u_x}{\frac{3}{2}kT}\right)^2 \tag{3.15a}$$

whereas at the low energies this becomes

$$\frac{nkT}{\sigma_R E_{rms}^2} \ll \frac{L_E}{V} \tag{3.15b}$$

Conditions common in the reentry problem are $L_E = 2$ cm, $u_x \simeq 1$ e.v., $T \simeq 2000^\circ$ K, $p = 1$ mm Hg, $V \simeq 10^5$ cm/sec, and we will take

$$\nu_{en} = 6\times10^9(p/T)c \tag{3.16}$$

where p is in mm Hg and T is in $^\circ$K. In Equation (3.16) one must take $c = \sqrt{2u_x/m}$ for Equation (3.15a) and $c \sim \sqrt{kT/m}$ for

Equation (3.15b). Substitution of these numbers gives from Equation (3.15a)

$$E_{rms} \gg 0.7 \text{ volt/cm} \tag{3.17a}$$

and from Equation (3.15b)

$$E_{rms} \gg 1.5 \text{ volts/cm} \tag{3.17b}$$

Since these minimum field strengths are only about 1 to 2 percent of the field strengths required for breakdown, one might infer from this that the relaxed distribution is fairly well achieved for breakdown problems in reentry. One should note, however, that if we set $L_E/V = \tau$ and take τ to be 1 microsecond, the analogous results become

$$E_{rms} \gg 7 \text{ volts/cm} \tag{3.18a}$$

and

$$E_{rms} \gg 15 \text{ volts/cm} \tag{3.18b}$$

for the high- and low-energy regions. Thus, for microsecond pulses under these conditions, the stationary RVDF may not be quite achieved.

Although this estimate only includes initial tendencies, it should give a reasonable estimate of the relaxation requirements.

3.1.3 The stationary distribution as a condition for use of d-c data

The use of the macroscopic Equations (2.1) or, equivalently, (3.12) does not in itself assume a relaxed RVDF. The only place the RVDF comes into such computations with the macroscopic equations is through D and ν, the diffusion and net ionization coefficients. The assumption of a relaxed RVDF comes in indirectly then when one uses data from experiments conducted under relaxed conditions.

Despite restriction (3.6), it is found in Appendix A that at zero frequency, $\omega = 0$, one obtains Equations (3.1) and (3.3) again with $\omega = 0$ and E_{rms} replaced with E_{d-c}. Then, it is immediately obvious that one obtains the same distribution function and macroscopic coefficients with a high-frequency a-c field as with the equivalently effective d-c field given by[4]

$$E_e = \frac{E_{rms}}{\left(1 + \frac{\omega^2}{\nu_{en}^2}\right)^{1/2}} \tag{3.19a}$$

Therefore, for cold air, one can use d-c measured data for high-frequency breakdown prediction. However, care must be taken because all existing d-c data were obtained under relaxed RVDF conditions and should be used only when relaxed RVDF conditions obtain.

The existing measurements of pulsed breakdown (e.g., Ref. 3) are also conducted under relaxed conditions. This may be seen by noting

$$\sigma_R E_{rms}^2 \equiv E_e^2 \left(\frac{ne^2}{m\nu_{en}}\right) \tag{3.19b}$$

Then, the conditions (3.15a) and (3.15b) become, respectively,

$$\left(\frac{E_e}{p}\right)^2 >> \left(\frac{V}{L_E}\right)\left(\frac{\frac{3}{2}kT}{u_x}\right)^2 \frac{1}{e^2} (6\times10^9) \frac{1}{pT} \sqrt{2mu_x^3} \tag{3.20a}$$

and

$$\left(\frac{E_e}{p}\right)^2 >> \left(\frac{V}{L_E}\right) \frac{1}{e^2} (6\times10^9) \frac{1}{pT} \sqrt{2mu^3} \tag{3.20b}$$

---

[4] A small correction to this equivalence will be discussed in Section 3.2.5.

where Equation (3.16) was used and $c = \sqrt{2u/m}$. For example, the data of Reference 3 were for

$$30 < \frac{E_e}{p} < 50 \text{ volts/cm-mm Hg}$$

$$1 < p < 1000 \text{ mm Hg}$$

$$\lambda = 10,\ 10.7 \text{ cm}$$

$$\tau \equiv L_E/V \simeq 1\ \mu \text{ sec}$$

Then, Equation (3.20b) gives with $u^2 \simeq (3/2)kT$ and $E_e/p \simeq 30$

$$\left(\frac{E_e}{p}\right)^2 \simeq 1000 \gg \frac{3.4}{p\sqrt{T}}$$

Equation (3.20a) is even easier to satisfy.

3.1.4 Determination of the relaxed distribution function

Equation (3.13d) has been solved exactly for the case of constant ν_{en} in terms of hypergeometric functions.[5] The method is, in general, very complicated and tedious. However, the main features of the distribution function may be obtained by the approximate method of Allis (Ref. 13), Brown (Ref. 1), and Smit (Ref. 21), which is much easier to use. We describe this below:

The usual procedure is to divide the problem into two different regions. The first, an inelastic region, corresponds to electron energies above the lowest inelastic threshold u_x, that is, all u, such that

$$u \geq u_x$$

---

[5]Reference 20. This work is reviewed in Reference 1, pp. 546-549.

Electron energies below this level are considered in the elastic regions. The slope of the logarithm of the distribution function in both these regions is required to be continuous. We consider first, very briefly, the inelastic region.

When inelastic collisions are present, they overpower all other collision processes because of the very large energy loss per collision. Also, ν_A and ν_R and, of course, q are small at large energies. The term involving m/M, which is due to heavy particle recoil, and the diffusion term are also neglected in this region. This reduces (3.13d) to an equation that is solved by use of the substitution $u^{1/2}f = e^{-s}$. The reason for this change of variable is to facilitate the requirement of good accuracy at u_x, the lowest inelastic level, and u_I, the ionization energy, while simultaneously requiring $f(\infty) = 0$. The resulting first-order equation for ds/du is solved with a power series in $1/u$. One coefficient in this power series is reserved for matching at u_x to the elastic range solution.

In the elastic range ν_I and ν_X are zero; however, qf must be considered. As noted in Section 3.1.1, $\bar{q} = 2\bar{\nu}_I + \bar{\nu}_X$. Also, q, the electron reappearance term, is appreciable only at low velocities, as are ν_A and ν_{en}. Then, multiplying Equation (3.13d) by $4\pi c^2 dc$ and integrating to a value of $u = (1/2)mc^2$ corresponding to moderate velocities, one obtains

$$\left(\bar{\nu}_I + \bar{\nu}_X - \Phi\right) = -\frac{4\pi}{3}\nu_{en}c^3\left(u_c\frac{df}{du} + \frac{3m}{M}f\right) \qquad (3.21)$$

where Φ is the diffusion term given by

$$\Phi \equiv \int_0^c \frac{1}{n}\nabla\cdot(\vec{\phi}nf)4\pi c^2 dc \qquad (3.22)$$

This term is usually small in the elastic region. It is much larger in the inelastic region but is usually neglected there because of

the overpowering effect of the inelastic collisions. If considered, it is generally replaced with some simplifying approximation.

The solution to Equation (3.21) is

$$f = \frac{e^{-w}}{4\pi} \int_{w_o}^{w} e^{w} \left(\bar{\nu}_I + \bar{\nu}_X - \Phi \right) \frac{dw}{c^3 \nu_{en}} \tag{3.23a}$$

where

$$w \equiv \int_{o}^{u} \frac{3m}{M} \frac{du}{u_c} \tag{3.23b}$$

This equation is valid only if c, and thus w, is large enough to be above the values at which $q(c)$, $\nu_A(c)$, and $\nu_R(c)$ contribute appreciably. Here, w_o is the value of w when $u = u_o$, and u_o is the average value of u above u_x at which inelastic collisions occur. It is generally slightly above u_x. In general, u_o must be determined by matching slopes at u_x to the solution in the inelastic region.

3.1.5 The form of the distribution function and the special cases of Maxwellian, Druyvestein, and Margenau distributions

By using the value of u_c from Equation (3.13b) in Equations (3.23a) and (3.23b), the form of the distribution function and various special cases may be predicted.

When the first inelastic energy level is so high and $w_o(u_o)$ so large (compared to average w) that the integral in Equation (3.23a) is dominated by the upper limit, the integral is approximately constant, and then f is

$$f \simeq (\text{const}) e^{-w} = (\text{const}) \exp \left(- \int_{o}^{\frac{1}{2} mc^2} \frac{du}{\frac{Me^2}{3m^2 \nu_{en}^2} E_e^2 + kT} \right) \tag{3.24}$$

This "Margenau distribution" was first derived in Reference 22. When

$$\left.\begin{aligned} &\frac{Me^2}{3m^2\nu_{en}^{\,2}}\,E_e^{\,2} \ll kT \\ \text{or}\quad &\frac{e^2E_e^{\,2}}{m\nu_{en}} = \sigma_R E_{rms}^{\,2} \ll \nu_{en}\left(\frac{2m}{M}\right)\frac{3}{2}\,kT \end{aligned}\right\} \qquad (3.25)$$

this reduces to the ordinary Maxwellian (temperature) distribution. The condition (3.25) is equivalent to the statement that the rate of heat input is negligible compared to the average energy exchanged between electrons and heavy particles.

When the inequality of Equation (3.25) is not satisfied and both sides are about equal, one obtains again a Maxwellian distribution at the new electron temperature

$$\frac{3}{2}\,kT_e = \frac{3}{2}\,kT + \sigma_R E_{rms}^{\,2}\left(\frac{m}{2M\nu_{en}}\right) \qquad (3.26)$$

if ν_{en} is approximately constant. Essentially, the average energy has been increased by the energy necessary for the electrons to lose an amount during collisions with heavy particles equal to what they gain between collisions from the electric field.

If one assumes that the mean-free path (rather than the collision frequency) is approximately independent of velocity, then $\nu_{en} \simeq c/l$, and if (3.25) is satisfied, one obtains the Druyvestein distribution (Ref. 23).

When u_o is not very much larger than the average u, one obtains a definite distribution by requiring continuous slope at u_x and matching (3.23) to the inelastic region. The form of the distribution function in such a situation will, for a strong electric field, be rather flat and fall off suddenly at $u = u_x$.

The slope at $u = u_x$ determines the number of particles diffusing into the inelastic region and thus undergoes inelastic collisions. This behavior is depicted schematically in Figure 3.1. A careful treatment of the computation of f for air using some recent (though not yet fully accepted) data for the rates of vibrational excitation by electron impact may be found in Reference 24. Careful computations with noble gases, H_2 and Heg gas (He with about 1-percent Hg) are in Reference 20.

3.2 Macroscopic Properties and Macroscopic Equations from Theory

Although the very poor state of our knowledge of $\nu_{en}(c)$, the momentum transfer collision frequency, $\nu_I(c)$, the net ionization frequency, etc., prevents a truly reliable prediction of macroscopic properties, useful formulas for extrapolating and interpreting experimental data may be obtained from theory.

3.2.1 The macroscopic equations

In Section 3.1.1 we derived the electron conservation equation from the kinetic equation. This, in addition, gave the macroscopic parameters for this equation. By taking velocity moments of the kinetic equation (3.3), all the other macroscopic equations could be likewise derived.

An alternate and completely equivalent procedure would be to write down the macroscopic equations from continuum mechanics and evaluate the necessary macroscopic parameters by use of Equation (3.1). It turns out that the equations dealing with electrons are not always independent of the equations governing the heavier ions and, therefore, an equation for heavy ion conservation will be included. The equations of interest are those which have been already averaged over the very short time $2\pi/\omega$ of the high-frequency oscillation. The time dependence remaining in the equations is for the much slower changes such as growth of ionization.

From continuum mechanics, the particle conservation equations are

$$\frac{\partial n}{\partial t} + \nabla \cdot \left(n \left\langle \vec{\bar{v}} \right\rangle \right) = \left\langle \bar{\nu}_I - \bar{\nu}_A - \bar{\nu}_R \right\rangle n \tag{3.27a}$$

$$\frac{\partial N_I}{\partial t} + \nabla \cdot \left(N_I \vec{\bar{v}}_I \right) = \frac{1}{Z_{av}} \left\langle \bar{\nu}_I - \bar{\nu}_A - \bar{\nu}_R \right\rangle n \tag{3.27b}$$

where eZ_{av} is the average charge per ion.[6] For breakdown studies, Z_{av} will be very close to unity. The average ionization $\bar{\nu}_I$ is a function of the precise mixture at every point and should go to zero as the number of ionizable particles is depleted. This latter property is not important in the computation of breakdown conditions. The bar denotes averages over the RVDF and the $\langle\ \rangle$ notation denotes time averages over $\Delta t = 2\pi/\omega$.

Let us write for the diffusion relation for electrons

$$\left\langle \vec{\bar{c}} \right\rangle \equiv \left\langle \vec{\bar{v}} \right\rangle - \vec{v} = - \frac{\vec{\nabla}(D_e n)}{n} - e\mu_e \vec{E}_D \tag{3.28a}$$

and for the heavy ions

$$\vec{\bar{v}}_I - \vec{v} = - \frac{D_I \vec{\nabla} N_I}{N_I} + Z_{av} e \mu_I \vec{E}_D \tag{3.28b}$$

Here we have assumed special forms for the diffusion which will be justified in the next section. The field $\vec{E}_D$ is due to the charge separation formed by the different diffusion rates of the ions and the electrons. It is given by Poisson's relation

$$\vec{\nabla} \cdot \left(\epsilon_o \vec{E}_D \right) = - ne + N_I Z_{av} e \tag{3.29}$$

where ϵ_o is the free space dielectric constant.

---

[6] In Equation (3.27b), the simplifying assumption is made of an average ion of charge $Z_{av}e$ and that ions of the opposite charge are not counted (attachment). This serves the purpose here since this equation is really only used for the discussion in Section 3.2.3 of ambipolar diffusion. More generally, one has a separate equation for each ion, and all the individual processes must be considered on the right-hand side of each equation.

An energy equation is not needed in this model since the assumption of a relaxed RVDF determined the energy as a function of local conditions. The energy is determined by the local balance between electromagnetic heating and collision losses.

3.2.2 Macroscopic properties

Equation (3.11) defined the average of a microscopic quantity when it is a function only of the magnitude of $\vec{c}$ and not its direction. For a more general function, one that is dependent on the direction of $\vec{c}$ as well as its magnitude, one must use F_e as given in Equation (3.1) to compute averages. This requires

$$n\,\overline{\eta(\vec{c})} = \int_0^\infty \eta(\vec{c}) F_e \, dc_x \, dc_y \, dc_z \tag{3.30}$$

It is easily seen that Equation (3.11) is a special case of (3.30). The subsequent average over $(2\pi/\omega)$ gives $n\left\langle \bar{\eta}(\vec{c})\right\rangle$. Because of the form of (3.1) it is always possible to reduce averages of the type (3.30) to averages over the RVDF as expressed by Equation (3.11). Let us proceed in this way to derive the necessary macroscopic relations. In deriving these relations the following identity is used

$$\int \vec{c}\,\vec{c}\cdot\vec{A}(c)dc_x\,dc_y\,dc_z = \int \frac{c^2}{3}\vec{A}(c)4\pi c^2 dc$$

where $\vec{A}$ is any vector that may be a function of the magnitude of $\vec{c}$. This result follows by symmetry. Some terms also require integration by parts.

In order to obtain an expression for the right-hand side of Equation (3.28a), another term must be added to Equation (3.1) to account for the d-c field E_D. This term is

$$\left(-e\vec{c}\cdot\vec{E}_D/mv_{en}c\right)\left(\partial F_o{}^o/\partial c\right)$$

as is evident from the derivation from the treatment of d-c fields in Appendix A. (Alternately one could use the existing last term in Eq. (3.1), use $\vec{E} = \sqrt{2}\,\vec{E}_{rms}\cos\omega t$ in all the derivations, and afterward replace $E_{rms}/\left[1 + (\omega^2/\nu_{en}^2)\right]^{1/2}$ with E_D, as required by Eq. (3.19).) With this extra term in Equation (3.1) we find

$$\left\langle \vec{\bar{c}} \right\rangle = \frac{\omega}{2\pi} \int_0^{2\pi/\omega} dt \left(\iiint \vec{c}\, F_e \, dc_x \, dc_y \, dc_z \right)$$

$$= \iiint \vec{c} \left(F_o^{\,o} - \frac{\vec{c} \cdot \nabla F_o^{\,o}}{\nu_{en}} + \frac{e\vec{c} \cdot \vec{E}_D}{m\nu_{en}c} \frac{\partial}{\partial c} F_o^{\,o} \right) dc_x \, dc_y \, dc_z$$

The alternating current term dropped out in the average over $2\pi/\omega$. The first term of this expression vanishes. The other two may be rewritten, by use of the identity above, as

$$\left\langle \vec{\bar{c}} \right\rangle = - \int \left(\frac{c^2}{3\nu_{en}} \nabla F_o^{\,o} - \frac{\vec{E}_D ec}{3m\nu_{en}} \frac{\partial}{\partial c} F_o^{\,o} \right) 4\pi c^2 dc$$

Using $F_o^{\,o} = nf$, integrating the second term by parts, and manipulation gives

$$\left\langle \vec{\bar{c}} \right\rangle = - \nabla \left[n \int f \left(\frac{c^2}{3\nu_{en}} \right) 4\pi c^2 dc \right] - n \int f \left(\frac{c^2}{3\nu_{en}} \nabla \ln \nu_{en} \right) 4\pi c^2 dc$$

$$+ \frac{ne}{m} \left[\int \left(\frac{1}{\nu_{en}} + \frac{c}{\nu_{en}} \frac{d \ln \nu_{en}}{dc} \right) f 4\pi c^2 dc \right] \vec{E}_D$$

or, by use of Equation (3.11),

$$n\left\langle\vec{\bar{c}}\right\rangle = -\nabla\left[\left(\overline{\frac{c^2}{3\nu_{en}}}\right)n\right] - n\left(\overline{\frac{c^2}{3\nu_{en}}\nabla \ln \nu_{en}}\right)$$

$$-\frac{ne}{m}\left[\left(\overline{\frac{1}{\nu_{en}}}\right)+\left(\overline{\frac{c}{\nu_{en}}\frac{d \ln \nu_{en}}{dc}}\right)\right]\vec{E}_D \qquad (3.31)$$

Generally the terms involving derivatives of $\ln \nu$ are quite small compared to the others, so that Equation (3.31) is written

$$n\left\langle\vec{\bar{c}}\right\rangle = -\nabla\left[\left(\overline{\frac{c^2}{3\nu_{en}}}\right)n\right] - \frac{ne}{m}\left(\overline{\frac{1}{\nu_{en}}}\right)\vec{E}_D \qquad (3.32)$$

Comparison with Equation (3.28a) gives

$$D_e = \left(\overline{\frac{c^2}{3\nu_{en}}}\right) \text{ and } \mu_e = \frac{1}{m}\left(\overline{\frac{1}{\nu_{en}}}\right) \qquad (3.33)$$

Analogous expressions for the right-hand side of Equation (3.28b) are obtained in kinetic theory textbooks (Ref. 25). They give

$$\vec{\bar{V}}_i - \vec{\bar{V}} = -\frac{kT}{M_I\nu_{In}}\left[\frac{\nabla N_I}{N_I} + k_T^I\left(\frac{\nabla T}{T}\right) - \frac{Ze}{kT}\vec{E}_D\right] \qquad (3.34)$$

The thermal diffusion ratio k_T^I is generally small because the ion mass is about equal to the average particle mass - this, in fact, is the essential reason for the different form of the diffusion terms in Equations (3.28a) and (3.28b). Comparison with Equation (3.28b) gives

$$D_I = \frac{kT}{M_I\nu_{In}} \text{ and } \mu_I = \frac{1}{M_I\nu_{In}} \qquad (3.35)$$

The average electron induced ionization frequency is, of course, given by Equation (3.30) as

$$\left\langle \overline{\nu_I} \right\rangle = \frac{\omega}{2\pi} \int_0^{2\pi/\omega} \left\{ \sum_i \int_{c_{Ii}}^{\infty} \left[\sigma_{Ii}(c) N_i \right] c f 4\pi c^2 dc \right\} dt \quad (3.36)$$

where $(1/2)mc_{Ii}^2$ is equal to the ionization potential of the i^{th} species, N_i is the number of neutrals of the i^{th} species, and $\sigma_{Ii}(c)$ is the cross section for ionization of the i^{th} species.

The instantaneous conductivity of the gas may be found by computing $\vec{J}$, the current density, using Equations (3.1) and (3.30) to obtain $\vec{\bar{c}}$, which gives

$$\sigma\vec{E} \equiv \vec{J} \equiv - ne\, \vec{\bar{c}} \equiv Re\left[\left(\sigma_R + j\sigma_I \right) e^{j\omega t} \vec{E}_o \right]$$

$$= \frac{ne^2}{m} Re\left(\left\{ \left(\overline{\frac{1}{\nu_{en} + j\omega}} \right) + \left[\overline{\frac{c}{\left(\nu_{en} + j\omega \right)^2} \frac{d\nu_{en}}{dc}} \right] \right\} e^{j\omega t} \vec{E}_o \right)$$

The second term is generally negligible so that

$$\sigma_R + j\sigma_I = \frac{ne^2}{m} \left(\overline{\frac{1}{\nu_{en} + j\omega}} \right) \quad (3.37)$$

The instantaneous heating rate is $\vec{J} \cdot \vec{E}$ or

$$\vec{J} \cdot \vec{E} = ne\, \vec{\bar{c}} \cdot \vec{E} = E_o^2 \left(\sigma_R \cos^2\omega t - \frac{1}{2} \sigma_I \sin 2\omega t \right) \quad (3.38)$$

so that

$$\left\langle \vec{J} \cdot \vec{E} \right\rangle = E_{rms}^2 \sigma_R \quad (3.39)$$

Since ν_{en} varies slowly with electron energy (Ref. 15), it is common to use in these expressions

$$\left.\begin{aligned} \overline{1/\nu_{en}} &\simeq 1/\overline{\nu_{en}} \quad ; \quad \overline{c^2/\nu_{en}} \simeq \overline{c^2}/\overline{\nu_{en}} \\ \left(\overline{\frac{1}{\nu_{en} + j\omega}}\right) &\simeq \frac{1}{\overline{\nu_{en}} + j\omega} \end{aligned}\right\} \quad (3.40a)$$

This is sometimes called the constant collision frequency approximation. Notice that with this approximation Equation (3.33) becomes

$$D_e = \overline{c^2}/3\overline{\nu_{en}} = \frac{2}{3}\left(1/m\overline{\nu_{en}}\right)\left(\frac{1}{2}\,\overline{mc^2}\right) = \frac{2}{3}\,\mu_e\left(\frac{1}{2}\,\overline{mc^2}\right) \qquad (3.40b)$$

3.2.3 Ambipolar diffusion phenomena

If in Equations (3.27a), (3.27b), and (3.29), with Equations (3.28a) and (3.28b), one assumes that $\partial n/\partial t \simeq \partial N_I/\partial t$ (i.e., the net charge density is approximately constant in time), then Allis and Rose (summarized in Ref. 13) have shown that the effect of the diffusion field E_D on the electrons may be accounted for by a new effective diffusion constant, D_t, and the behavior of the heavy ions then ignored. That is, they have shown that the movement of the electrons may be described by Equation (3.27a) but with $\langle\vec{\vec{c}}\rangle = \langle\vec{\vec{v}}\rangle - \vec{V}$ given by

$$n\langle\vec{\vec{c}}\rangle = -\nabla(D_t n)$$

where the new effective constant D_t was obtained by numerical solution of Equations (3.27a), (3.27b), (3.29), (3.28a), and (3.28b) with the assumption of constant D_e, D_I, μ_e, and μ_I. It is believed that taking these parameters constant does not greatly disturb the results.

The numerical results for D_t are given in Figure 8 of Reference 13 and may be represented approximately by the formula

$$\log\left(\frac{D_t}{D_e}\right) - \log(0.9) = \frac{1}{4}\left[\log\left(\frac{D_a}{D_e}\right) - \log(0.9)\right]\left[\log\left(\frac{4\pi\Lambda^2}{\lambda_D^2}\right) - \log(0.018)\right] \tag{3.41a}$$

when $1 \leq (D_t/D_e) \leq (D_a/D_e)$. Otherwise,

$$\max\,(D_t/D_e) = 1 \quad , \quad \min\,(D_t/D_e) = D_a/D_e \tag{3.41b}$$

Here λ_D is the Debye distance given by

$$\lambda_D = \left(\frac{\overline{mc^2/3}}{4\pi ne^2}\right)^{1/2} \tag{3.42}$$

Λ is the "diffusion length," $\Lambda = \nabla^2 n/n$, and D_a is the ambipolar diffusion constant given by

$$D_a = \frac{\mu_I D_e + \mu_e D_I}{\mu_I + \mu_e} \tag{3.43}$$

Equation (3.41) states that the logarithm of D_t/D_e varies linearly from zero (<u>free diffusion</u> where $D_t = D_e$ and $4\pi\Lambda^2/\lambda_D^2 = 0.018$) to $\log D_a/D_e$ (full <u>ambipolar diffusion</u> where $D_t = D_a$ and $4\pi\Lambda^2/\lambda_D^2 = 180$). Then three regions can be distinguished

$$\left.\begin{aligned} &\text{Free diffusion:} && \left(\frac{\Lambda}{\lambda_D}\right)^2 \leq 1.2\times10^{-3} \quad , \quad D_t = D_e \\ &\text{Transition:} && 1.2\times10^{-3} \leq \left(\frac{\Lambda}{\lambda_D}\right)^2 \leq 14 \quad , \quad D_e > D_t > D_a \\ &\text{Full ambipolar:} && \left(\frac{\Lambda}{\lambda_D}\right)^2 \geq 14 \quad , \quad D_t = D_a \end{aligned}\right\} \tag{3.44}$$

Since $m \ll M_I$, Equations (3.33) and (3.35) indicate $\mu_e \gg \mu_I$ and, using (3.40), that (3.43) may be written to good approximation

$$D_a \simeq \mu_I \left(\frac{2}{3} \frac{\overline{mc^2}}{2} + kT \right) \tag{3.45a}$$

With a relatively cold gas in an applied field under stationary conditions, the average electron energy would be about (see, e.g., Fig. 3.1 and Ref. 24 for strong fields)

$$\overline{mc^2}/2 \simeq (2/3)u_x \gg kT$$

where u_x is the lowest excitation potential and is about an electron volt for oxygen. Then Equation (3.45a) may be written approximately

$$D_a \simeq (4/9)\mu_I u_x \tag{3.45b}$$

If we take $(3/2)(\overline{mc^2}/2) \simeq u_x \simeq 1$ ev in Equations (3.42) and (3.44), we find for the three regions

$$\left.\begin{array}{ll} \text{Free diffusion:} & \Lambda^2 n \leq 2.9\times10^2 \text{ cm}^{-1} \\ \text{Transition diffusion:} & 2.9\times10^2 \leq \Lambda^2 n \leq 3.5\times10^6 \text{ cm}^{-1} \\ \text{Full ambipolar:} & \Lambda^2 n \geq 3.5\times10^6 \text{ cm}^{-1} \end{array}\right\} \tag{3.46}$$

Thus it is seen that in re-entry problems the diffusion will be transition or full ambipolar.

Diffusion constants for ions and, therefore, the ambipolar diffusion constant may be determined from the polarizability δ of the neutral particles by use of the formula (see Ref. 25, Eq. (14.2_2))

$$D_I = \frac{3}{8\left(\frac{\rho}{M}\right)(0.0422)\Gamma\left(3 - \frac{1}{2}\right)}\left[\frac{kT\left(M_I + M\right)}{2\pi M_I M}\right]^{1/2}\left(\frac{2kT}{K_{12}}\right)^{1/2} \quad (3.47)$$

where $K_{12} = 2\delta(e/\epsilon)^2$, Γ is the usual gamma function, δ is the average polarizability of the neutral molecules and ϵ is the dielectric constant.

3.2.4 The ionization oscillation correction of Gould and Roberts

In Reference 3 high-frequency breakdown condition computations were made with the use of d-c cold-air data. The relationship between the a-c and d-c parameters used was a generalization of the use of Equation (3.19).

In Appendix A, it is noted that a second harmonic heating contribution to the equation governing the RVDF is assumed negligible at very high frequencies. In Reference 3 an attempt was made to re-introduce this correction in a somewhat phenomenological way. Gould and Roberts noted that if the electron energy actually oscillated (i.e., was modulated) with time, then some correction for this oscillation should be necessary in computing $\langle\overline{\nu_I}\rangle$, since $\overline{\nu_I}$ depends strongly on the number of electrons with energy above the ionization potential. They computed the energy modulation by use of the macroscopic energy equation with the instantaneous heating term as given by Equation (3.38) and with energy loss per unit time determined from experiment. With this modulated energy, the new average $\langle\overline{\nu_I} - \overline{\nu_A} - \overline{\nu_R}\rangle$ is determined from

$$\langle\nu\rangle \equiv \langle\overline{\nu_I} - \overline{\nu_A} - \overline{\nu_R}\rangle = \langle\left[\alpha_T(\bar{u}) - \eta_a(\bar{u})\right] V_d(\bar{u})\rangle \quad (3.48)$$

where $\bar{u}$ is the function of time computed from the energy equation, $\alpha_T(\bar{u})$ is the d-c experimentally determined ionizations per unit drift length (Townsend coefficient), $\eta_a(\bar{u})$ is the d-c experimentally determined attachments per unit drift length, and $V_d(\bar{u})$ is the d-c experimentally determined drift velocity, $V_d \equiv \langle\vec{\bar{c}}\rangle$, determined from $V_d(E/p)$ and $\bar{u}(E/p)$.

The $\langle\nu\rangle$ determined in this way is plotted in Figure 3.2 as a function of E_e/p for various values of $p\lambda$. The energy modulation correction goes to zero for very high frequencies ($p\lambda = 0$) and then the relationship between a-c and d-c may be expressed by Equation (3.19) alone. It should be noted that p used for Figure 3.2 is not the actual pressure but instead

$$p^* = 760 \frac{\rho}{\rho_o} Z \quad \text{mm Hg}$$

where Z is the particle multiplicity factor usually used in the equation of state in the form $p = \rho ZRT$, and ρ_o is the sea level density. In our computations (see Sections 4 and 7) ρ/ρ_o is about 10^{-3} to 10^{-4}, $Z \simeq 2$, and $\lambda \simeq 100$ cm. Then the value of $p\lambda$ to be used is about 7.2 to 72. It is seen in Figure 3.2 that the modulation correction here will be considerably less than 1 volt/mm Hg and, therefore, no modulation correction is needed.

3.3 Data for Cold Air

In order to check the accuracy of the model used in computation, it is desirable to compare some computed results with experimental results for the same antenna configuration. This is done in Section 6. Since these experiments were conducted in cold air under zero velocity conditions, only the high-frequency ionization coefficient ζ for cold air is needed.

3.3.1 The high-frequency ionization coefficient

In Reference 5, Figure 2, data for ν and D have been reduced and plotted in the convenient form of $\zeta = \nu/DE_e^2$ as a function of E_e/p. The E/p axis of this figure must be shifted 6 volts, so that the abscissa reads about 6 volts higher, because a full energy modulation correction has been made which, as previously discussed, does not apply here (see Section 3.2.4). This figure (see Fig. 3.3) is matched to within 4-percent accuracy by the equation

$$\zeta_{cold} = (0.243)\left(\frac{E_e}{p} - 30\right) \times 10^{-4}\left(\frac{cm}{volt}\right)^2 \qquad (3.49)$$

with

$$\frac{E_e}{p} \leq 110 \quad \text{volts/cm-mm Hg}$$

This curve was derived by expressing ζ in terms of ionization and attachment coefficients as

$$\zeta = \frac{3}{2}\,\frac{(\alpha_T/p) - (\eta_a/p)}{u_{av}(E_e/p)} \qquad (3.50)$$

The data of $(\alpha_T/p) - (\eta_a/p)$ were derived from Reference 29a and values of u_{av} as a function of E/p were taken from References 29b and 29c. Although some extrapolation of this data is possible we believe that our results should not be applied to situations for which E_e/p is appreciably above 110 volts/cm-mm Hg.

3.3.2 The free diffusion coefficient

For computing breakdown in gaseous flows of cold air one would need D_e in addition to ζ. These cold air values will also be useful in estimating the diffusion for hot air. From theory, D_e is given by Equation (3.40b). By using drift velocity measurements in an applied field from Reference 28, page 542, one can obtain μ_e. The average electron energy may be taken from Reference 2a, page 83. The D_e obtained from these data are plotted in Figure 3.4.

3.4 Data for Hot Air

Because of the extreme paucity of data in hot air, the estimates here will have to be guided almost entirely from theory. For this purpose, the formulation for the RVDF and $\bar{u} = (1/2)\overline{mc^2}$ given by Allis (Ref. 13) will be used.

3.4.1 Average energy and diffusion coefficients

If in Equation (3.23a) and (3.23b) the diffusion term Φ is neglected or assumed to be about constant in the elastic region and if the approximation (3.40a) is used ($\nu_{en} \simeq$ const), one may rewrite the distribution function (3.23) as

$$f \sim e^{-\frac{3m}{M}\frac{Mc^2}{2u_c}} \int_c^{c_o} e^{\frac{3m}{M}\frac{mc^2}{2u_c}} \frac{1}{c^2}\, dc \qquad (3.51)$$

As pointed out in the derivation of (3.23) this equation does not apply down to $c = 0$, but all the necessary integrals in which f is used converge and contribute little from the region of small c. From this Allis (Ref. 13) derives

$$\bar{u} = \frac{3}{10} u_o \left[\frac{1 + \left(4W_o/21\right) + \left(2W_o^2/63\right)\cdots}{1 + \left(W_o/5\right) + \left(4W_o^2/105\right)\cdots} \right] \qquad (3.52a)$$

where

$$W_o = \frac{3}{2}\,\frac{m}{M}\left(\frac{mc_o^2}{2}\right) \Bigg/ \left(\frac{e^2E_e^2}{2m\nu_{en}^2} + \frac{3mkT}{2M}\right) \qquad (3.52b)$$

where

$$u_o = \frac{mc_o^2}{2} \quad \text{and} \quad u_x = \frac{mc_x^2}{2}$$

Here, as mentioned in Section 3.1.4, u_o is usually slightly larger than u_x (the difference $u_o - u_x$ is larger for larger field strengths), and then c_o is slightly larger than c_x. The term in brackets in (3.52a) is slightly less than unity and varies very slowly. Thus it is seen that $\bar{u}$ varies very slowly and will be about equal to or slightly above $3u_x/10$.

For a choice of u_x, it is noted that the lowest excitation energy that has been found to be excited by electrons in air or air constituents was reported by Schulz in Reference 30. Schulz reported a "... large inelastic process in N_2 for electrons with energies around 2.3 ev and that vibrational levels of the nitrogen molecule, up to $v = 8$, are excited." The cross section for the process is not known.

If $u_x = 2.3$ ev is taken and if it is assumed that $W_x \leq 1$ and that $u_o \simeq u_x$ then

$$\bar{u} \simeq \left(\frac{3}{10}\right)(2.3) = 0.7 \text{ ev} \qquad (3.53)$$

Calculations of the electron energy distribution based upon the 2.3 ev level reported by Schulz were made by Carleton and McGill (Ref. 24). These quite involved calculations led to mean energies of 0.6 to 1.0 ev for fairly large values of E/p. This agrees quite well with Equation (3.53).

Crompton and Sutton (Ref. 31) obtained average electron energies in cold air by measuring $e\mu_e E/D$ under conditions such that mobility was balanced against diffusion. Then from Equations (3.28a) and (3.40b) one obtains

$$\bar{u} = \frac{3}{2} e\mu(D/e\mu_e E) = \frac{3}{2}(D/\mu_e)$$

Their results are given in Figure 3.5. It is seen that the data match a u_x of somewhere between 6 and 8 volts much better than 0.7 ev given by Equation (3.53). It should also be noted that the lowest readily excitable (by electron impact) stable states of the main constituents were previously reported to be 6.1 ev for N_2 and 7.9 ev for O_2 (Ref. 2a). These results imply that the earlier mentioned 2.3 ev is either relatively difficult to excite or readily gives up its energy in a future impact or that the value of $\bar{u} = (3/10)u_x$ cited by Allis is too low for strong fields.

In hot air still other phenomena may occur. Since the boundary layer may contain highly dissociated O_2, the metastable level of atomic oxygen at 1.97 ev (Ref. 2a) may play an important role. However, since this possibility is uncertain, we have adopted $u_x = 6.1$ ev and used Equation (3.52) to obtain Figure 3.6. Then using Equations (3.40b) and (3.45a), the results shown in Figures 3.7 and 3.8 were computed for the free and ambipolar diffusion coefficients. The free-electron mobilities for Equation (3.40b) and Figure 3.7 were taken from the collision frequency curves for high-temperature air in Reference 15. The ion mobilities for Equation (3.45a) and Figure 3.8 were computed from Equation (3.47) wherein the average molecular weight of the ions and of the neutrals were taken from Reference 33 and the average polarizabilities for hot air were taken from Reference 34.

3.4.2 The effective ionization rate

During preparation of this report we have found virtually no data for ν_I or ν_A in hot air. Presumably the number of particles making their way to energies that are sufficiently high to cause ionization would be increased by the higher temperatures because of the decreased ability to transfer this energy to the heavy particles. However, this effect should be slight because the largest part of the energy is lost in inelastic collisions and almost all particles will be in their ground states.

Another possibility at temperatures of 2000° to 4000° K and pressures of around 1 mm Hg is that the presence of NO in significant amounts may decrease the effective energy necessary to cause ionization because of its lower ionization potential. However, breakdown measurements in relatively pure NO (Ref. 2b) indicate, surprisingly, that it is actually slightly more difficult to break down NO than pure N_2 or pure O_2. Therefore we have assumed $\bar{\nu}_I - \bar{\nu}_R - \bar{\nu}_A$ to be unchanged in hot air relative to its cold air value. This involves using the cold air result of Equation (3.49) to obtain

$$\zeta_{hot} = \frac{\nu}{D_{hot}E^2} = \frac{D_{cold}}{D_{hot}}\zeta_{cold} = \left(\frac{D_{cold}}{D_{hot}}\right)(0.243)\left(\frac{E_e}{p^*} - 30\right)\times 10^{-4}\left(\frac{cm}{volt}\right)^2$$

$$= \left(\frac{D_{cold}}{D_{hot}}\right)(0.243)\left[\frac{E_e}{760z(\rho/\rho_o)} - 30\right]\times 10^{-4}\left(\frac{cm}{volt}\right)^2 \qquad (3.54)$$

3.5 Mixtures, Impurities, and Use of Experimental Data

The effects of small amounts of impurities or admixtures in certain gases have been discussed by Brown (Ref. 1) and he shows that, for selected gases, small concentrations of gases added to the main gas can cause large changes in breakdown conditions. The effect of the impurity gas has not always been well understood but the following phenomena are known to occur:

(a) The impurity may have a low, easily excited excitation energy and will thus strongly influence the electron RVDF. The relationship of the RVDF to pertinent macroscopic properties was discussed in Sections 3.1.4, 3.2.2, and 3.4.

(b) The presence of a low ionization potential species in the mixture may greatly increase the ionization coefficient. This was why, in Section 3.4.2, the presence of NO in air was expected to increase the ionization rate. The fact that pure NO was more difficult to break down than O_2 and N_2 is probably due to the phenomenon (a) above. Since NO has a strong permanent dipole moment, it is probably much easier to excite its low states by electron impact than it would be to excite O_2 or N_2.

(c) High-energy metastable states are more difficult to excite in the presence of small quantities of low-ionization energy impurities such as Hg.

(d) Ramsauer effects in the impurity gas or changes in the velocity distribution (as in (a) above) induced by the impurity gas may have large influence upon the electron mobility and diffusion coefficient. As a possible example of this phenomenon, consider the effect upon mobility of adding small amounts of

nitrogen to argon compared to the pure electron mobilities as depicted in Reference 2a, Figures 3.8, 3.9, and 3.12, when addition of 1 percent of N_2 to A results in a sixfold increase in mobility over pure argon at $E/p = 1$ volt/cm-mm Hg. The mobility is also more than twice that of pure nitrogen.

(e) Attachments and recombinations may be strongly affected by the presence of certain species.

Thus, it is seen that macroscopic properties pertinent in breakdown may be strongly altered by the presence of a small amount of impurity or by the presence, in sufficient amounts, of a specie formed only at high temperatures. Because of these effects, measurements of breakdown in impure hot gases produced in devices such as arc jets may have little meaning.

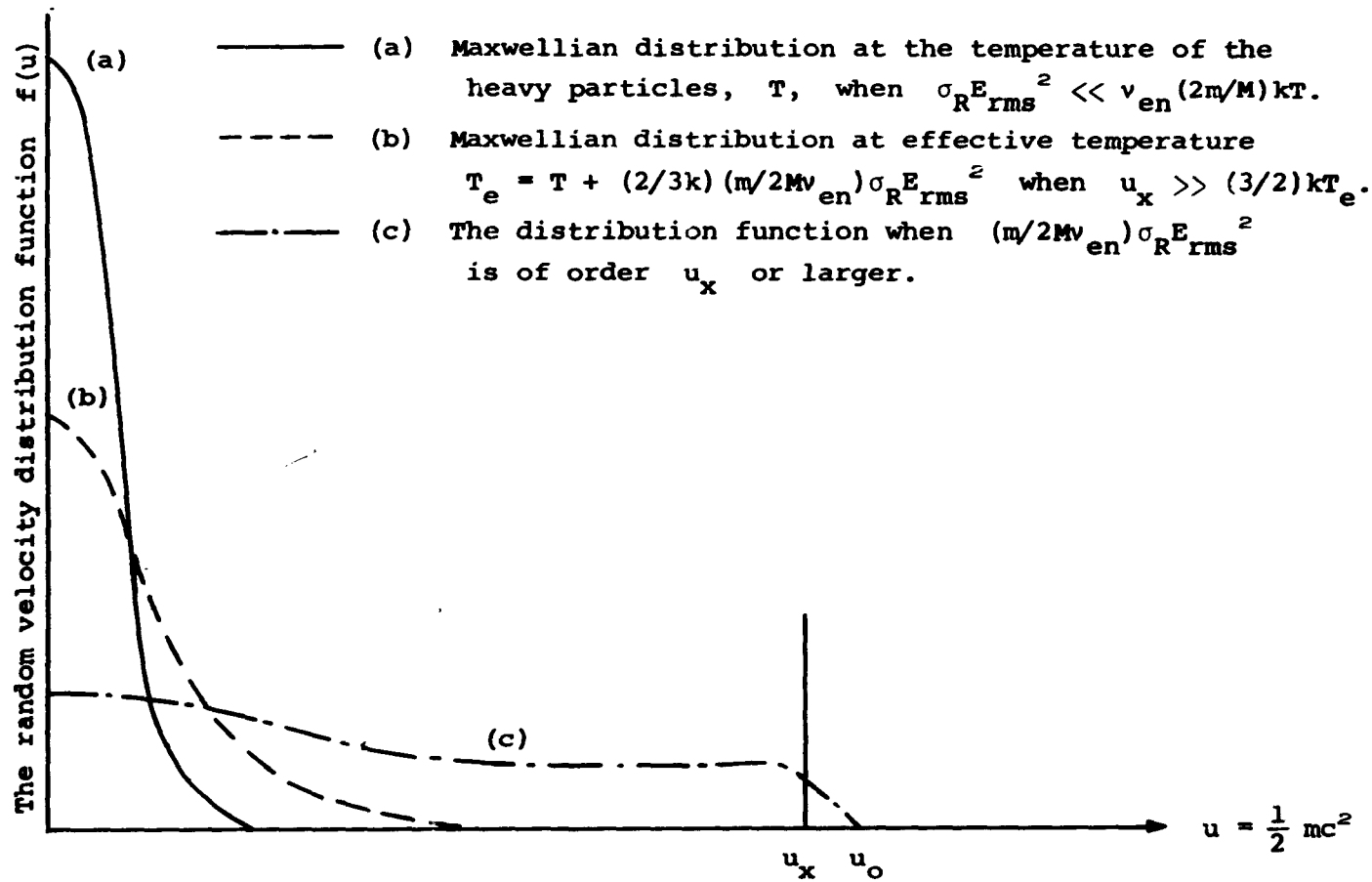

Figure 3.1.- Schematic of the shape of the random velocity distribution function for three different field strengths. This distribution function is normalized to one when multiplied by $4\pi c^2 dc$ and integrated.

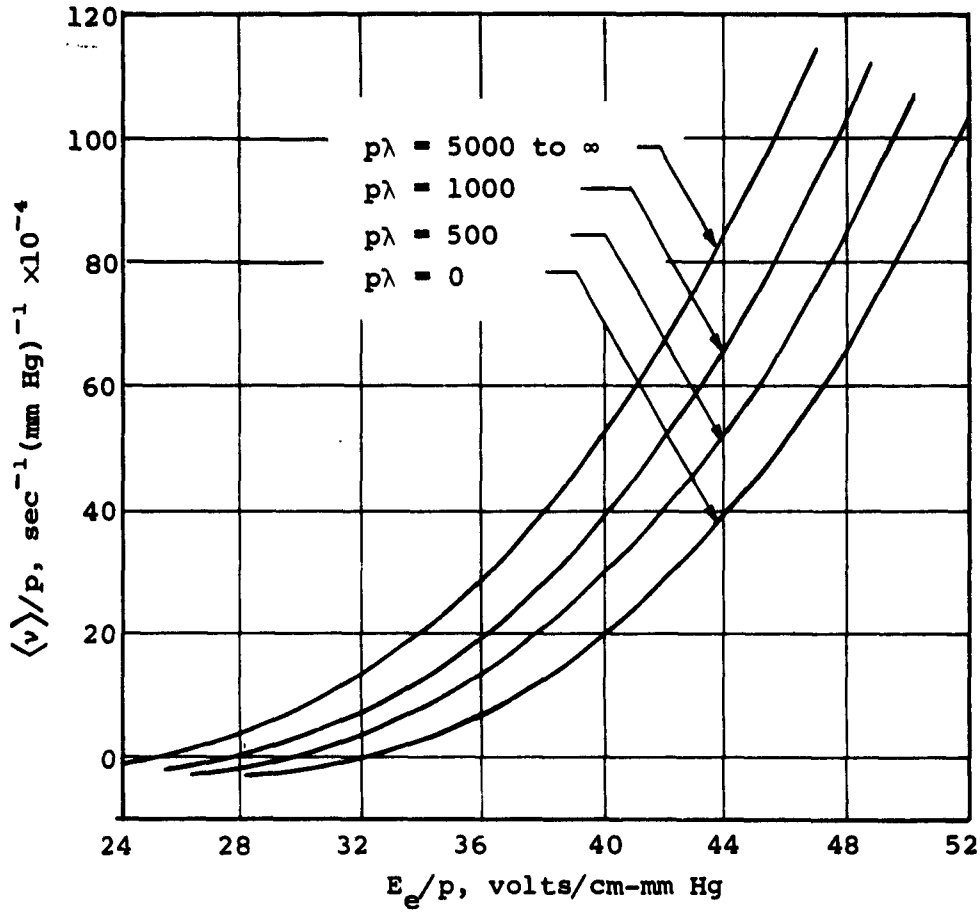

Figure 3.2.- The net ionization frequency $\langle \nu(E_e/p) \rangle$ for various wavelengths λ. Taken from Reference 3.

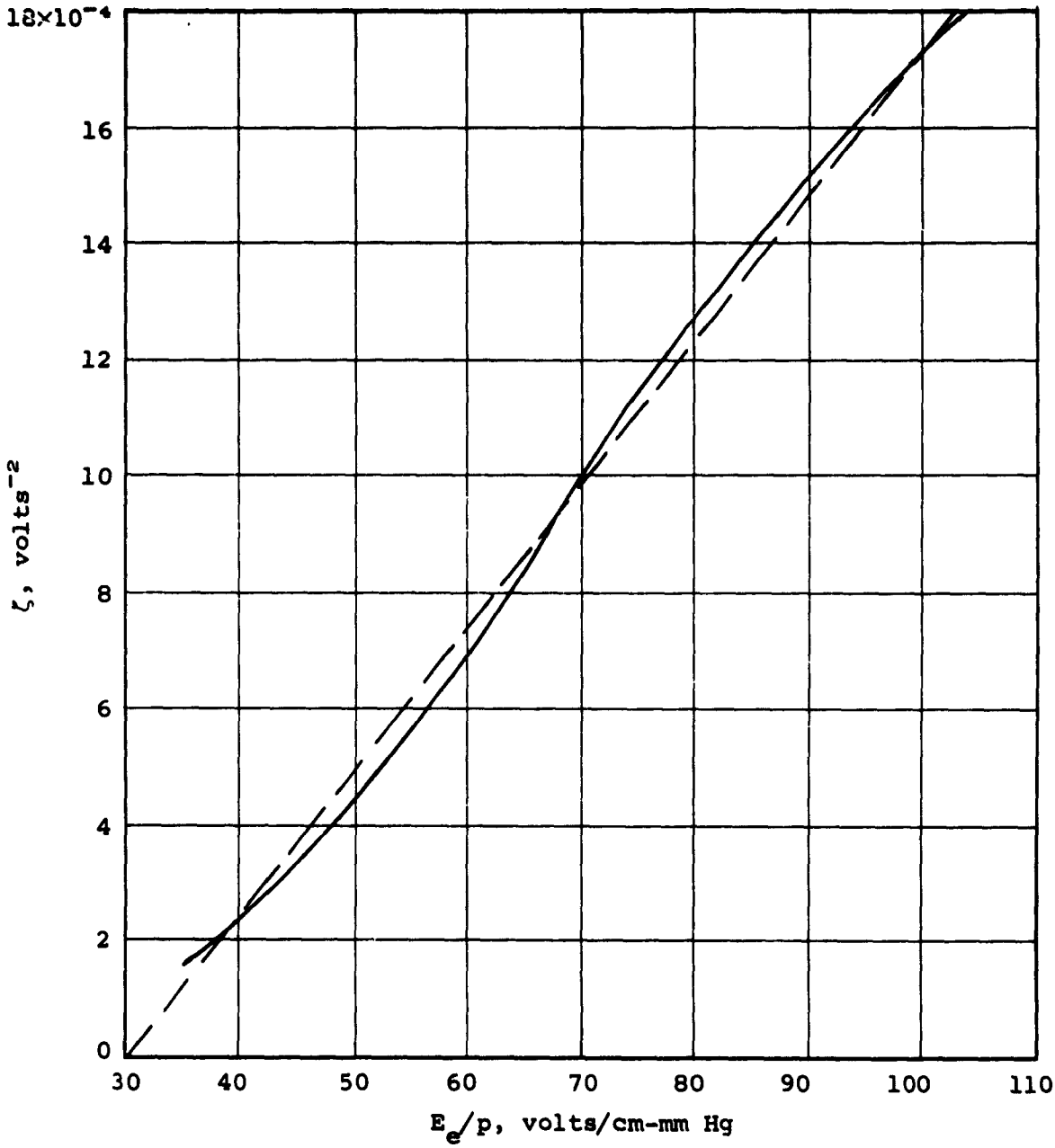

Figure 3.3.- The cold air high frequency ionization coefficient from Reference 5 (with abscissa shifted 6 volts to compensate for the full oscillation correction which was used in Ref. 6 but which is not applicable here). The dashed line is the function used in this report.

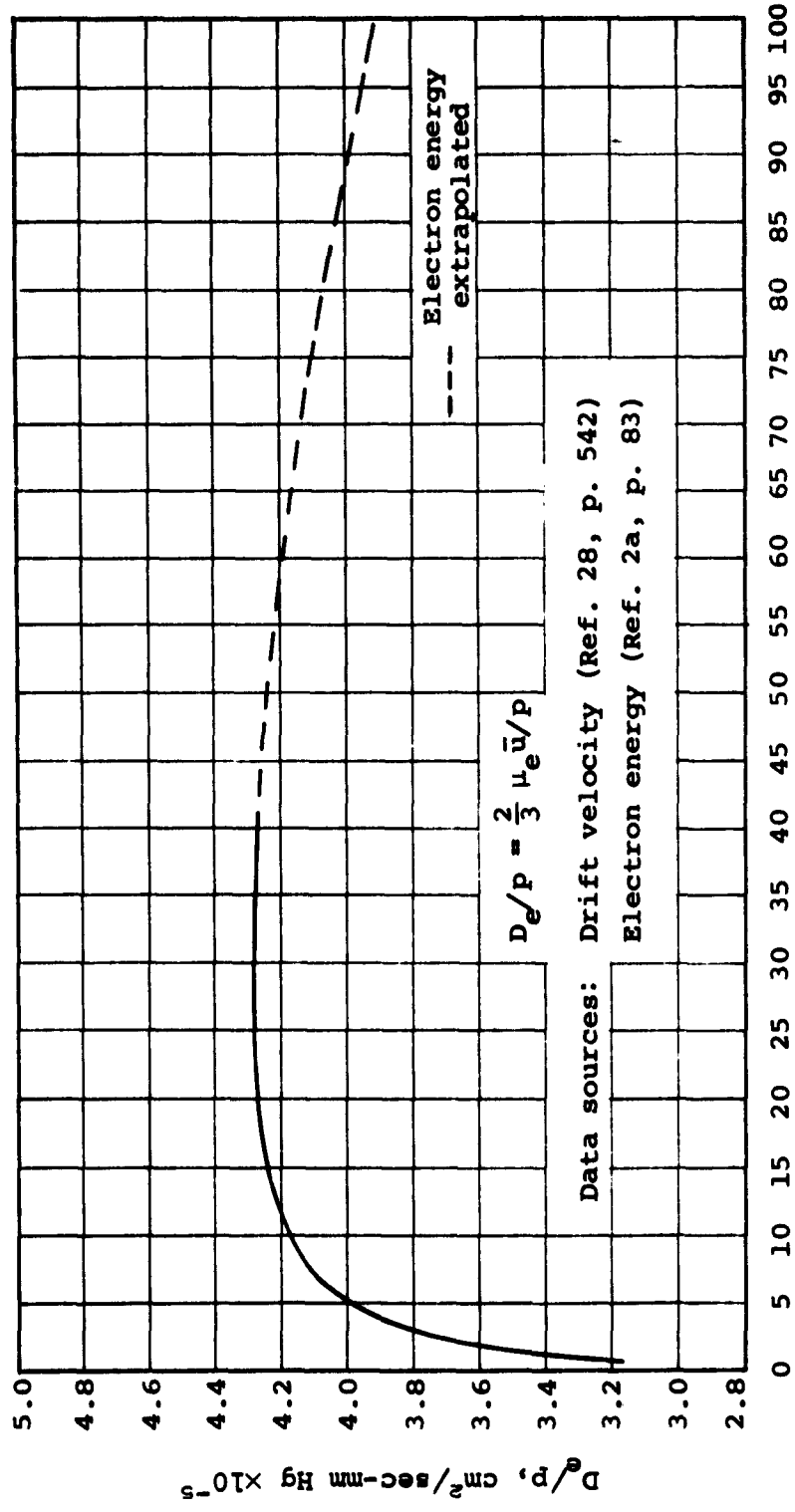

Figure 3.4.- Free electron diffusion coefficient for cold air.

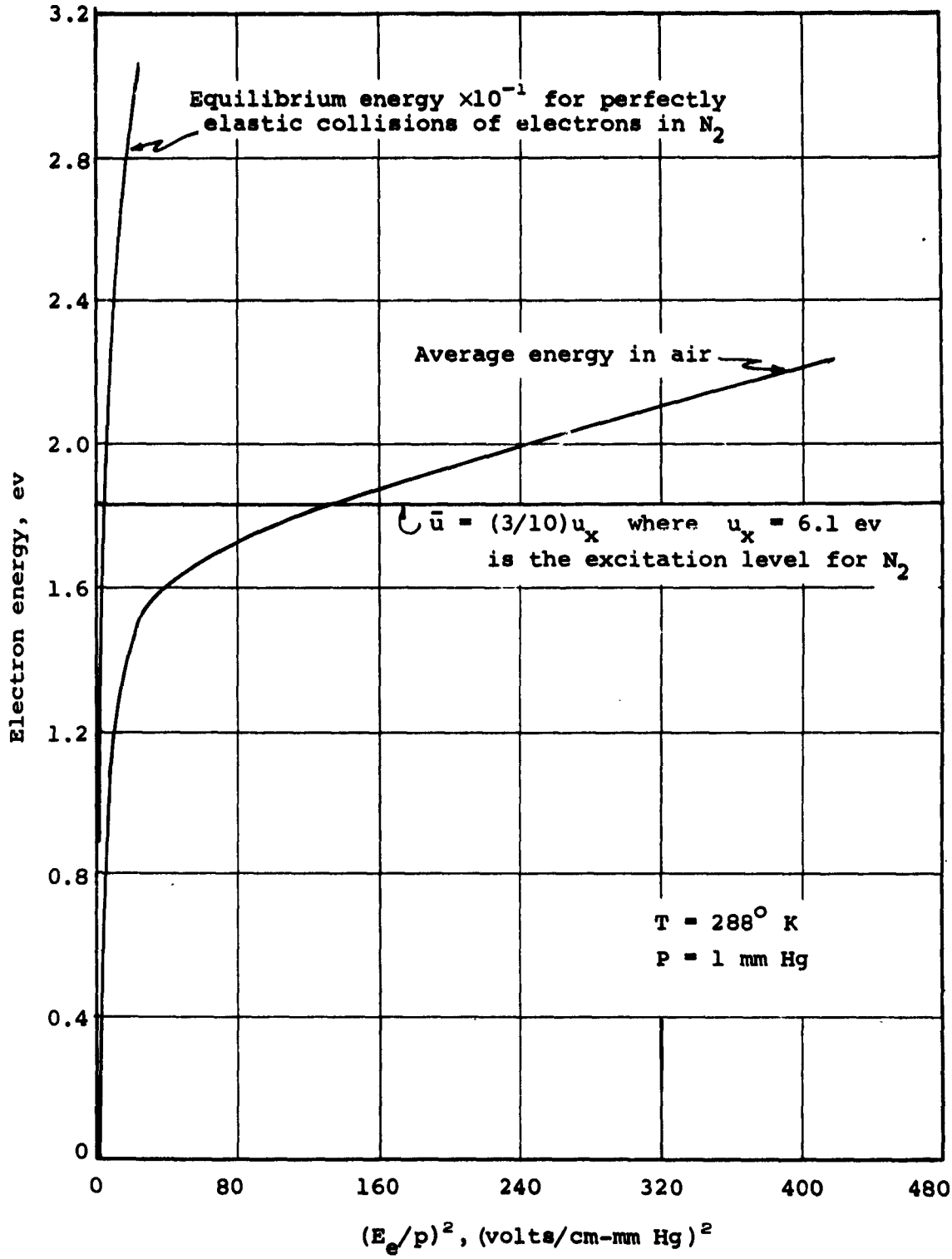

Figure 3.5.- Average energy for electrons in cold air versus $(E_e/p)^2$, data from Crompton and Sutton (Ref. 31).

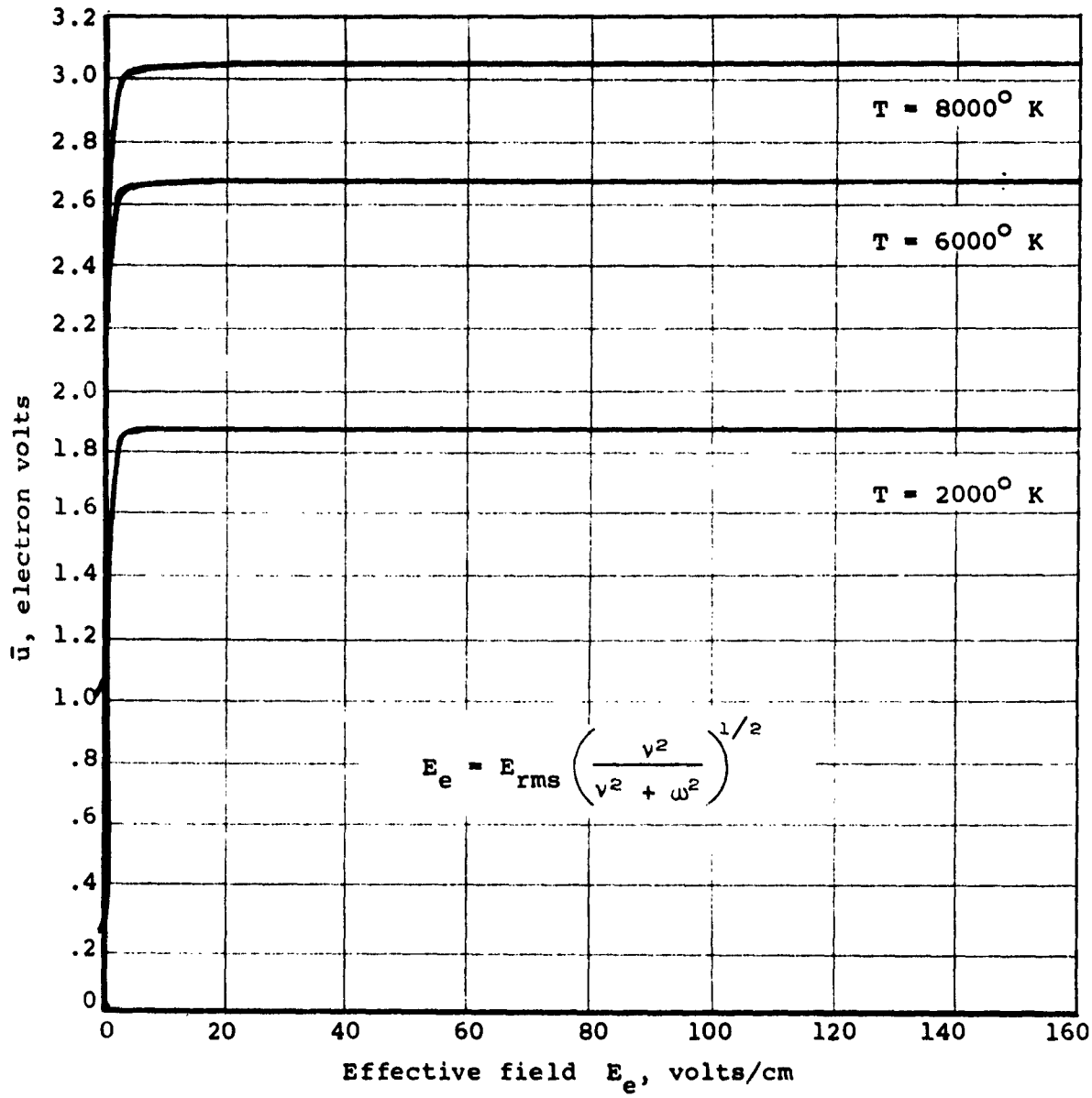

(a) $\rho/\rho_o = 10^{-3}$

Figure 3.6.- Average energy of electrons as a function of E_e for various gas temperatures.

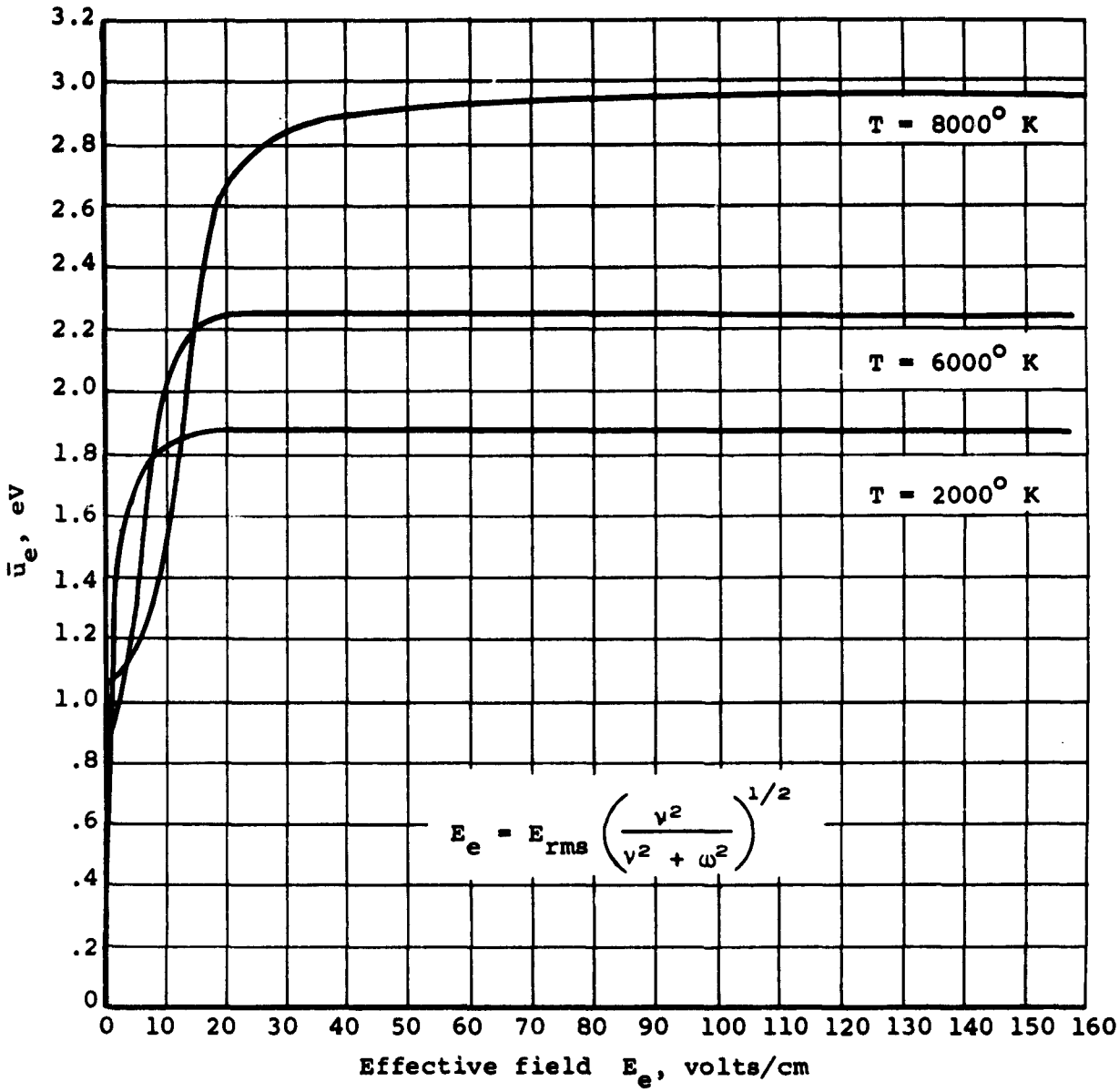

(b) $\rho/\rho_o = 10^{-2}$.

Figure 3.6.- Concluded.

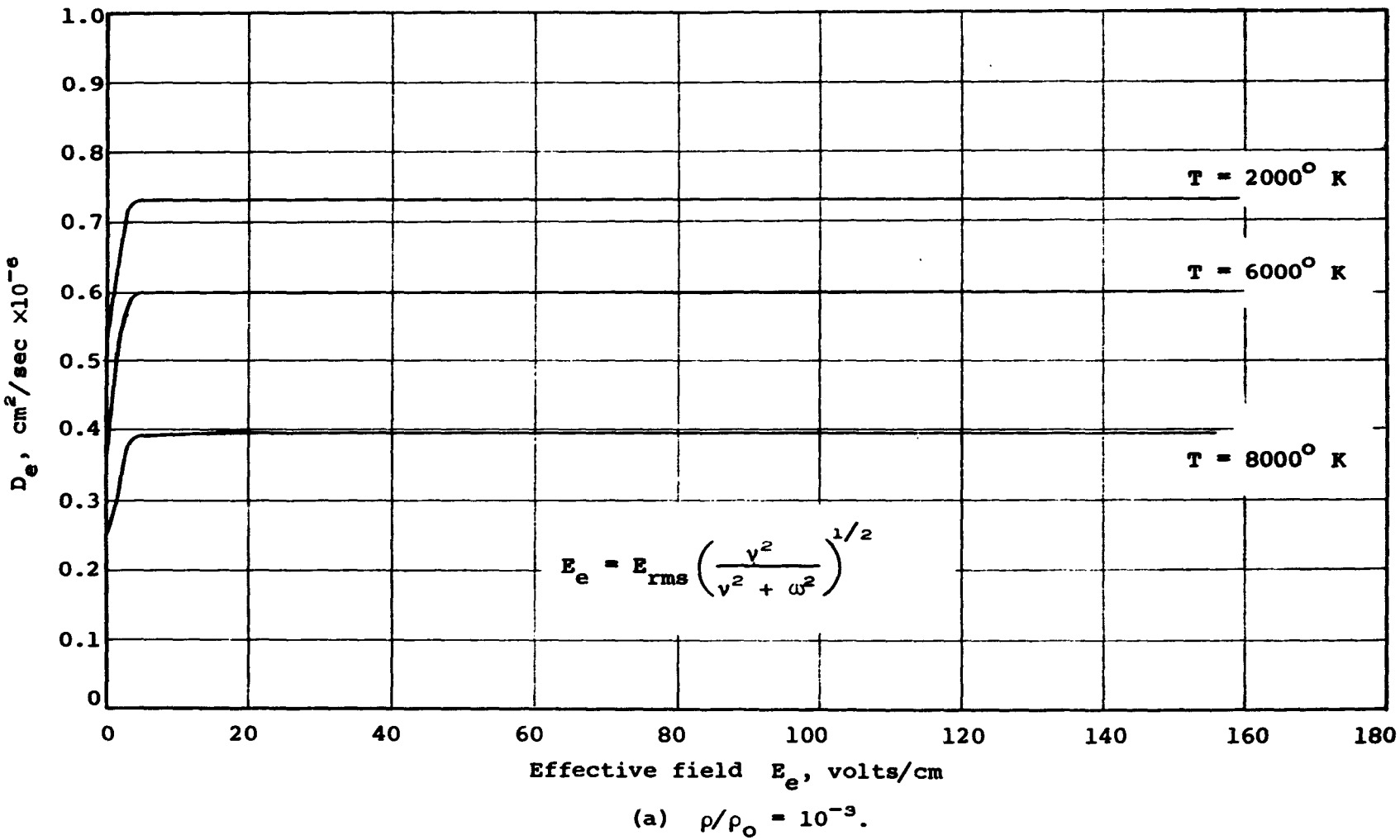

(a) $\rho/\rho_o = 10^{-3}$.

Figure 3.7.- Free electron diffusion coefficient in air as a function of E_e for various gas temperatures.

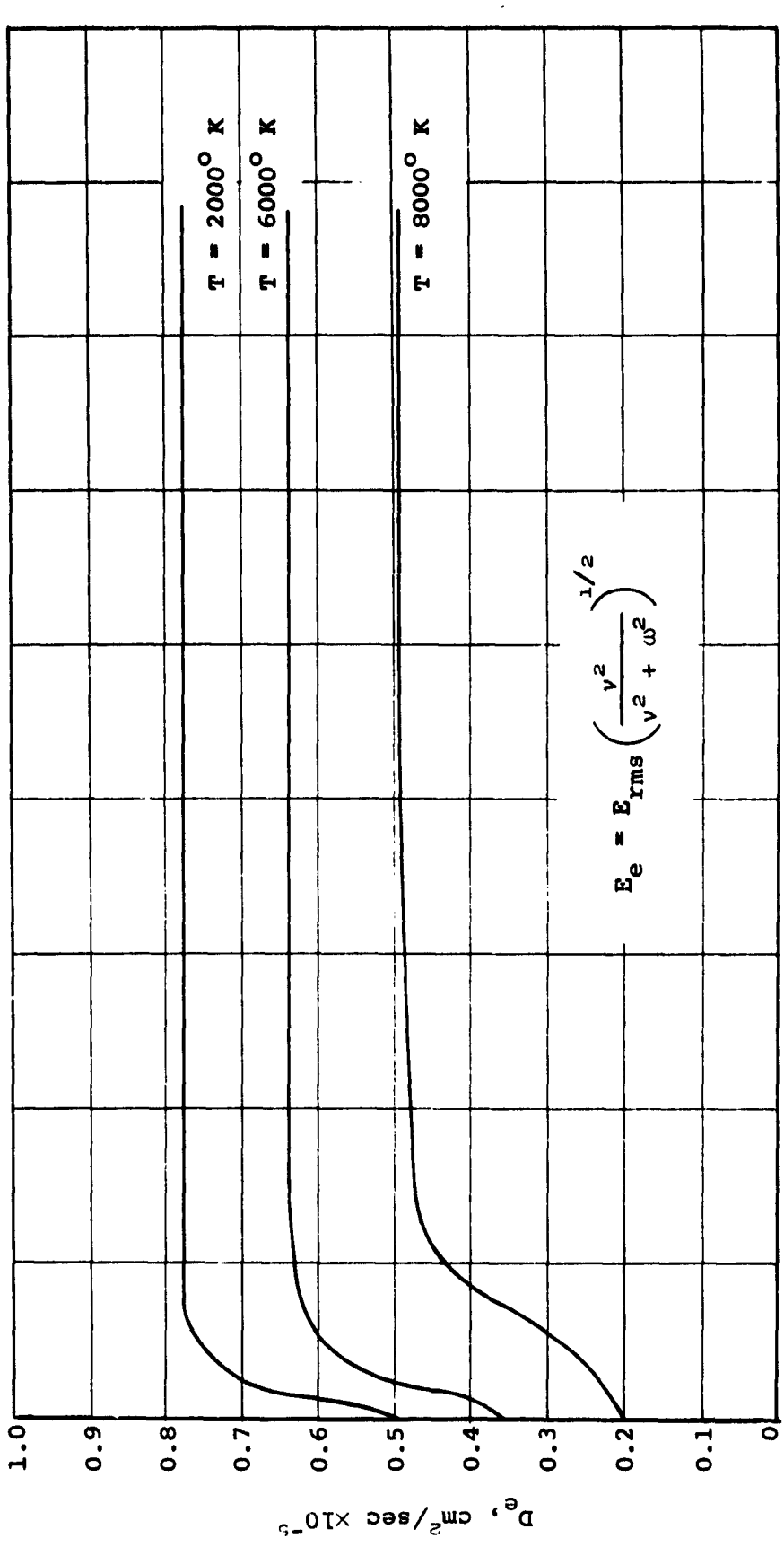

(b) $\rho/\rho_o = 10^{-2}$.

Figure 3.7.- Concluded.

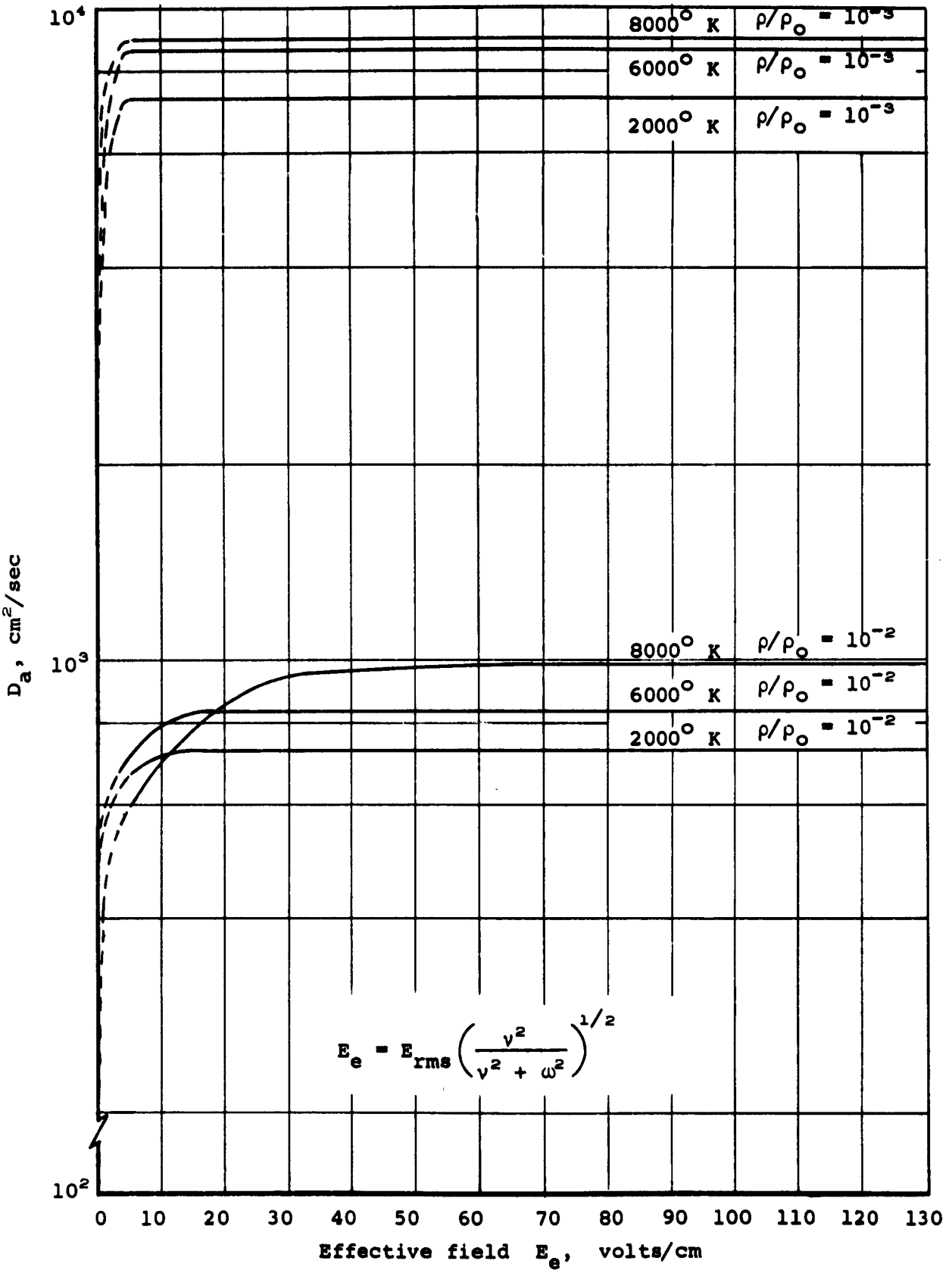

Figure 3.8.- Ambipolar diffusion coefficient in air as a function of E_e.

4. PROPERTIES OF TYPICAL AERODYNAMIC FLOW FIELDS

The local dynamical and thermodynamical properties of typical aerodynamic flow fields surrounding reentry bodies are required as inputs for the breakdown computations. In this section, we present the results of computations for two simplified geometrical shapes involving a wedge and a sharp-nosed cone. Both the inviscid and viscous regions of the flow field have been treated including both laminar and turbulent regions. Assumptions made involve: (1) The use of equilibrium, thermodynamic properties for the air in the flow, (2) neglect of foreign species induced by ablation or transpiration into the flow, (3) neglect of displacement of effective body surface location by the boundary layer in the inviscid region, and (4) negligible shock front thickness.

Quantities calculated for these regions include local velocity, temperature, density, enthalpy for both the inviscid and viscous regions as well as electron concentration, weak field electron collision frequency and strong field electron collision frequency for the viscous boundary layer. Electron concentrations and collision frequencies are computed from the thermodynamic state of the gas. These calculations have been incorporated into the computer program for the viscous flow field, as described in Reference 36.

4.1 Inviscid Flow-Field Calculations

4.1.1 Inviscid flow field - wedges

The inviscid flow fields surrounding a two-dimensional wedge have been calculated using the method of W. E. Moeckel (Ref. 37). The equations used in these calculations are:

$$\frac{p_2}{p_1} = (1 - u_r)\,\frac{\rho_1 V_1^2}{p_1}\sin^2\theta + 1 \qquad (4.1)$$

$$\frac{h_2}{h_1} = \left(1 - u_r^2\right)\left(\frac{\rho_1 V_1^2}{p_1} - M_1^2\right)\frac{\sin^2\theta}{2} + 1 \qquad (4.2)$$

$$\tan (\theta - \Lambda) = u_r \tan \theta \qquad (4.3)$$

where subscript 1's refer to free-stream quantities and subscript 2's, to quantities in the flow field and

$$u_r = \frac{u_1}{u_2} \qquad (4.4)$$

is the ratio of the components of velocities V_1 and V_2, normal to the oblique shock wave. The quantity, Λ refers to the angle between the surface of the wedge and the direction of the free-stream velocity vector, and θ is the oblique shock angle with respect to the direction of the same vector.

The equations above are solved by iteration, using various input conditions. The ARDC 1959 Atmosphere (Ref. 38) has been used throughout this work, as well as for the conical cases.

The results of the calculations for the inviscid flow fields are presented in Tables 4.1(a) through (d). Because stream lines in the flow field are parallel to the body surface, the quantities plotted are constant throughout the flow field and so represent the values next to the body surface.

4.1.2 Inviscid flow field - sharp-nosed cones

The inviscid flow-field parameters associated with the hypersonic flight of a sharp-nosed cone at zero angle of attack have been derived from the work of Romig (Ref. 39) using the ARDC 1959 atmospheric data (Ref. 38). Her work assumes continuum flow, negligible boundary-layer thickness, negligible shock-front thickness, and steady-state flow. The results of these calculations for a number of typical cases are given in Tables 4.2(a) through (d). The quantities plotted are those calculated for the region adjacent to the body surface.

4.2 Boundary-Layer Flow-Field Calculations

The viscous flows associated with each of the geometric shapes described in the previous sections have been calculated using the method of Reference 36. This reference describes a computational procedure and computer program based upon a method proposed by Rubesin (Ref. 34). A detailed discussion of the procedure is given in Reference 36. The inviscid flow fields discussed in the previous sections furnish the inputs to this program.

In the case of cones, the boundary-layer properties were calculated at distances back from the apex along the surface such that the antennas used would fit into the space available. These distances along the surface occurred at distances of 5.73, 3.82, and 2.86 feet for the 10^{o}, 15^{o}, and 20^{o} cones, respectively.

Sample results of the application of this program to the flow-field calculation are given in Figures 4.1 through 4.7. Complete results of these calculations are available from Vidya, Inc. However, since the results of these calculations are quite lengthy for the number of cases and the number of variables considered, only sample results are presented. Furthermore, in applying the results of these calculations to the breakdown calculation, certain approximations have been used, as are discussed in the next section.

4.3 Representation of the Boundary-Layer Profile with the Function B

The calculations of the previous section are now used to obtain values for the quantity $\vec{B} = \vec{V}/D$, defined in Section 2.1.2. Two formulations for breakdown computations discussed in the next section involve the use of (a) a mean constant value for the diffusion coefficient D, and (b) a variable diffusion coefficient which is a function of the local conditions at each point throughout the flow field. As described in Section 7, the computations of breakdown have been done initially for the constant D case.

The velocity profile $\vec{V}(y)$ was approximated by the function

$$\vec{V} = \vec{V}_o \ (1 - e^{-by}) \qquad (4.5)$$

where the parameter b was adjusted to give the best fit to the velocity profile in the boundary layer, and $\vec{V}_o$ is given by the velocity at the edge of the boundary layer. These data are tabulated in Table 4.3.

The values for D were taken at a point in the boundary layer corresponding to the position at which the electric field had fallen to one-half its value at $z = 0$ on the surface (see also Section 7). The antenna for which the calculations have been performed is a slot 1/2 inch wide by 17 inches long, oriented on the surface with its width normal to the gaseous flow direction. The near field of this antenna has been examined by Scharfman and Morita (Ref. 4). As discussed in Section 6.1, their results show that the field at $z = 0$ may be approximated by $E = E_o \ e^{-\epsilon_1 y}$ where $\epsilon_1 = 0.540 \ cm^{-1}$, so that at $E/E_o = 1/2$, $y = 1.293$ cm $= 0.0425$ feet.

The values for the temperature, density, and electron density on the boundary layer were obtained at $y = 0.0425$ feet, and values of D were obtained from Figures 3.7 and 3.8. These values are listed in Table 4.3 for each of the flow situations considered. Finally, values of $B_o = V_o/D$ are also given in Table 4.3.

TABLE 4.1.- INVISCID FLOW-FIELD CALCULATIONS FOR CONES.

(a) h = 80,000 ft.

$T_1 = 390^\circ$ R, $\rho_1 = 2.79 \times 10^{-3}$ lb/ft^3, $p_1 = 58.1$ lb/ft^2, $h_1 = 93.9$ Btu/lb

$h_{wall} = 646$ Btu/lb, $T_{wall} = 2500^\circ$ K, Prandtl No. = 0.75

Λ (deg)	V_1 (ft/sec $\times 10^{-3}$)	v_2 (ft/sec $\times 10^{-3}$)	ρ_2 (lb/ft^3 $\times 10^2$)	p_2 (lb/ft^2)	h_2 (Btu/lb)	T_2 ($^\circ$R)
10	25	24.393	1.537	1820	530	2028
15	25	23.77	1.942	4011	1020	3685
20	25	22.804	2.417	6684	1440	4875
10	15	-	1.145	726.6	235	1014
15	15	14.142	1.425	1511	415	1677
20	15	13.675	1.676	2616	678	2613
10	10	-	.950	372	150	663
15	10	-	1.145	726.6	320	975
20	10	8.832	1.327	1162	345	1404

TABLE 4.1.- CONTINUED.

(b) h = 120,000 ft.

$T_1 = 451.37^{\circ}$ R, $\rho_1 = 4.0851 \times 10^{-4}$ lb/ft^3, $p_1 = 9.8372$ lb/ft^2

$h_1 = 1.085 \times 10^2$ Btu/lb, $h_{wall} = 646$ Btu/lb, $T_{wall} = 2500^{\circ}$ K

Prandtl No. = 0.75

Λ (deg)	V_1 (ft/sec $\times 10^{-3}$)	V_2 (ft/sec $\times 10^{-3}$)	ρ_2 (lb/ft^3 $\times 10^3$)	p_2 (lb/ft^2)	h_2 (Btu/lb)	T_2 ($^{\circ}$R)
10	35	34.321	2.63	501.7	930	3430
15	35	33.541	3.74	1151	1710	5281
20	35	32.434	4.40	1869	3165	6996
10	25	24.454	2.14	275.4	625	2076
15	25	23.979	2.74	570.6	1055	3792
20	25	23.238	3.53	1003	1600	5055
10	15	-	1.70	102.3	240	1038
15	15	14.177	2.02	216.4	430	1738
20	15	13.820	2.41	373.8	690	2686

TABLE 4.1.- CONTINUED.

(c) h = 200,000 ft.

$T_1 = 449^{\circ}$ R, $\rho_1 = 1.97 \times 10^{-5}$ lb/ft^3, $p_1 = 0.472$ lb/ft^2, $h_1 = 108$ Btu/lb

$h_{wall} = 646$ Btu/lb, $T_{wall} = 2500^{\circ}$ K, Prandtl No. = 0.75

Λ (deg)	V_1 (ft/sec $\times 10^{-3}$)	v_2 (ft/sec $\times 10^{-3}$)	ρ_2 (lb/ft^3 $\times 10^4$)	p_2 (lb/ft^2)	h_2 (Btu/lb)	T_2 ($^{\circ}$R)
10	45	44.16	1.6	40.08	1210	4131
15	45	43.19	2.2	84.87	2925	5927
20	45	41.71	2.4	150.9	4590	8531
10	35	34.35	1.3	24.05	1080	3772
15	35	33.54	1.9	55.17	1590	4714
20	35	32.43	2.2	91.94	3130	6151
10	25	24.45	1.1	13.20	525	2065
15	25	23.94	1.4	27.35	1080	3772
20	25	23.13	1.8	48.57	1500	4580
10	10	-	.7	2.829	190	727.4
15	10	-	.8	5.187	230	1033
20	10	-	1.0	8.393	360	1459

TABLE 4.1.- CONCLUDED.

(d) h = 250,000 ft.

$T_1 = 328.2^{\circ}$ R, $\rho_1 = 2.493 \times 10^{-6}$ lb/ft^3, $p_1 = 0.0436$ lb/ft^2

$h_1 = 78.9$ Btu/lb, $h_{wall} = 646$ Btu/lb, $T_{wall} = 2500^{\circ}$ K

Prandtl No. = 0.75

Λ (deg)	V_1 (ft/sec $\times 10^{-3}$)	v_2 (ft/sec $\times 10^{-3}$)	ρ_2 (lb/ft^3 $\times 10^5$)	p_2 (lb/ft^2)	h_2 (Btu/lb)	T_2 ($^{\circ}$R)
10	15	-	1.1	0.6110	230	919
15	15	14.07	1.4	1.309	387	1575
20	15	13.42	1.6	2.182	685	2461
10	25	24.31	1.5	1.658	490	1969
15	25	23.56	2.2	3.404	750	2855
20	25	22.87	2.9	6.022	950	3446
10	35	34.10	2.0	3.011	720	2757
15	35	33.02	3.0	6.546	1160	3545
20	35	31.46	3.1	11.35	2760	5382

TABLE 4.2.- INVISCID FLOW-FIELD CALCULATIONS FOR WEDGES.

(a) h = 80,000 ft.

$T_1 = 390^{\circ}$ R, $\rho_1 = 2.79 \times 10^{-3}$ lb/ft^3, $p_1 = 58.1$ lb/ft^2, $h_1 = 93.9$ Btu/lb

$h_{wall} = 646$ Btu/lb, $T_{wall} = 2500^{\circ}$ K, Prandtl No. = 0.75

Λ (deg)	V_1 (ft/sec $\times 10^{-3}$)	θ (deg)	v_2 (ft/sec $\times 10^{-3}$)	ρ_2 (lb/ft^3 $\times 10^2$)	p_2 (lb/ft^2)	h_2 (Btu/lb)	T_2 ($^{\circ}$R)	M_2 Mach No.
10	25	12.2	24.45	1.57	2052	635	2450	10.4
15	25	17.8	23.8	1.84	4354	1280	4420	7.7
20	25	23.1	23.0	2.22	7343	2030	5987	6.5
10	15	13.0	14.63	1.22	824	375	1266	8.5
15	15	18.6	14.24	1.50	1674	535	2102	6.52
20	15	24.3	13.71	1.68	2814	690	3136	5.18
10	10	14.3	9.72	.953	431	210	848	6.84
15	10	19.7	9.45	1.22	818	310	1260	5.50
20	10	25.4	9.08	1.41	1336	435	1778	4.49

TABLE 4.2.- CONTINUED.

(b) h = 120,000 ft.

$T_1 = 451.37^{\circ}$ R, $\rho_1 = 4.0851 \times 10^{-4}$ lb/ft^3, $p_1 = 9.8372$ lb/ft^2

$h_1 = 1.085 \times 10^2$ Btu/lb, $h_{wall} = 646$ Btu/lb, $T_{wall} = 2500^{\circ}$ K

Prandtl No. = 0.75

Λ (deg)	V_1 (ft/sec $\times 10^{-3}$)	θ (deg)	v_2 (ft/sec $\times 10^{-3}$)	ρ_2 (lb/ft^3 $\times 10^2$)	p_2 (lb/ft^2)	h_2 (Btu/lb)	T_2 ($^{\circ}$R)	M_2 Mach
10	35	11.9	34.3	2.61	566	1150	4056	11.6
15	35	17.0	33.4	3.57	1188	2200	5853	9.5
20	35	22.2	32.4	4.26	2026	3520	7544	7.49
10	25	12.3	24.4	2.26	302	645	2514	10.3
15	25	17.8	23.8	2.71	637	1360	4392	7.8
20	25	22.9	23.1	3.39	1068	2020	5620	6.72
10	15	13.2	14.6	1.73	123	372	1337	8.28
15	15	18.7	14.2	2.14	247	550	2167	6.42
20	15	24.4	13.7	2.43	414	850	3197	5.13

TABLE 4.2.- CONTINUED.

(c) h = 200,000 ft.

$T_1 = 449^{\circ}$ R, $\rho_1 = 1.97 \times 10^{-5}$ lb/ft^3, $p_1 = 0.472$ lb/ft^2, $h_1 = 108$ Btu/lb

$h_{wall} = 646$ Btu/lb, $T_{wall} = 2500^{\circ}$ K, Prandtl No. = 0.75

Λ (deg)	V_1 (ft/sec $\times 10^{-3}$)	θ (deg)	v_2 (ft/sec $\times 10^{-3}$)	ρ_2 (lb/ft^3 $\times 10^4$)	p_2 (lb/ft^2)	h_2 (Btu/lb)	T_2 ($^{\circ}$R)	M_2 Mach
10	45	11.4	44.1	1.62	43.0	-	4770	14.1
15	45	16.5	43.2	2.20	91.7	-	6568	10.6
20	45	21.8	41.8	2.45	158.0	-	9365	8.63
10	35	11.8	34.27	1.29	27.2	1130	3938	11.9
15	35	16.8	33.52	1.87	56.6	1383	5204	10.1
20	35	22.1	32.4	2.18	97.0	2870	6974	7.64
10	25	12.2	24.4	1.09	14.5	646	2510	10.3
15	25	17.6	23.9	1.35	30.5	1240	4179	8.14
20	25	22.6	23.1	1.77	50.8	1950	5032	7.13
10	10	14.5	9.71	.644	3.15	220	916	6.58
15	10	19.9	9.44	.829	5.88	320	1331	5.36
20	10	25.5	9.07	.970	9.53	452	1844	4.41

TABLE 4.2.- CONCLUDED.

(d) h = 250,000 ft.

$T_1 = 328.2^{\circ}$ R, $\rho_1 = 2.493 \times 10^{-6}$ lb/ft^3, $p_1 = 0.0436$ lb/ft^2

$h_1 = 78.9$ Btu/lb, $h_{wall} = 646$ Btu/lb, $T_{wall} = 2500^{\circ}$ K

Prandtl No. = 0.75

Λ (deg)	V_1 (ft/sec $\times 10^{-3}$)	θ (deg)	v_2 (ft/sec $\times 10^{-3}$)	ρ_2 (lb/ft^3 $\times 10^5$)	p_2 (lb/ft^2)	h_2 (Btu/lb)	T_2 ($^{\circ}$R)	M_2 Mach No.
10	15	12.9	14.640	1.130	0.7205	293	1197	8.73
15	15	18.5	14.251	1.363	1.480	515	2037	6.62
20	15	24.2	13.718	1.527	2.496	820	3066	5.26
10	25	12.2	24.456	1.427	1.817	615	2389	10.5
15	25	17.5	23.863	1.786	3.821	1203	3955	8.44
20	25	22.5	23.124	2.385	6.380	1875	4654	7.43
10	35	11.76	34.281	1.689	3.405	1095	3755	12.34
15	35	16.69	33.541	2.529	7.102	2045	4798	10.52
20	35	23.03	32.464	2.846	12.23	3580	6703	7.81

TABLE 4.3.- INPUT DATA FOR ANTENNA BREAKDOWN COMPUTATIONS.

(a) Cones.

Parameters \ Case No.	2	3	4	5	6
Altitude (ft)	250,000	250,000	250,000	250,000	250,000
Velocity (ft/sec)	15,000	15,000	25,000	25,000	25,000
Body half angle (deg)	15	20	10	15	20
V_o (cm/sec)	4.58×10^5	4.58×10^5	7.63×10^5	7.63×10^5	7.63×10^5
D (cm^2/sec)	1.1×10^5	5.8×10^4	1.5×10^5	6.5×10^4	2.4×10^4
b (cm^{-1})	0.56	0.699	0.495	0.784	1.21
B_o (cm^{-1})	4.16	7.90	5.09	11.7	31.8
Z	1.10	1.10	1.21	1.20	1.17
Temperature (^oK)	2320	2340	3550	3280	2665
Pressure (mm Hg)	0.4695	0.785	0.595	1.220	2.160
Density (ρ/ρ_o)	6.88×10^{-5}	1.17×10^{-4}	4.98×10^{-5}	1.13×10^{-4}	2.79×10^{-4}
D_e/D_a	89	90	87.5	84	90

TABLE 4.3.- CONTINUED.

(a) Continued.

Parameters \ Case No.	7	8	9	10L	10T
Altitude (ft)	250,000	250,000	250,000	200,000	200,000
Velocity (ft/sec)	35,000	35,000	35,000	45,000	45,000
Body half angle (deg)	10	15	20	10	10
V_o (cm/sec)	1.068×10^6	1.068×10^6	1.068×10^6	1.37×10^6	1.37×10^6
D (cm^2/sec)	1.3×10^5	5.5×10^4	3.0×10^4	3.7×10^3	1.0×10^4
b (cm^{-1})	0.620	1.022	1.288	2.93	3.87
B_o (cm^{-1})	8.23	19.45	35.6	371	137
Z	1.35	1.32	1.24	1.04	1.53
Temperature (^oK)	4660	4555	4135	2300	5120
Pressure (mm Hg)	1.081	2.345	4.075	14.38	14.38
Density (ρ/ρ_o)	6.12×10^{-5}	1.46×10^{-4}	2.87×10^{-4}	2.22×10^{-3}	8.29×10^{-4}
D_e/D_a	72.5	77	87	100	84.5

TABLE 4.3.- CONTINUED.

(a) Continued.

Parameters \ Case No.	11L	11T	12L	12T	13L
Altitude (ft)	200,000	200,000	200,000	200,000	200,000
Velocity (ft/sec)	45,000	45,000	45,000	45,000	35,000
Body half angle (deg)	15	15	20	20	10
V_o (cm/sec)	1.37×10^{6}	1.37×10^{6}	1.37×10^{6}	1.37×10^{6}	1.068×10^{6}
D (cm^2/sec)	3.1×10^{3}	4.6×10^{3}	2.5×10^{3}	2.5×10^{3}	5.5×10^{3}
b (cm^{-1})	4.03	4.14	4.77	4.53	1.86
B_o (cm^{-1})	442	298	548	548	194.5
Z	1.12	1.24	1.25	1.25	1.05
Temperature (^{o}K)	3290	4720	4740	4740	2090
Pressure (mm Hg)	30.4	30.4	54.1	54.1	8.65
Density (ρ/ρ_o)	2.87×10^{-3}	1.87×10^{-3}	3.03×10^{-3}	3.03×10^{-3}	1.45×10^{-3}
D_e/D_a	94	83	84	94	99.5

TABLE 4.3.- CONTINUED.

(a) Continued.

Parameters \ Case No.	13T	14L	14T	15L	15T
Altitude (ft)	200,000	200,000	200,000	200,000	200,000
Velocity (ft/sec)	35,000	35,000	35,000	35,000	35,000
Body half angle (deg)	10	15	15	20	20
V_o (cm/sec)	1.068×10^{6}	1.068×10^{6}	1.068×10^{6}	1.068×10^{6}	1.068×10^{6}
D (cm^2/sec)	1.1×10^{4}	2.2×10^{3}	3.2×10^{3}	2.7×10^{3}	2.7×10^{3}
b (cm^{-1})	3.9	3.28	6.95	3.88	7.48
B_o (cm^{-1})	97	486	334	396	396
Z	1.21	1.06	1.10	1.17	1.17
Temperature (^{o}K)	3580	2620	2980	3417	3417
Pressure (mm Hg)	8.65	19.8	19.8	32.9	32.9
Density (ρ/ρ_o)	7.35×10^{-4}	3.80×10^{-3}	2.18×10^{-3}	2.94×10^{-3}	2.94×10^{-3}
D_e/D_a	87	99	95.5	94	94

TABLE 4.3.- CONTINUED.

(a) Concluded.

Case No. / Parameters	16L	16T	17	18
Altitude (ft)	200,000	200,000	200,000	200,000
Velocity (ft/sec)	25,000	25,000	25,000	25,000
Body half angle (deg)	10	10	15	20
V_o (cm/sec)	7.63×10^5	7.63×10^5	7.63×10^5	7.63×10^5
D (cm^2/sec)	5×10^3	1.2×10^4	4.5×10^3	3×10^3
b (cm^{-1})	1.86	3.75	2.15	3.04
B_o (cm^{-1})	152.6	63.6	169.5	254
Z	1.00	1.13	1.01	1.06
Temperature (^oK)	1145	2650	2090	2540
Pressure (mm Hg)	4.73	4.73	9.81	17.45
Density (ρ/ρ_o)	1.50×10^{-3}	5.97×10^{-4}	1.64×10^{-3}	2.39×10^{-3}
D_e/D_a	100	93	100	99

TABLE 4.3.- CONTINUED.

(b) Wedges.

Parameters \ Case No.	19	20	21	22	23
Altitude (ft)	250,000	250,000	250,000	250,000	250,000
Velocity (ft/sec)	15,000	15,000	15,000	25,000	25,000
Body half angle (deg)	10	15	20	10	15
V_o (cm/sec)	4.58×10^5	4.58×10^5	4.58×10^5	7.63×10^5	7.63×10^5
D (cm^2/sec)	1.8×10^5	8×10^4	5×10^4	9.5×10^4	7.9×10^4
b (cm^{-1})	0.244	0.341	0.462	0.341	0.525
B_o (cm^{-1})	2.54	5.7	9.2	8.04	9.67
Z	1.05	1.09	1.06	1.21	1.22
Temperature (^oK)	2167	2310	2427	3333	3890
Pressure (mm Hg)	0.261	0.531	0.895	0.652	1.37
Density (ρ/ρ_o)	4.17×10^{-5}	7.89×10^{-5}	1.26×10^{-4}	5.85×10^{-5}	1.06×10^{-4}
D_e/D_a	88	89	89	82	79.5

TABLE 4.3.- CONTINUED.

(b) Continued.

Case No. / Parameters	24	25	26	27	31L
Altitude (ft)	250,000	250,000	250,000	250,000	200,000
Velocity (ft/sec)	25,000	35,000	35,000	35,000	35,000
Body half angle (deg)	20	10	15	20	10
V_o (cm/sec)	7.63×10^{5}	1.068×10^{6}	1.068×10^{6}	1.068×10^{6}	1.068×10^{6}
D (cm^2/sec)	4.5×10^{4}	1.2×10^{5}	5.6×10^{4}	4.3×10^{4}	4.7×10^{3}
b (cm^{-1})	0.644	0.414	0.614	0.772	2.01
B_o (cm^{-1})	17	8.91	19.1	24.8	227
Z	1.23	1.34	1.40	1.42	1.02
Temperature (^{o}K)	4060	4580	4830	5060	2130
Pressure (mm Hg)	2.29	1.22	2.55	4.39	9.75
Density (ρ/ρ_o)	1.68×10^{-4}	6.97×10^{-5}	1.35×10^{-4}	2.24×10^{-4}	1.58×10^{-3}
D_e/D_a	80	73	75	75	100

TABLE 4.3.- CONTINUED.

(b) Continued.

Parameters \ Case No.	31T	32L	32T	33L	33T
Altitude (ft)	200,000	200,000	200,000	200,000	200,000
Velocity (ft/sec)	35,000	35,000	35,000	35,000	35,000
Body half angle (deg)	10	15	15	20	20
V_o (cm/sec)	1.068×10^{6}	1.068×10^{6}	1.068×10^{6}	1.068×10^{6}	1.068×10^{6}
D (cm^2/sec)	1.15×10^{4}	2.6×10^{3}	6×10^{3}	2.5×10^{3}	4×10^{3}
b (cm^{-1})	1.57	3.17	2.12	3.47	2.13
B_o (cm^{-1})	93	414	178	427	267
Z	1.27	1.07	1.23	1.18	1.25
Temperature (^{o}K)	4670	2890	4500	3870	4830
Pressure (mm Hg)	9.75	20.3	20.3	34.8	34.8
Density (ρ/ρ_o)	5.76×10^{-4}	2.90×10^{-3}	1.33×10^{-3}	3.31×10^{-3}	1.95×10^{-3}
D_e/D_a	79.5	97	83	91	82

TABLE 4.3.- CONTINUED.

(b) Continued.

Case No. / Parameters	34L	34T	35L	35T	36L
Altitude (ft)	200,000	200,000	200,000	200,000	200,000
Velocity (ft/sec)	25,000	25,000	25,000	25,000	25,000
Body half angle (deg)	10	10	15	15	20
V_o (cm/sec)	7.63×10^5	7.63×10^5	7.63×10^5	7.63×10^5	7.63×10^5
D (cm^2/sec)	7.8×10^3	1.35×10^4	4.5×10^3	6.8×10^3	3.8×10^3
b (cm^{-1})	1.86	1.78	2.09	3.59	2.57
B_o (cm^{-1})	98	56.6	171	112	206
Z	1.00	1.15	1.07	1.13	1.07
Temperature (^oK)	1875	3000	2319	3055	2895
Pressure (mm Hg)	5.21	5.21	10.95	10.95	18.2
Density (ρ/ρ_o)	9.84×10^{-4}	5.38×10^{-4}	1.68×10^{-3}	1.12×10^{-3}	2.19×10^{-3}
D_e/D_a	98.5	90	98	93	96

TABLE 4.3.- CONTINUED.

(b) Concluded.

Case No. / Parameters	36T	37L	37T	38L	38T	39L
Altitude (ft)	200,000	200,000	200,000	200,000	200,000	200,000
Velocity (ft/sec)	25,000	10,000	10,000	10,000	10,000	10,000
Body half angle (deg)	20	10	10	15	15	20
V_o (cm/sec)	7.63×10^{5}	3.05×10^{5}	3.05×10^{5}	3.05×10^{5}	3.05×10^{5}	3.05×10^{5}
D (cm^2/sec)	4.4×10^{3}	3.2×10^{4}	2.5×10^{4}	1.7×10^{4}	1.25×10^{4}	1.0×10^{4}
b (cm^{-1})	3.42	0.543	1.785	0.770	3.25	0.922
B_o (cm^{-1})	173	9.54	12.2	17.9	24.4	30.5
Z	1.16	1.00	1.00	1.00	1.00	1.00
Temperature (^{o}K)	3220	1872	1373	1778	1340	1655
Pressure (mm Hg)	18.2	1.13	1.13	2.11	2.11	3.3
Density (ρ/ρ_o)	1.73×10^{-3}	2.17×10^{-4}	2.94×10^{-4}	4.28×10^{-4}	5.68×10^{-4}	7.34×10^{-4}
D_e/D_a	93	94	95	96	97	98

TABLE 4.3.- CONCLUDED.

(c) Special conical geometry cases for investigation of effects of velocity term.

Parameters \ Case No.	13LA	13LB	13LC	13LD	13LE
Altitude (ft)	200,000	200,000	200,000	200,000	200,000
Velocity (ft/sec)	35,000	35,000	35,000	35,000	35,000
Body half angle (deg)	10	10	10	10	10
V_o (cm/sec)	1.068×10	1.068×10	1.068×10	1.068×10	1.068×10
D (cm^2/sec)	5.5×10^6	5.5×10^6	5.5×10^6	5.5×10^6	5.5×10^6
b (cm^{-1})	1.86	0.54	5.40	54.0	0
B_o (cm^{-1})	194.5	194.5	194.5	194.5	194.5
Z	1.05	1.05	1.05	1.05	1.05
Temperature (^oK)	2090	2090	2090	2090	2090
Pressure (mm Hg)	8.65	8.65	8.65	8.65	8.65
Density (ρ/ρ_o)	1.45×10^{-3}	1.45×10^{-3}	1.45×10^{-3}	1.45×10^{-3}	1.45×10^{-3}
D_e/D_a	99.5	99.5	99.5	99.5	99.5

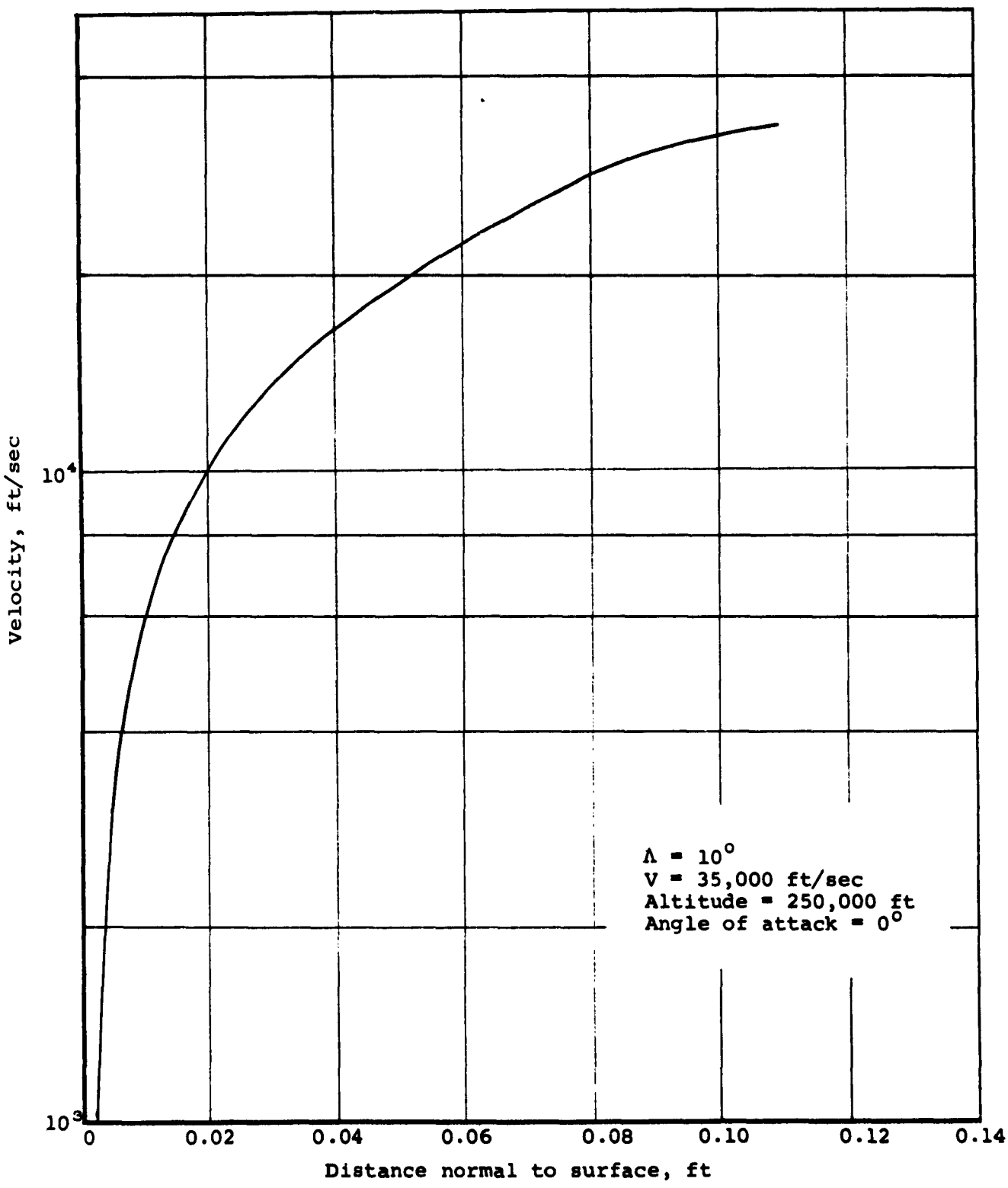

Figure 4.1.- Boundary-layer velocity profile at 5.76 feet from conical apex.

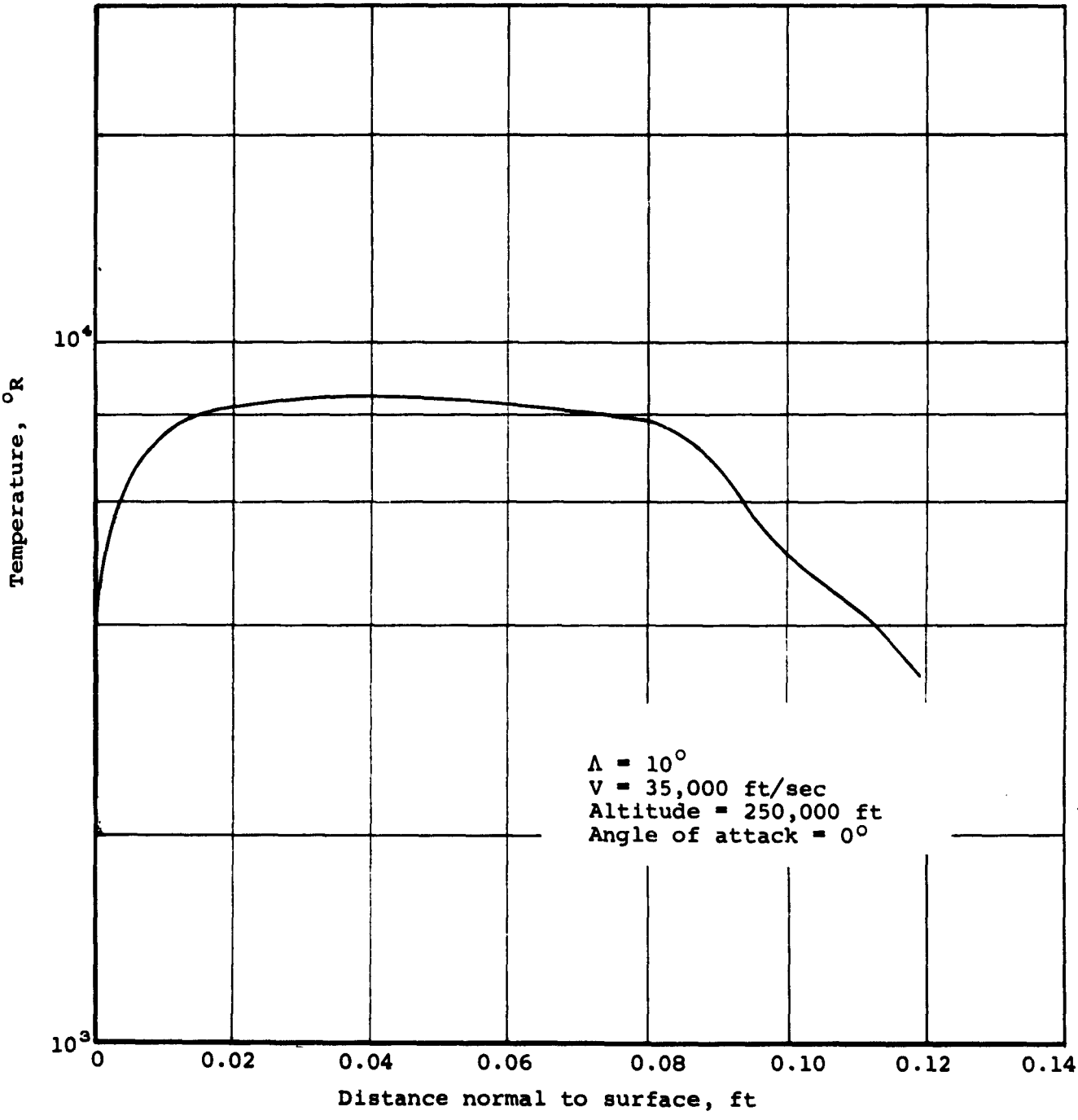

Figure 4.2.- Boundary-layer temperature profile at 5.76 feet from conical apex.

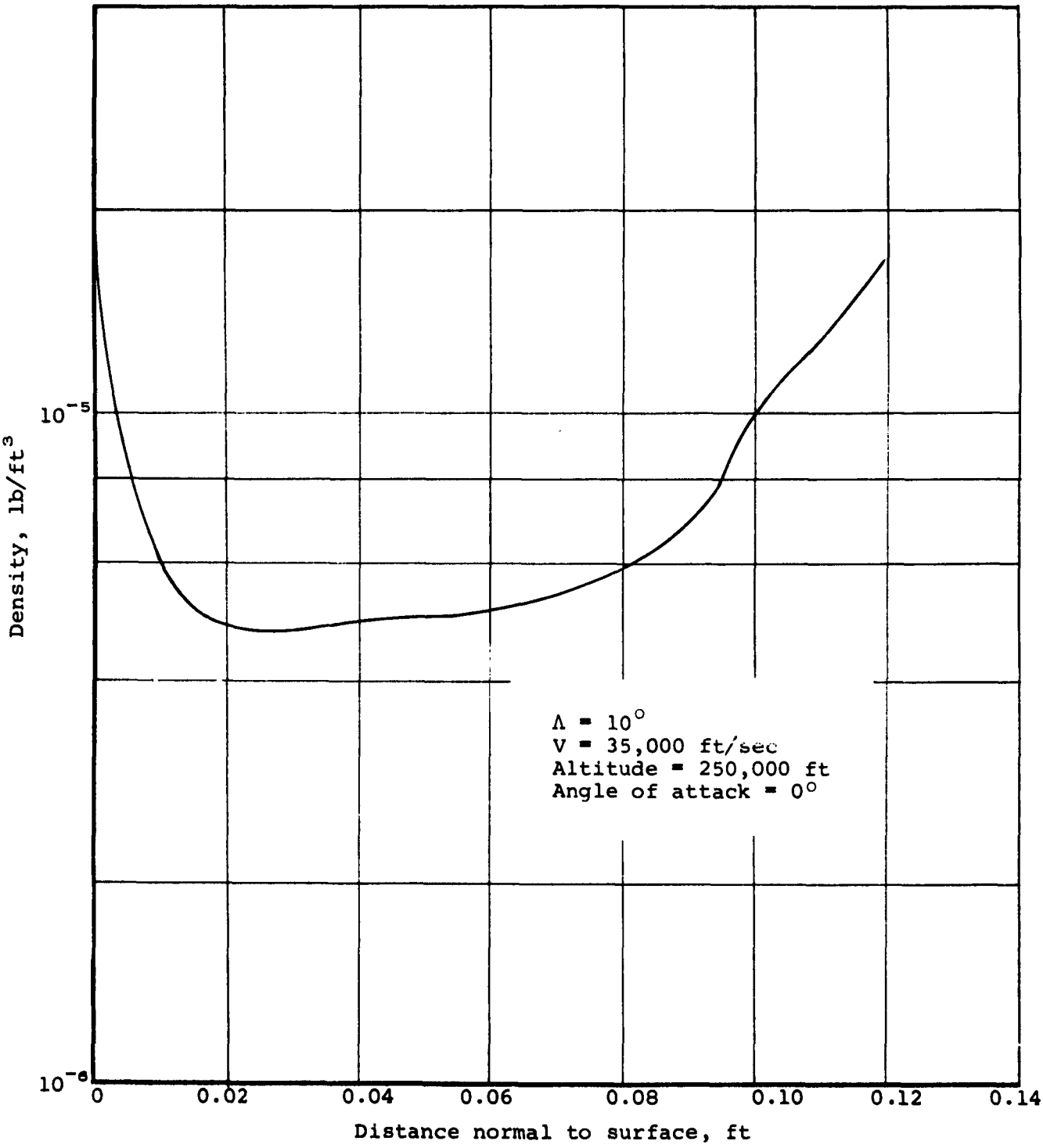

Figure 4.3.- Boundary-layer density profile at 5.76 feet from conical apex.

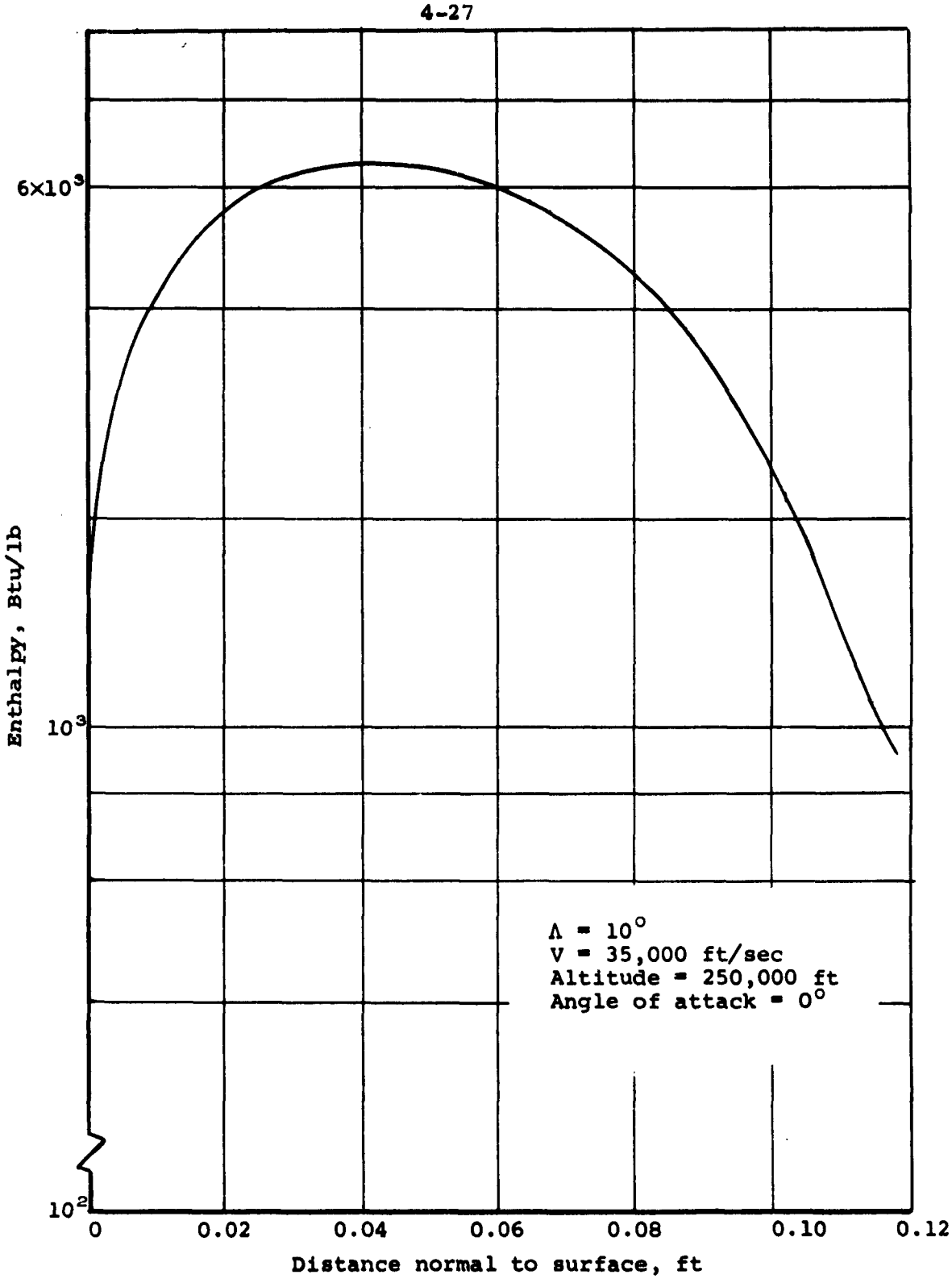

Figure 4.4.- Boundary-layer enthalpy profile at 5.76 feet from conical apex.

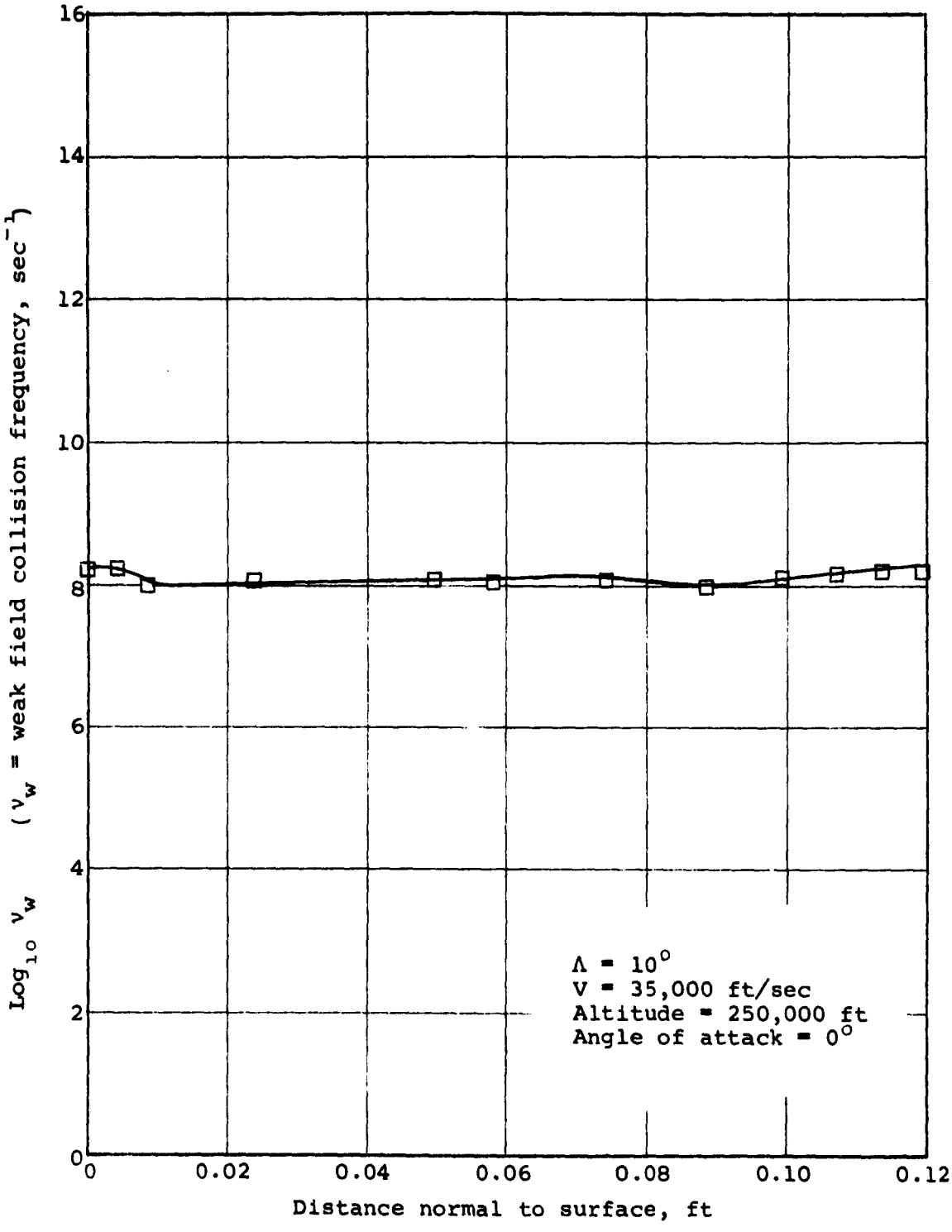

Figure 4.5.- Profile of weak field collision frequency through the boundary layer at 5.76 feet from conical apex.

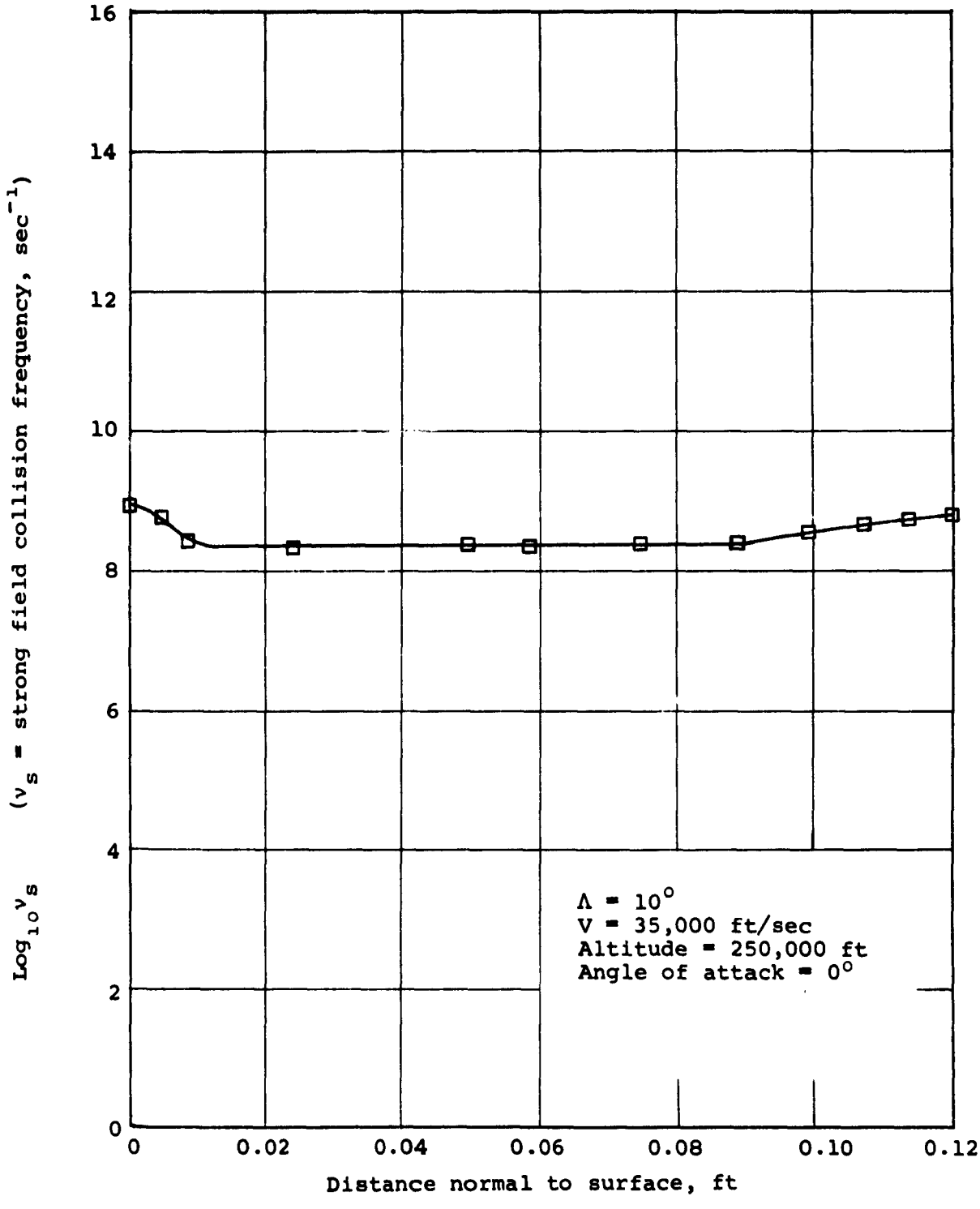

Figure 4.6.- Profile of strong field collision frequency through the boundary layer at 5.76 feet from conical apex.

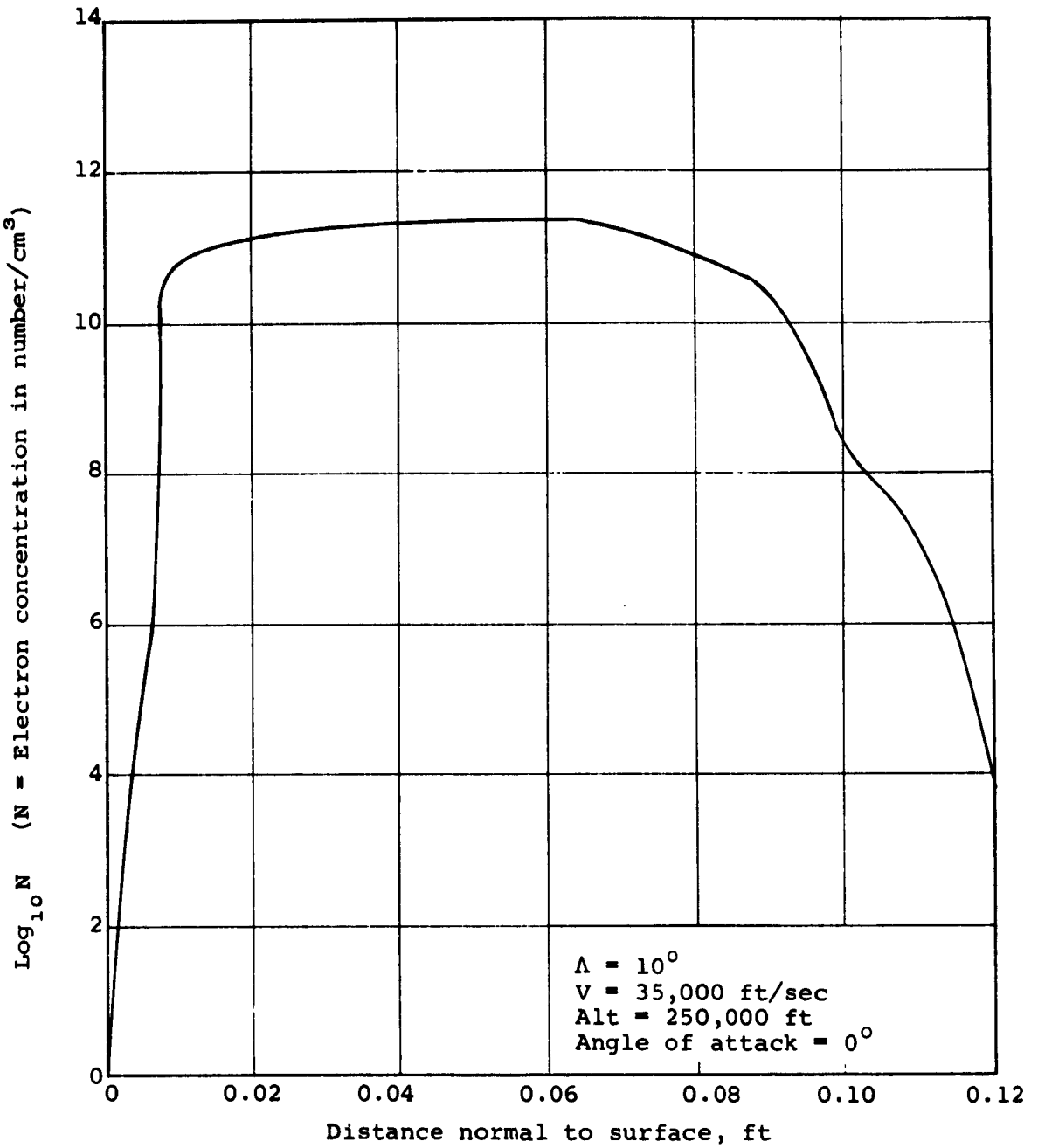

Figure 4.7.- Electron density profile at 5.76 feet from apex of cone along the conical surface.

5. VARIATIONAL METHOD FOR COMPUTATION OF THE C-W BREAKDOWN FIELD STRENGTH

In this section a variational technique will be fully developed in terms of orthogonal polynomials for the computation of breakdown field strengths. This variational principle is a special case of one listed in Reference 26, page 1109, (see also Appendix B).

Suppose Equation (2.13) is multiplied through by $\tilde{\psi}$ and integrated over all space. Upon solving for the eigenvalue one obtains

$$k^2 = -\int \tilde{\psi}\left[\nabla^2 - \vec{\nabla}\cdot(\vec{B}\,]\right)\psi\, d\tau \Big/ \int \tilde{\psi} G \psi\, d\tau \qquad (5.1)$$

where

$$\int d\tau \equiv \iiint dx\, dy\, dz$$

If this expression vanishes to first order with variations in ψ and $\tilde{\psi}$ (independently), and if ψ and $\tilde{\psi}$ both vanish on the boundaries of the region, then ψ satisfies Equation (2.13) and $\tilde{\psi}$ satisfies (see Appendix B)

$$(\nabla^2 + \vec{B}\cdot\vec{\nabla})\tilde{\psi} = -k^2 G\tilde{\psi} \qquad (5.2)$$

Here $\tilde{\psi}$ is called the adjoint of ψ and Equation (5.2) is the adjoint equation. This variational principle, $\delta(k^2) = 0$, is particularly good for the determination of eigenvalues since the error in k^2 is second order in its dependence on the errors in ψ and $\tilde{\psi}$ because we are demanding that the first-order variation vanish.

The numerical determination of k^2 for boundary-layer flow will now be formulated for several cases of increasing complexity. First, the special case of constant D is considered. This

assumes that D does not vary significantly in the region of appreciable induced electron production. This approximation should approximate reality fairly well since Equations (3.33) and (3.40) indicate $D \simeq \overline{mc^2}/3m\overline{\nu_{en}}$ and analysis indicates that the electron RVDF and thus $(1/2)mc^2$ varies quite slowly with electric field strength when the effective field strength is above a few volts (Sections 3.3 and 3.4). In regions of lower field strength, the RVDF varies considerably. However, there is no increase in ionization in such regions and diffusion has little effect, except on the downstream side of the applied field. Downstream of the applied field the electrons quickly (in about three mean free paths) achieve a Maxwellian RVDF among themselves but remain fairly well insulated from the heavy particles. Thus, downstream of the field, the average energy will change considerably (probably to about one-half its value in the field). This will cause some error in the downstream diffusion rate and thus in the eigenvalue and the breakdown field strength. Likewise there is a corresponding error in the cross-flow diffusion rate perpendicular to the surface. This model is formulated below in two and three dimensions.

Following the constant-D formulations, the variable-D problem is formulated. This latter development was not used in the computations, however, because it would have necessitated the use of either a larger computing machine or a significantly slower program. The accuracy of the input data for the computation does not appear to warrant such meticulosity.

5.1 Formulation for Diffusion Coefficient Constant Throughout the Field

When D is constant, Equations (2.13) and (5.2) become identical except for the sign of the $\vec{B} \cdot \vec{\nabla}$ term. Since $\vec{V}$ is in the z direction, a change of variable $z \rightarrow -z$ transforms one equation into the other. Thus $\psi(-z) = \tilde{\psi}(z)$, so that $\tilde{\psi}$ need not be varied as an independent function. It will be seen, subsequently, that this simplification cuts the number of equations to be considered exactly in half.

Let us assume that the dependence of ζ on field strength may be written

$$\zeta = \sum_i a_i(\vec{r}) \left(\frac{E}{p^*}\right)^{d_i} \tag{5.3}$$

where $p^* = \rho Z(RT)_{cold} = (\rho/\rho_o)Z(760)\text{mm}$ and ρ/ρ_o is the density ratio, ρ_o being the density under STP and Z the compressibility. For cold air this polynomial is given by Equation (3.49). Then, with Equations (2.11) and (2.12), G becomes

$$G = \frac{\sum a_i (E'/p^*)^{d_i} F^{d_i+2}}{\sum a_i (E'/p^*)^{d_i}} \equiv \sum g_i F^{d_i+2} \tag{5.4a}$$

and

$$G_{cold} = \left[\frac{(E/p^*) - 30}{(E'/p^*) - 30}\right]\left(\frac{E}{E'}\right)^2 \equiv F^2\left[F\left(\frac{p^*}{p^{*\prime}}\right) - 30P\right]\frac{1}{1 - 30P} \tag{5.4b}$$

where

$$g_i = \frac{\left(\frac{p^*}{p^{*\prime}}\right)^{d_i} a_i P^{d_i}}{\sum_j a_j P^{d_j}} \quad \text{and} \quad P = \left(\frac{p^{*\prime}}{E'}\right) = \left[\frac{760Z(\rho'/\rho_o)}{E'}\right]\frac{\text{mm-cm}}{\text{volt}} \tag{5.5}$$

and for truly cold air $p_{cold} = p^*$. Also, from Equation (2.10)

$$k^2 = \left(p^{*\prime}\right)^2 \sum a_i P^{-(d_i+2)} \tag{5.6a}$$

and for cold air

$$k_{cold}^2 = \left(p^{*\prime}\right)^2 (0.243)\left(\frac{1 - 30P}{P^3}\right)\times 10^{-4} \tag{5.6b}$$

Thus for a given $p^{*\prime}$, P fixes k^2 and k^2 fixes P. In the following formulation we have initially neglected the variation of p^* and have taken $p^* = p^{*\prime}$ = value of p^* at one-half power point (see Section 5.3).

For $\vec{B}$ we use Equation (4.5). A definite electric field will now be chosen.

5.1.1 Exponential - Gaussian field in two dimensions

For the two-dimensional problem, it is assumed that all quantities are constant in the x direction (flow over an infinite surface and an infinite antenna). This problem approximates the solution for the case where the antenna illuminates the gas evenly for a very long distance across the flow as compared to the downstream illumination width.

Let us take a field such that (see Fig. 2.1)

$$F = E/E' = \exp\left(-\epsilon_1 y - \epsilon_2 z^2\right) \tag{5.7}$$

The y-dependence resembles well the induction field measured just outside slot antennas (see Section 6.1). The z-dependence seems reasonable but is chosen arbitrarily. Any field, however, may be represented by multiplying Equation (5.7) by polynomials (e.g., Laguerre y-representation and Hermite z-representation). Also, as will be evident in the analysis below, little extra complication arises with such representation over that involved from the use of Equation (5.7) alone.

For a trial function we take an orthogonal polynomial expansion for

$$\psi = \sum_{m,n} A_{m,n}\psi_{m,n} \tag{5.8}$$

where

$$\psi_{m,n} = \left[e^{-\frac{\alpha}{2}y}\, yL_m^{\alpha,2}(y)\right]\left[e^{-\frac{\gamma}{2}z^2}\, H_n^{\gamma}(z)\gamma^{-\frac{n}{2}}\right] \tag{5.9}$$

Here $L_m^{\alpha,2}$ is the Laguerre polynomial given by[7]

---

[7] $L_m^{\alpha,2}$ is the $L_m(y,\alpha,3)$ of Reference 27.

$$L_m^{\alpha,2} = e^{\alpha y}\, y^{-2}\, \frac{d^m}{dy^m}\left(e^{-\alpha y}\, y^{m+2}\right) \tag{5.10a}$$

and H_n^{γ} is the Hermite polynomial given by[8]

$$H_n^{\gamma} = (-1)^n\, e^{\gamma z^2}\, \frac{d^n}{dz^n}\, e^{-\gamma z^2} \tag{5.10b}$$

The $A_{m,n}$ are the parameters to be varied, and γ and α are parameters which may be arbitrarily selected for the computation. However, very large or very small values of α and γ compared to ϵ_1 and ϵ_2, respectively, will necessitate the use of more terms in Equation (5.8) for good accuracy.

If Equations (5.8), (4.5), and (5.4a) or (5.4b) are substituted into Equation (5.1) with $\tilde{\psi} = \psi(-z)$, one obtains (Appendixes C, D, and E)

$$-k^2 = \frac{\sum_{m,n}\sum_{m',n'} (-1)^{n'} \left(Q_{m',n'}^{m,n} - N_{m',n'}^{m,n}\right) A_{m',n'} A_{m,n}}{\sum_{m,n}\sum_{m',n'} (-1)^{n'}\, M_{m',n'}^{m,n}\, A_{m',n'} A_{m,n}} \tag{5.11}$$

where

$$Q_{m',n'}^{m,n} = \gamma^{-\left(\frac{n+n'}{2}\right)} \left\{ {}^{2}J_{m,m'}^{\alpha,0} \left[\frac{1}{4}\, I_{n',n+2}^{\gamma;0} - \left(\frac{1}{2} + n\right)\gamma\, I_{n',n}^{\gamma;0} + n(n-1)\gamma^2 I_{n',n-2}^{\gamma;0}\right] \right.$$
$$\left. + I_{n',n}^{\gamma;0} \left[(m+3)\, {}^{0}J_{m',m}^{\alpha,0} - \alpha(m+2)\, {}^{1}J_{m',m}^{\alpha,0} + \frac{\alpha^2}{4}\, {}^{2}J_{m',m}^{\alpha,0} - {}^{0}J_{m',m+1}^{\alpha,0}\right]\right\} \tag{5.12}$$

---

[8] H_n^{γ} is the $H_n(z,\alpha)$ defined in Reference 27.

$$N^{m,n}_{m',n'} = B_o\,\gamma^{-\left(\frac{n+n'}{2}\right)}\left({}^{2}J^{\alpha,o}_{m',m} - {}^{2}J^{\alpha,b}_{m',m}\right)\left(-\frac{1}{2}\,I^{\gamma,o}_{n',n+1} + n\gamma\,I^{\gamma,o}_{n',n-1}\right) \tag{5.13}$$

$$M^{m,n}_{m',n'} = \gamma^{-\left(\frac{n+n'}{2}\right)}\sum_i g_i\left\{\left[{}^{2}J^{\alpha,(d_i+2)\epsilon_1}_{m',m}\right]\left[I^{\gamma,(d_i+2)\epsilon_2}_{n',n}\right]\right\} \tag{5.14a}$$

or, for cold air,

$$\left(M^{m,n}_{m',n'}\right)_{cold} = \gamma^{-\left(\frac{n+n'}{2}\right)}\frac{1}{1-30P}\left[\left({}^{2}J^{\alpha,3\epsilon_1}_{m',m}\right)\left(I^{\gamma,3\epsilon_2}_{n',n}\right) - 30P\left({}^{2}J^{\alpha,2\epsilon_1}_{m',m}\right)\left(I^{\gamma,2\epsilon_2}_{n',n}\right)\right] \tag{5.14b}$$

Here

$$I^{\gamma,\eta}_{m,n} = \int_{-\infty}^{\infty} e^{-(\gamma+\eta)z^2}\,H^{\alpha}_m\,H^{\alpha}_n\,dz = I^{\gamma,\eta}_{n,m} \tag{5.15}$$

and

$${}^{c}J^{\alpha,\eta}_{m,n} = \int_{o}^{\infty} e^{-(\alpha+\eta)y}\,y^{c}\,L^{\alpha,2}_m\,L^{\alpha,2}_n\,dy = {}^{c}J^{\alpha,\eta}_{n,m} \tag{5.16}$$

It is shown in Appendix D that

$$I^{\gamma,\eta}_{n,n} = 2(2n-1)\left(\frac{\gamma^2}{\gamma+\eta}\right)I^{\gamma,\eta}_{n-1,n-1} - 4(n-1)^2\,\frac{\gamma^2(\gamma-\eta)}{\gamma+\eta}\,I^{\gamma,\eta}_{n-2,n-2} \tag{5.17}$$

$$I^{\gamma,\eta}_{m,m+2\nu} = \left(\frac{m+2\nu}{m+1}\right)\frac{\gamma}{\eta}\,I^{\gamma,\eta}_{m+2\nu-1,m+1} - \frac{1}{2(m+1)}\left(\frac{\gamma+\eta}{\gamma\eta}\right)I^{\gamma,\eta}_{m+2\nu,m+2} \tag{5.18}$$

and $I_{m,m+2\nu+1} = 0$. The lowest members are

$$I^{\gamma,\eta}_{o,o} = \sqrt{\frac{\pi}{\gamma + \eta}}$$

and

$$I^{\gamma,\eta}_{1,1} = \frac{2\gamma^2}{\gamma + \eta}\sqrt{\frac{\pi}{\gamma + \eta}}$$

Similarly in Appendix E it is shown that

$$(\alpha+\eta)\ {}^{c}J^{\alpha,\eta}_{m,n} = \left[(n-m+1-c)\alpha+(2n+1)\eta\right]\ {}^{c}J^{\alpha,\eta}_{m,n-1} - (n^2-1)\eta\ {}^{c}J^{\alpha,\eta}_{m,n-2}$$

$$+ m(m+2)\alpha\ {}^{c}J^{\alpha,\eta}_{m-1,n-1} \qquad (5.19)$$

The lowest members are

$${}^{c}J^{\alpha,\eta}_{o,o} = \frac{c!}{(\alpha + \eta)^{c+1}}\ ,\quad {}^{c}J^{\alpha,\eta}_{1,o} = \frac{c!}{(\alpha + \eta)^{c+2}}\left[(2 - c)\alpha + 3\eta\right]$$

These reduction relations allow all the I's and J's to be generated from the lowest members. The normalization integrals for Hermite and Laguerre polynomials are special cases of the I's and J's. They are

$$I^{\gamma,o}_{m,n} = \sqrt{\frac{\pi}{\gamma}}\, n!\,(2\gamma)^n\,\delta^n_m\ ,\quad {}^{2}J^{\alpha,o}_{m,n} = \frac{n!\,(n+2)!}{\alpha^3}\,\delta^n_m$$

where δ^n_m is a Kronecker delta.

If one now evaluates $\partial k^2/\partial A_{m,n}$ from Equation (5.11) and sets them equal to zero, as required by the variational principle, one finds[9]

---

[9]Here the symmetry of $Q^{m,n}_{m',n'}$ and $M^{m,n}_{m',n'}$ and the antisymmetry of $N^{m,n}_{m',n'}$ in the primed and unprimed indices has been used, for example, $Q^{m,n}_{m',n'} = Q^{m',n'}_{m,n}$ but $N^{m,n}_{m',n'} = -N^{m',n'}_{m,n}$.

$$\sum_{m',n'} \left\{ \left[(-1)^{n'} + (-1)^{n} \right] \left[Q^{m,n}_{m',n'} + k^2 M^{m,n}_{m',n'} \right] - \left[(-1)^{n'} - (-1)^{n} \right] N^{m,n}_{m',n'} \right\} A_{m',n'} = 0 \quad (5.20)$$

Setting the determinant of coefficients of this set of equations (for the $A_{m,n}$) equal to zero determines k^2. Alternately, one could specify one of the $A_{m,n}$ and use all but one of these equations along with Equation (5.11) to determine k^2. These approaches are completely equivalent. We want the lowest value of k^2, that is, we want the lowest value of k^2 that permits the vanishing of the determinant.

5.1.2 Exponential - Gaussian field in three dimensions

The extension of Section 5.1.1 to three dimensions is straightforward. For the electric field we now take

$$F = E/E' = e^{-\epsilon_1 y} e^{-\epsilon_2 z^2 - \epsilon_3 x^2} \quad (5.21)$$

Again, as discussed earlier after Equation (5.7), multiplication by various polynomials allows adequate representation of any field without introducing significant extra work.

In place of Equation (5.8) we have

$$\psi = \sum_{l,m,n} A_{l,m,n} \psi_{l,m,n} \quad (5.22)$$

with

$$\psi_{l,m,n} = e^{-\frac{\alpha}{2} y} L^{\alpha,2}_{m}(y) e^{-\frac{1}{2}(\beta x^2 + \gamma z^2)} H^{\beta}_{l}(x) H^{\gamma}_{n}(z) \beta^{-\frac{l}{2}} \gamma^{-\frac{n}{2}} \quad (5.23)$$

Equation (5.11) now becomes

$$-k^2 = \frac{\sum_{l,m,n}\sum_{l',m',n'} (-1)^{n'} \left(Q^{l,m,n}_{l',m',n'} - N^{l,m,n}_{l',m',n'}\right) A_{l,m,n} A_{l',m',n'}}{\sum_{l,m,n}\sum_{l',m',n'} M^{l,m,n}_{l',m',n'} A_{l',m',n'} A_{l,m,n}} \tag{5.24}$$

where

$$\begin{aligned}\left(\gamma^{\frac{1}{2}(n+n')}\ \beta^{\frac{1}{2}(l+l')}\right) Q^{l,m,n}_{l',m',n'} &= \left\{ {}^{2}J^{\alpha;o}_{m',m}\ I^{\beta;o}_{l',l}\left[\frac{1}{4}\, I^{\gamma;o}_{n',n+2} - \left(\frac{1}{2}+n\right)\gamma\ I^{\gamma;o}_{n',n} + n(n-1)\gamma^2\ I^{\gamma;o}_{n',n-2}\right]\right. \\ &+ {}^{2}J^{\alpha;o}_{m,m}\ I^{\gamma;o}_{n',n}\left[\frac{1}{4}\, I^{\beta;o}_{l',l+2} - \left(\frac{1}{2}+l\right)\beta\ I^{\beta;o}_{l',l} + l(l-1)\beta^2\ I^{\beta;o}_{l',l+2}\right] \\ &\left. + I^{\beta;o}_{l',l}\ I^{\gamma;o}_{n',n}\left[(n+3)\ {}^{o}J^{\alpha;o}_{m',m} - \alpha(m+2)\ {}^{1}J^{\alpha;o}_{m',m} + \frac{\alpha^2}{4}\ {}^{2}J^{\alpha;o}_{m',m} - {}^{o}J^{\alpha;o}_{m',m+1}\right]\right\}\end{aligned} \tag{5.25}$$

$$N^{l,m,n}_{l',m',n'} = B_o \gamma^{-\frac{1}{2}(n+n')}\ \beta^{-\frac{1}{2}(l+l')}\ I^{\beta;o}_{l',l}\left({}^{2}J^{\alpha;o}_{m',m} - {}^{2}J^{\alpha;b}_{m',m}\right)\left(-\frac{1}{2}\, I^{\gamma;o}_{n',n+1} + n\gamma\ I^{\gamma;o}_{n',n-1}\right) \tag{5.26}$$

$$M^{l,m,n}_{l',m',n'} = \gamma^{-\frac{1}{2}(n+n')}\ \beta^{-\frac{1}{2}(l+l')} \sum_i g_i \left\{\left[I^{\beta,(d_i+2)\epsilon_3}_{l',l}\right]\left[{}^{2}J^{\alpha,(d_i+2)\epsilon_1}_{m',m}\right]\left[I^{\gamma,(d_i+2)\epsilon_2}_{n',n}\right]\right\} \tag{5.27a}$$

and for cold air

$$M^{l,m,n}_{l',m',n'} = \gamma^{-\frac{1}{2}(n+n')} \beta^{-\frac{1}{2}(l+l')} \frac{1}{1 - 30P} \left(I^{\beta,3\epsilon_3}_{l',l} J^{2\alpha,3\epsilon_1}_{m',m} I^{\gamma,3\epsilon_2}_{n',n} - 30P\, I^{\beta,2\epsilon_3}_{l',l} J^{2\alpha,2\epsilon_1}_{m',m} I^{\gamma,2\epsilon_2}_{n',n} \right) \tag{5.27b}$$

5.2 Formulation for Nonconstant Diffusion Coefficient

In Sections 3.3 and 3.4 it was pointed out that the diffusion coefficient is a function largely of the local composition in the regions of interest and of the heavy particle temperature. In addition, the diffusion coefficient depends on the electric field strength also in the weak field regions, that is, field strengths less than about 10 volts. Although, as pointed out earlier, one can get fairly good results with the constant-D formulation, a truly accurate treatment for the case of strong mixture gradients and large changes in the electric field, both of which are absent in the usual closed cavity breakdown studies, should include variable-D effects.

In general, it will always be possible to obtain reasonable fits to data in the form

$$\vec{B} = \frac{\vec{V}}{D} = \vec{B}_o \sum_{i,j,k} C_{i,j,k}\, y^j\, e^{-Y_i y}\, E^{\tau_i} \tag{5.28}$$

$$\zeta = \frac{\nu}{DE^2} = \sum_{i,j,k} a_{i,j,k}\, y^j\, e^{-Y_i y}\, E^{d_i} \tag{5.29}$$

When D is not constant, one cannot obtain $\tilde{\psi}$ from ψ by merely taking $\psi(z \rightarrow -z)$. The trial function for $\tilde{\psi}$ must be varied independently. The trial function for ψ may again be taken as Equation (5.8) with (5.9) for the two-dimensional case and (5.22)

with (5.23) for the three-dimensional case. Since the three-dimensional case is a simple generalization of the two-dimensional case, only the development of the two-dimensional case will be fully demonstrated.

5.2.1 Exponential - Gaussian field in two dimensions, nonconstant D

For the $\tilde{\psi}$ trial function we may take

$$\tilde{\psi} = \sum_{m,n} B_{m,n}\psi_{m,n} \tag{5.30}$$

Here again $\psi_{m,n}$ is given by Equation (5.9).

For k^2 we find

$$-k^2 = \frac{\sum_{m,n}\sum_{m',n'}\left(Q^{m,n}_{m',n'} - N^{m,n}_{m',n'}\right) B_{m',n'}A_{m,n}}{\sum_{m,n}\sum_{m',n'} M^{m,n}_{m',n'} B_{m',n'}A_{m,n}} \tag{5.31}$$

Here $Q^{m,n}_{m',n'}$ is still given by Equation (5.12); however, $N^{m,n}_{m',n'}$ and $M^{m,n}_{m',n'}$ are now changed. For any specific case they may be readily developed by multiplying Equations (5.28) and (5.29) by $\psi_{m',n'}$ and $\psi_{m,n}$, integrating and making use of the reduction formula (C.2a) (see Appendix C) and the integrals (5.15) and (5.16).

The set of equations $\partial k^2/\partial A_{m,n} = \partial k^2/\partial B_{m,n} = 0$ become

$$\sum_{m',n'}\left(Q^{m,n}_{m',n'} - N^{m,n}_{m',n'} + k^2 M^{m,n}_{m',n'}\right) B_{m',n'} = 0$$

$$\sum_{m',n'}\left(Q^{m,n}_{m',n'} + N^{m,n}_{m',n'} + k^2 M^{m,n}_{m',n'}\right) A_{m',n'} = 0$$

where we have made use of the symmetry of Q and M and anti-symmetry of N with respect to the primed and unprimed indices.

5.3 Discussion of Approximation that Particle Density or p* is Constant

At the end of the introduction to Section 5.1 the approximation $p^* = p^{*'}$ was made and the value selected for these quantities was the value of p^* at a distance above the aperture center corresponding to one-half the field strength at the aperture (see Section 7.1). Since $p^* = 760Z(\rho/\rho_o)$, this is equivalent to assuming that the particle density is constant in the boundary layer. The error involved should not be too important in view of the uncertainty in the values already used for the ionization frequency.

The consideration of the variable-p^* problem is actually no more difficult than the constant-p^* problem. This may be done by using a polynomial fit to the y-dependence of p^*. The additional integrals occurring in the variational principle give extra terms in Equation (5.14b) which may be written down immediately in terms of the $I_{m,n}^{\gamma,\eta}$ and $J_{m,n}^{c\alpha,\eta}$'s. This unnecessary approximation was actually the result of an oversight. Since almost all experimental breakdown studies have been conducted at room temperature, the macroscopic coefficients derived from these experiments have usually been represented as functions of E/p, where p was the actual gas pressure, although the truly meaningful physical variable should be E divided by particle density. In our initial calculation, therefore, we had used p instead of p^* in Equations (5.4) to (5.6). Also, p is constant through the boundary layer so that $p = p'$. Thus, effectively, the computations were conducted with the net ionization frequency corresponding to a constant density of about a factor of three to an order of magnitude too high but with the diffusion constant at the proper density. These results are presented in Section 7.2.1, although incorrect, because they depict qualitatively all the phenomena to be expected with breakdown in a boundary layer. When the oversight was noted, some results were quickly recomputed at

the more reasonable, but still constant, particle densities and the results presented in Section 7.2.2.

There is, of course, no constant-p* approximation necessary in the zero-velocity (no flow) breakdown computations of Section 6.

6. ZERO VELOCITY BREAKDOWN COMPUTATIONS AND COMPARISON WITH EXPERIMENT

In this section, computations for zero velocity will be compared with experiments conducted with antenna configurations similar or equivalent to a type of slot antenna commonly used for reentry vehicles (Ref. 4).

6.1 The Shape of the Electric Field

The breakdown studies of Reference 4 includes probe measurements of the electric field strength of slot antennas at various distances away from the antenna surface along the line perpendicular to the aperture surface of its geometric center. These data are plotted in Figure 6.1 as E/E_s versus y/d, where y is distance above the aperture surface, d is the small dimension of the aperture, and E_s is the field strength at the aperture surface. Notice that all the data cluster quite well about the representative curve drawn except for one of the flared horns.

Although, as pointed out in Section 5.1.1, it is possible to match this representative curve with any desired accuracy in the breakdown computations, it was found sufficient to merely match the initial slope. Thus, ϵ_1 in Equation (5.7) is taken to be

$$\epsilon_1 = 0.686/d \tag{6.1}$$

For the electric field variation across the gap, there are no data. A theoretical computation of such a near field is very difficult. We have taken ϵ_2 in Equation (5.7) such that the power falls to half at $z = \pm d/2$, that is,

$$\left(e^{-\epsilon_2 z^2}\right)^2 = \frac{1}{2} \quad \text{at} \quad z = d/2$$

or

$$\epsilon_2 = \frac{1.388}{d^2} \tag{6.2}$$

This type of field variation will reasonably represent the "size" of the field and seems to yield good agreement between computed and experimental breakdown field strengths.

The x-dependence is not important here because the aperture is taken to be very long in the x-direction so that a two-dimensional treatment applies (see Section 5.1).

The relationship between breakdown field strength and the radiated power level at breakdown may be obtained using a result from Reference 4, page 81. In this reference it is shown that for a long narrow slot, less than 1/2 wavelength long the power is related to the slot field strength by

$$P = E_s^2 d^2 \frac{R_s}{z_s^2} \tag{6.3}$$

where d is the slot width, z_s is the complex slot impendance, and R_s is the real part of z_s. In turn, z_s is related to z_d, the impedance of a dipole of diameter $d/2$. This relation is

$$z_s = \frac{70,952}{z_d} \tag{6.4}$$

The dipole impedance may be determined from Reference 32 (pp. 154-179).

6.2 Convergence with 4×4 Term Representation

The coefficient functions for Equation (5.20) were generated as indicated in Section 5.1. The lowest eigenvalues of Equation (5.20) were determined by solving for the k^2 that allows the determinant of Equation (5.20) to vanish. This was done by iteration on an IBM 1620. The breakdown voltage is then given by Equations (5.5) and (5.6b). Our computations have utilized four Hermite polynomials and four Laguerre polynomials. This gives a total of sixteen coefficients to vary or a 16×16 determinant.

Theory tells us (see Ref. 26 regarding variational techniques with positive definite operators) that the better the accuracy,

the lower the computed eigenvalue; that is, the eigenvalue is approached from above. In the present case, this implies that any alteration in the trial functions that produces a lower breakdown voltage is a desirable alteration and gives a more accurate eigenvalue.

To examine the accuracy of the 4×4 term representation, the breakdown field was computed with 2×2, 3×3, and 4×4 terms with various values of α and γ and the results plotted in Figure 6.2. It is seen that with $\alpha = 2\epsilon_1$ and $\gamma = 1/2\epsilon_2$ the change of the breakdown field is not large with addition of terms and that the rate of change at $n = 4\times4$ is quite small. This indicates that our results are at most 2 volts, or less than 5 percent, above the result which would be obtained for this model using many more terms in the expansion. All our computations used $\alpha = 2\epsilon_1$ and $\gamma = 1/2\epsilon_2$.

It should be noted that 2×2 representation is so crude that it does not even allow variation of the z-dependence curvature in the electron density function at $z = 0$.

6.3 Comparison of Breakdown Field Strength with Experiment

The only controlled experiments on antenna breakdown in air have been performed in ambient temperature air at rest. The results (Ref. 4) of one series of these experimental measurements for a 17-inch long slot antenna of width d operating at 380 megacycles is given in Figure 6.3 (solid line). For comparison purposes, the results of a two-dimensional constant-D model computation of breakdown are given as a dotted line. For these calculations, the values $\gamma = 0.5\epsilon_2$ and $\alpha = 2.0\epsilon_1$ were used with slot widths of 0.1, 1.27, and 2.54 centimeters.

The computed points agree well with experiment in the region in which the input data for ζ are valid, that is, for $E/p \leq 110$ volts-cm^{-1}-mm^{-1}Hg. Marked deviation from the experimental curve

occurs, as should be expected, for $E/p > 200$ volts-cm^{-1}-mm^{-1}, since the extrapolation of measured macroscopic coefficients into this regime is expected to yield poor values for ζ. The comparison supports the validity of the model for the simple geometry investigated here.

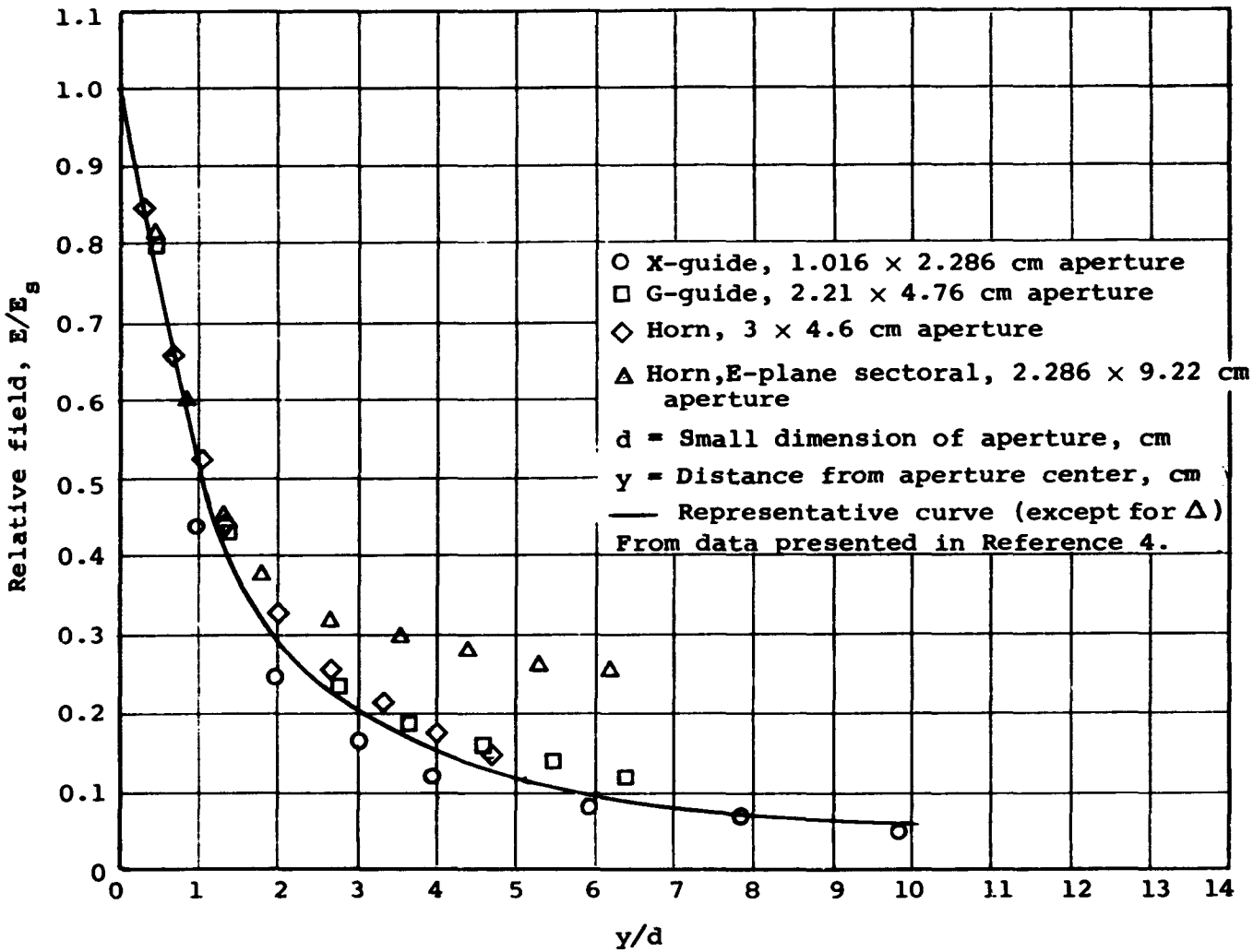

Figure 6.1.- Variation of field strength with distance for various apertures.

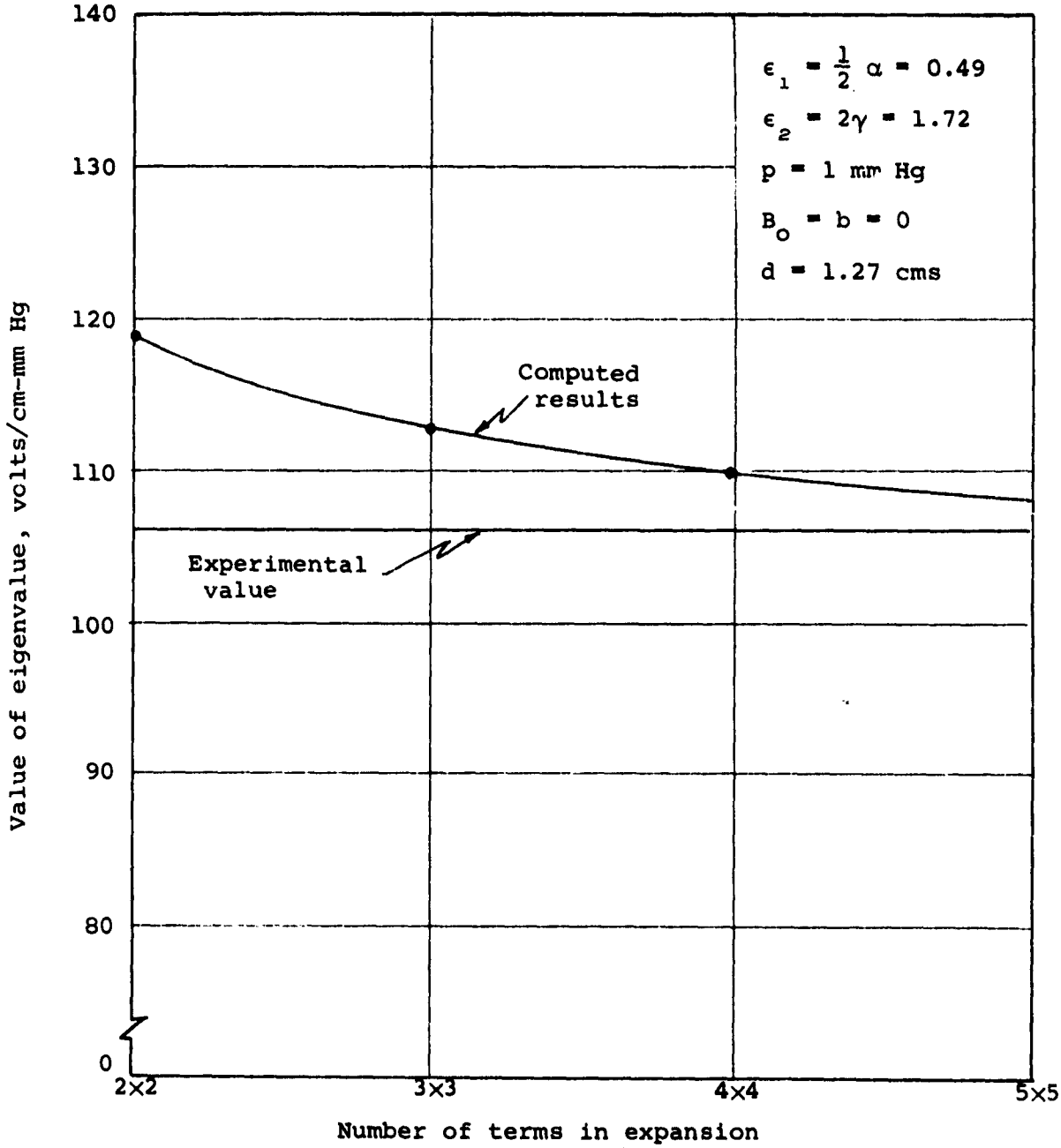

Figure 6.2.- Figure illustrating the convergence of the computed eigenvalue as a function of the number of terms used in the expansions.

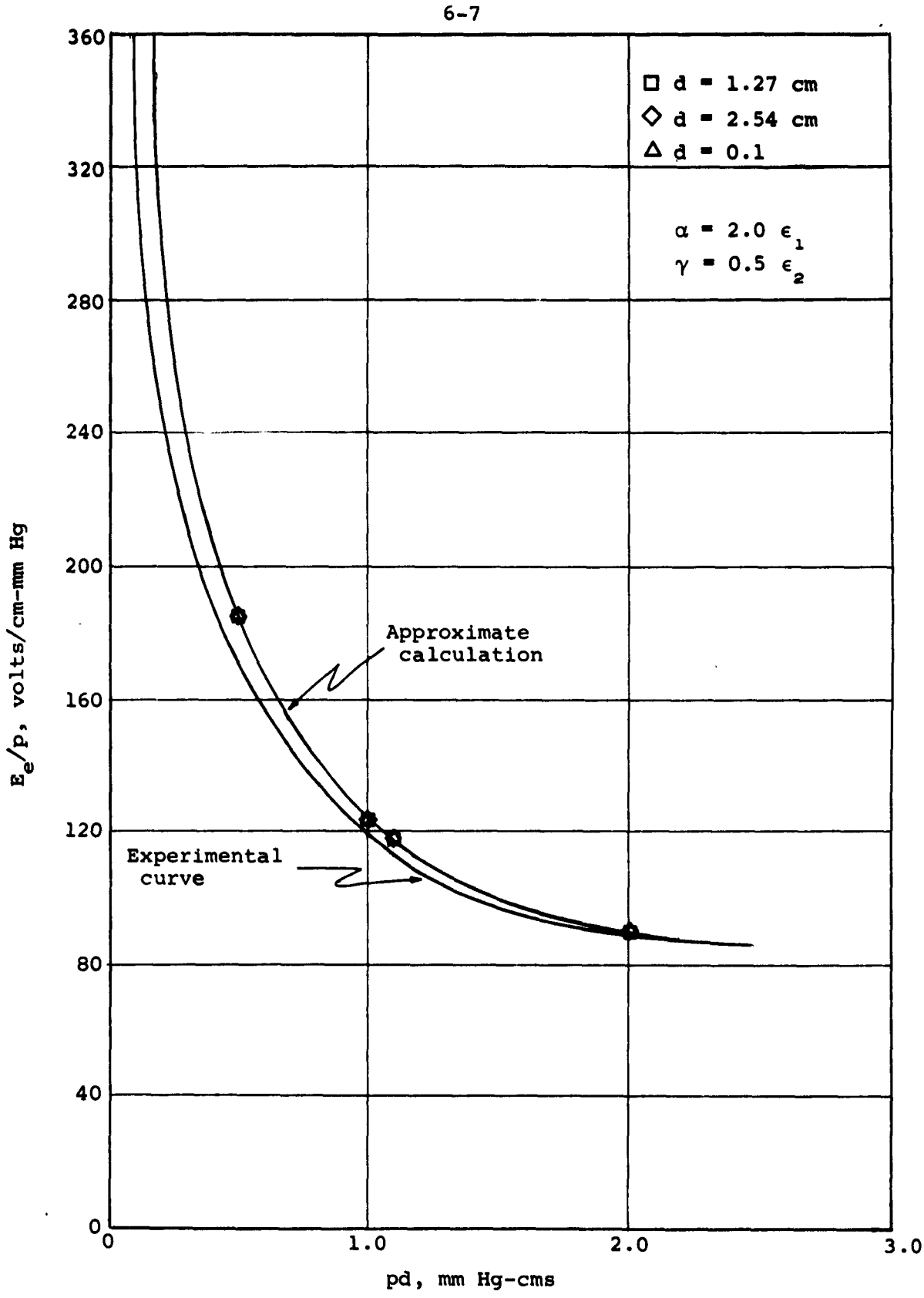

Figure 6.3.- Comparison of breakdown computation with experiment for a narrow slot and zero velocity flow.

7. COMPUTATIONS WITH FLOW RESEMBLING BOUNDARY LAYERS ENCOUNTERED IN HIGH-SPEED FLIGHT

7.1 Review of Input Assumptions

The inviscid and viscous layer properties for cones and wedges at various altitudes and reentry velocities were computed as described in Section 4. The boundary-layer velocity profile divided by D was represented as discussed in Section 4.3. In this representation of V/D, it was assumed that the diffusion was fully ambipolar and the diffusion coefficient, computed for hot air as described in Section 3.4.1, was evaluated for gas temperatures and densities at a distance from the antenna surface corresponding to a point where the electric field intensity is one half of its value in the aperture. The reason for this choice is that the ambipolar theory requires that D_a be evaluated at the point where breakdown first tends to occur. This would, for example, be at the center of a cavity for closed cavity breakdown. It would be about a diffusion length, $\Lambda = \left\{ \left[d^2(nD)/dy^2 \right] / (nD) \right\}^{-1/2}$ from the surface in the present case and would require iteration for Λ to evaluate properly.[10] The error will not be large by the choice indicated. The more accurate iteration treatment is not warranted because of the poor state of knowledge of the data used for the other inputs.

The value of the ionization coefficient, ζ, is taken as indicated by the choice of ν in Section 3.4.2. It is given by Equation (3.54)

$$\zeta_{hot} = \zeta_{cold}(P) \left[(D_e)_{cold} / (D_a)_{hot} \right]$$

---

[10] That is, select Λ, evaluate D_a at this point, solve for $\left\{ \left[d^2(nD)/dy^2 \right] / (nD) \right\}^{-1/2}$, compare, correct Λ, and repeat.

where ζ_{cold} is given by Equation (3.49) and $P = p^*/E$. This value of ζ_{hot} is taken such that D_a was evaluated a distance from the aperture as discussed above for V/D_a, and $p^{*'}$, the effective pressure as defined on page 3-26, taken at the center of the antenna aperture, was evaluated as discussed in Section 5.3. Initially, as noted in Section 5.3, due to an oversight, many computations were made with the ionization frequency evaluated at an improperly high density corresponding to p rather than p^*. This is equivalent to having a net ionization frequency of about an order of magnitude or more higher than the actual values. Although incorrect, these results do depict qualitatively the type of breakdown behavior expected in a boundary layer and are therefore discussed in Section 7.2.1. All such results are clearly labeled illustrative only. With the oversight corrected some of the computations were repeated and these results are discussed in Section 7.2.2.

The electric field adopted approximates that for a narrow slot antenna, as described in Section 6.1, and corresponds to a gap width of 1/2 inch. The arbitrary parameters α and γ were taken as in Section 6.2 for good convergence with 4×4 representation when there is no flow ($\alpha = 2\epsilon_1$, $\gamma = (1/2)\epsilon_2$). This model compares well with experiment for cold air without flow in the same geometry (Section 6.3). However, it was found that with flow the 4×4 term representation used proved inadequate for many of the computations of Section 7.2.2 with the proper density or p^* used, and further results would require the use of more terms. The method of solution is the same as in Section 6, namely, the determinant of the coefficients of Equation (5.20) is set equal to zero and solved by iteration for k^2 or P, the relationship between k^2 and P being given by Equation (5.6b).

Since the gap antenna was assumed very long, the two-dimensional formulation of Section 5.1.1 was used for both cones and wedges. The development of the variational principle used could be reformulated in cylindrical coordinates for antennas mounted in cones.

In fact, there would be fewer terms in such a formulation because the Laguerre polynomials behave more simply with the cylindrical coordinate differential operator. However, the antenna is assumed to be placed sufficiently far downstream in this model that the conical problem may quite accurately be approximated by the "two-dimensional" Cartesian problem and, therefore, a separate program was unwarranted.

Computations were attempted for several flight velocities between 10,000 and 45,000 feet per second at altitudes of 200,000 and 250,000 feet for both cones and wedges of 10°, 15°, and 20° half angles. The gap antenna was assumed placed at a distance sufficiently downstream that a 2-foot body total width or diameter existed at that point. This was

$$L(\text{ft}) \approx 1 \Big/ \begin{pmatrix} \text{half angle} \\ \text{in radians} \end{pmatrix} \tag{7.1}$$

At 200,000 feet these conditions made transition to turbulent flow probable, so that computations for this altitude were attempted for both a laminar and a turbulent boundary layer. However, even with use of a proper ionization frequency, the results of the calculations for the turbulent cases cannot be considered adequate since the effective electron diffusion rates are probably significantly different in a turbulent region (see, e.g., Ref. 35), whereas they are assumed unaltered by turbulence in this computation.

7.2 Discussion of Computed Breakdown Field Strengths

7.2.1 Illustrative computations using <u>improper</u> ionization frequency

The input data for the illustrative computations conducted with the ionization frequency evaluated at improper particle densities (discussed in Sections 7.1 and 5.3) are listed in Table 4.3, Cases 2 through 39, and the results of these computations are depicted in Figures 7.1 through 7.6.

In Figures 7.1 through 7.4 the breakdown field strength[11] in the antenna aperture is plotted versus the vehicle velocity. It is seen that, in all cases, the breakdown field strength climbs significantly with vehicle velocity and thus this appears to suggest that, other things being equal, one may transmit at a significantly higher power level at higher velocities. When plotted as E_B/p, as in Figures 7.5 and 7.6, the curves are relatively flat and even slightly decrease with increasing vehicle velocity. This implies that the increase in computed breakdown field strength with velocity is largely a pressure (or actually density - see Section 5.3) effect, that is, due to the increased shock-wave compression at higher velocities. Notice also the effect of density in the larger values of E_B at 200,000 feet relative to those at 250,000 feet, whereas the values of E_B/p at these two altitudes are only slightly different.

In order to examine the effect of the flow velocity profile itself at the antenna position, Case 13L (laminar) was rerun several times with various values of b, all other parameters remaining constant. This adjusts the velocity profile so that it climbs to the free-stream value at various rates with distance away from the wall. Very high b corresponds to a boundary-layer velocity profile of negligible thickness - as if the flow were uniform over the surface. Smaller values correspond to thicker velocity profiles, whereas $b = 0$ corresponds to no flow or, equivalently, an infinite boundary-layer thickness. The input data for these calculations are listed as Cases 13L, 13LB, 13LC, and 13LD of Table 4.3, and the results are plotted in Figure 7.7. It is seen that by sweeping out electrons the local flow velocity does play a significant role in breakdown at the actual boundary-layer

---

[11] Note that the quantity determined here is E_e, the effective field strength defined by Equation (3.19a). For air $E_e \simeq \dfrac{E_{rms}}{\left[1 - (36/p\lambda)^2\right]^{1/2}}$. For $p_\lambda > 200$ mm Hg-cm, $E_e \simeq E_{rms}$.

thickness (but, recall, an improperly high ionization frequency) and also that a velocity profile with $b = 10\epsilon_1$ or larger will give about the same result as uniform flow over the surface. However, the density effect, due to shock-wave compression, is considerably larger than the effect of local flow velocity. The velocity effect would be stronger if a more proper ionization frequency were used (Section 7.2.2).

7.2.2 Computations with a more proper ionization frequency

Computations were attempted with the corrected ionization frequency for the same vehicles, vehicle velocities, and altitudes as were used in Section 7.2.1. However, it was discovered that only a very few of the eigenvalues or breakdown voltages could then be found using the 4×4 term representation (16 constants to vary), that is, with 4 terms each for the y- and z-expansions, respectively. Analysis shows that the use of a few more terms in the trial function would alleviate this problem. In fact, 4×5 term representation (5 for the z-dependence at each y) would probably give all the eigenvalues but 4×7 is desirable for good accuracy.

Before discussing the analysis leading to these conclusions and presenting the few computed results obtained, let us examine why this difficulty arose here but not in Section 7.2.1, where the velocities were the same but the ionization frequency was evaluated at the wrong p^* or density.

If the quantity p^*, the modified pressure defined in connection with Equation (5.3), were actually utilized, instead of the improper p, and if p^* is taken constant over all space (at $\left(\frac{E}{E'}\right)_{z=0} = \frac{1}{2}$) in Equations (5.5) and (5.6), the effect is as if the net ionization frequency were a smaller function of P than used in Section 7.2.1 by the factor $(p^*/p)^2$. This factor varies between about 10^{-1} and 10^{-2}. The functional dependence of the ionization frequency on $P = p^*/E'$ and $F(y,z) = E/E'$ is (the product of Eqs. (5.4b) and (5.6b))

$$\frac{\nu}{D} \propto F^2(F - 30P)/P^3 \qquad (7.2)$$

When the coefficient of this function is reduced by the factor $(p^*/P)^2$, the quantity P must become smaller at breakdown. That this is so becomes clear if one notes in Equation (7.2) that when P is smaller, the region of space above the aperture over which ν is positive, and thus gives net electron production rather than loss by attachment, is increased. This causes the diffusion to be spread over a larger volume and results in a decreased diffusion loss rate. This decreased diffusion rate is necessary for the breakdown conditions since the ionization frequency has been reduced by the factor $(p^*/p)^2$. If there were no flow, both the overall diffusion term and net production term are smaller, but balance at breakdown. Thus here the velocity convection term need not be as large to effect the breakdown relation as in Section 7.2.1. Since the velocity term, $(\vec{V}/D) \cdot \nabla(nD)$, tends to vary inversely as the length of the field containing region whereas the diffusion term tends to vary inversely as the square of such a length, one should expect phenomena associated with local flow velocity to be significantly larger due to the smaller ionization frequency. This is, in fact, what was found.

In order to examine numerically the behavior of these eigenvalues with increasing free-stream velocity, the input data of Table 4.3, Case 5, (with the more proper value p^*) were used except with varying values of B_o. With the proper value of $B_o = 31.8$, no eigenvalue could be found for these conditions with 4×4 term representation. With the use of an even more crude 2×2 term representation, the determinant of the coefficients of Equation (5.20) was plotted versus P for various values of B_o in Figure 7.8. (Note the use of a hybrid scale for the value of the determinant.) The first crossing of the "zero axis"[12]

[12] It should be noted that for plotting convenience in Figure 7.8 a value of the determinant of $\pm 10^3$ was considered small enough, relatively, to be considered zero.

gives the eigenvalue (in terms of P which is uniquely related to k^2 and E') for each case. It is seen that the eigenvalue disappears between $B_o = 6$ and $B_o = 7$. The 4 by 4 term representation was then used with $B_o = 7$ and the eigenvalue readily computed and found to be $P = 3.33$ or $E' = 22.3$ volts/cm. This demonstrates that the use of more terms does allow one to obtain eigenvalues that could not be obtained with fewer terms.

The "physical reason" for the above phenomena may be seen as follows: The probable shape of the z-dependence (at a constant y) of the eigenfunctions are sketched schematically in Figure 7.9 for expansions using two-term, three-term, four-term, and five-term functions corresponding to a high value of B_o. Since H_n, the Hermite polynomial, is a polynomial of degree n and is odd if n is odd and even if n is even, these eigenfunctions behave like polynomials of first, second, third, and fourth order multiplied by $e^{-\gamma z^2/2}$. If the loops in Figure 7.9 containing a region of negative slope to the left of the actual maximum (velocity to the right) occur in a region where ν is positive then only "breakdown" can occur and there can be no critical breakdown condition. This is because, at a point in such a loop, the diffusion term is toward the point, tending to increase the electron density, and in the forward part of the loop (slope down) the velocity term is also tending to increase the electron density. Thus all terms in the conservation equation "produce" electrons. The phenomena is absent at lower velocities because the asymmetry demanded of the eigenfunction is smaller at lower velocities.

Finally, in Figures 7.10 and 7.11 we present the only eigenvalues which were obtained using the 4 by 4 representation. The field strengths here may be somewhat in error for the model since high accuracy is not possible here using only a 4 by 4 term representation. The short lines through the single points indicate the estimated behavior of the breakdown curve.

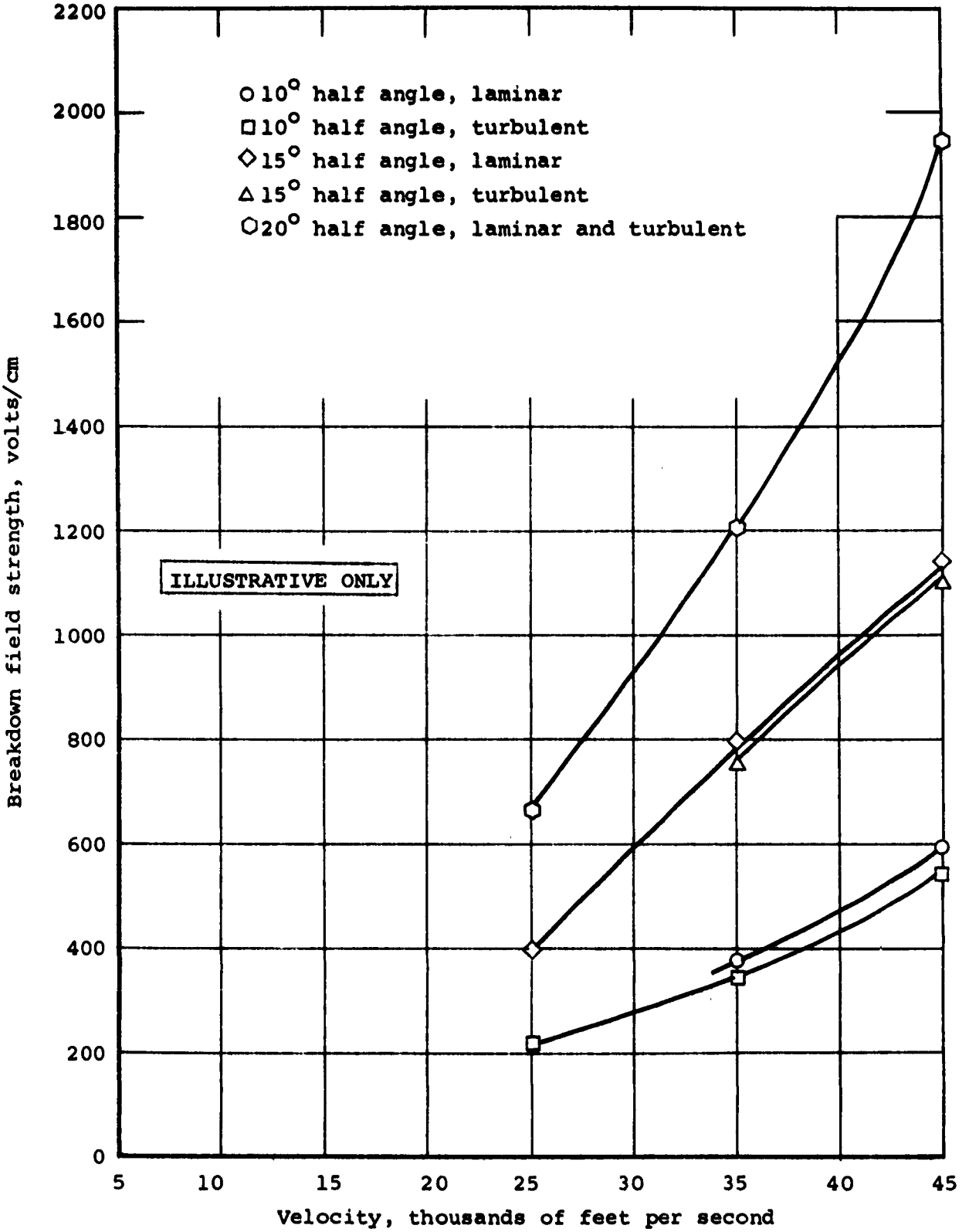

Figure 7.1.- Aperture breakdown field strength versus vehicle velocity for a cone at 200,000-foot altitude and zero angle of attack. For purposes of illustration only. (Improper ionization frequency used. See Section 7.1.)

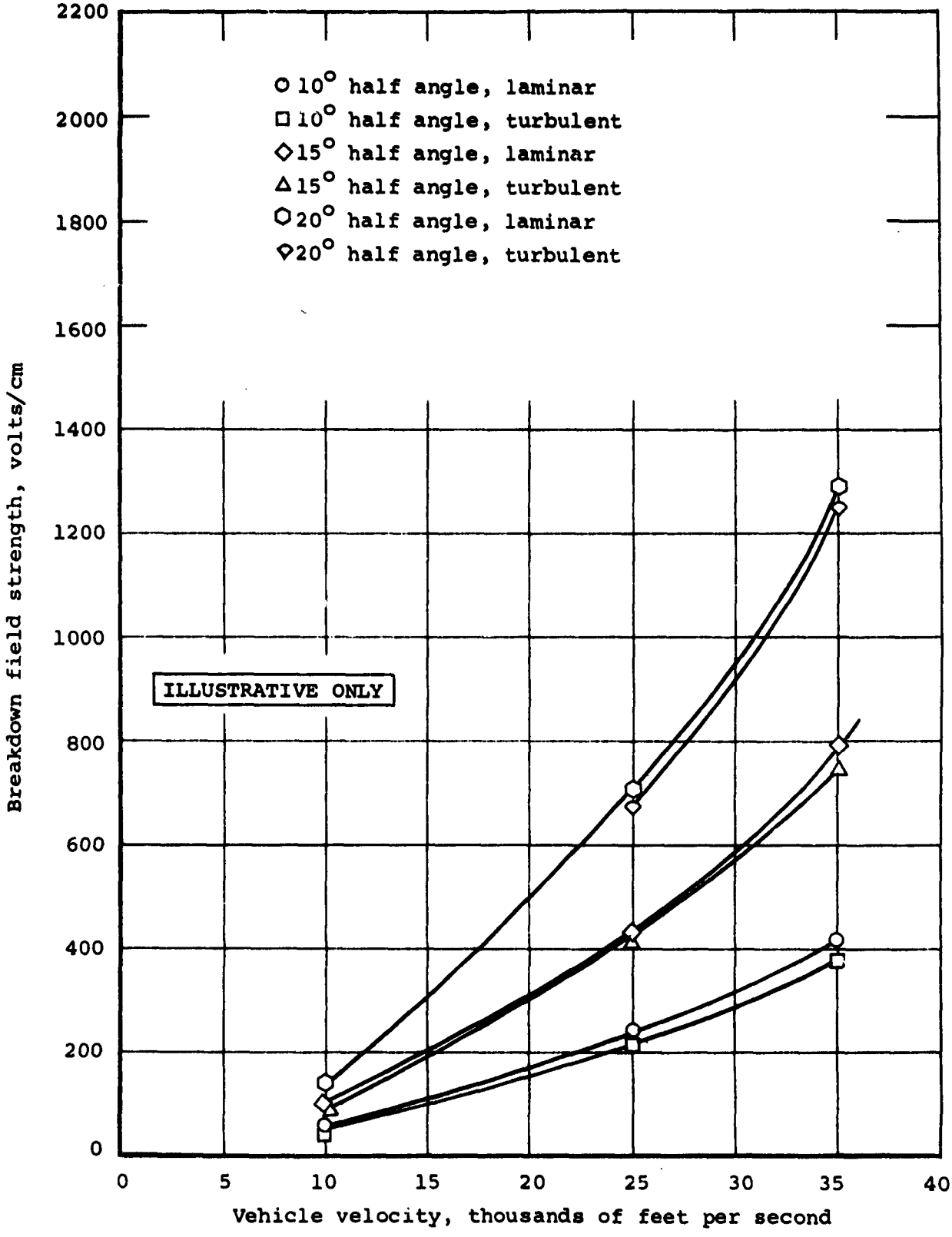

Figure 7.2.- Aperture breakdown field strength versus vehicle velocity for a wedge at 200,000-foot altitude at zero angle of attack. For purposes of illustration only. (Improper ionization frequency used. See Section 7.1.)

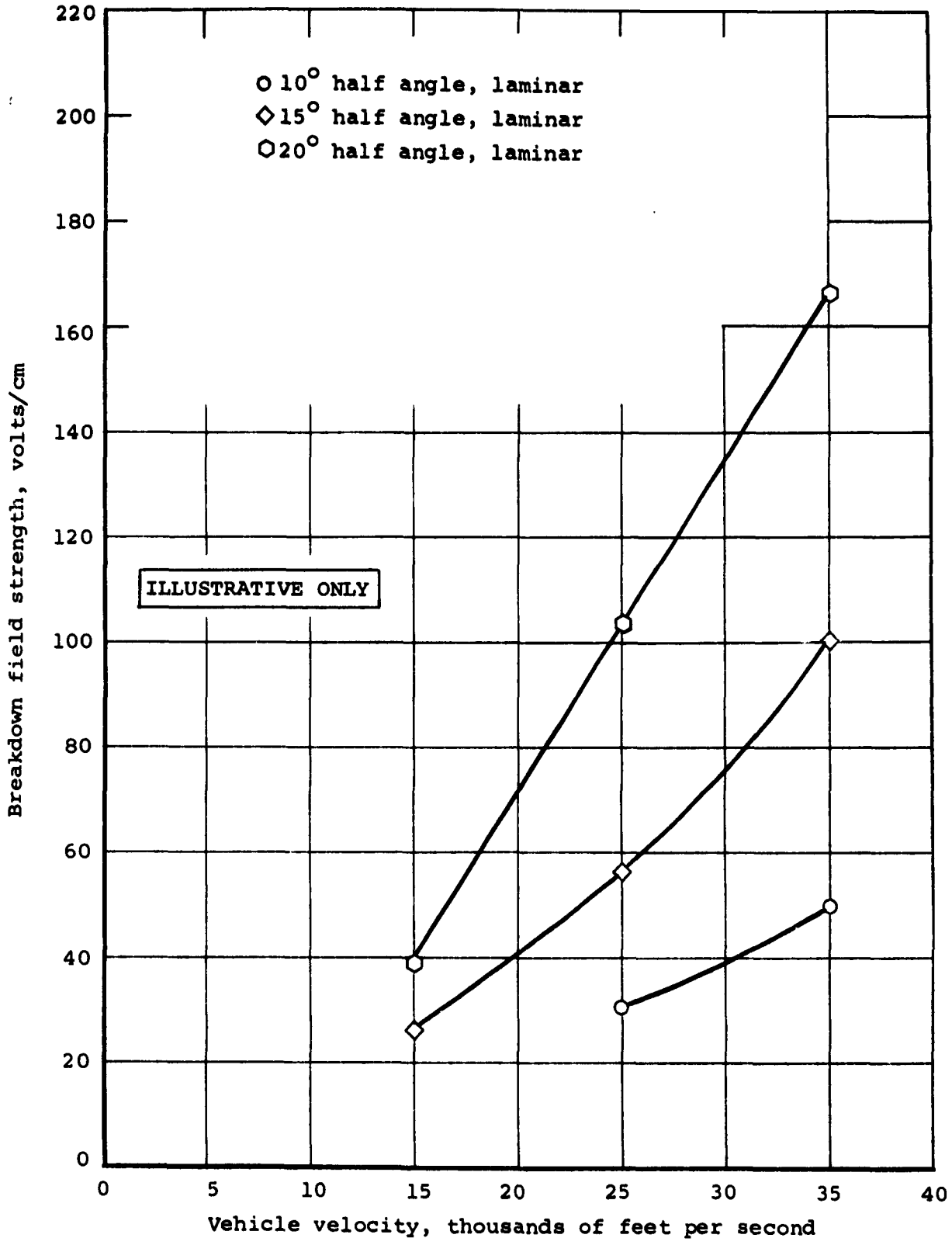

Figure 7.3.- Aperture breakdown field strength versus vehicle velocity for a cone at 250,000-foot altitude at zero angle of attack. For purposes of illustration only. (Improper ionization frequency used. See Section 7.1.)

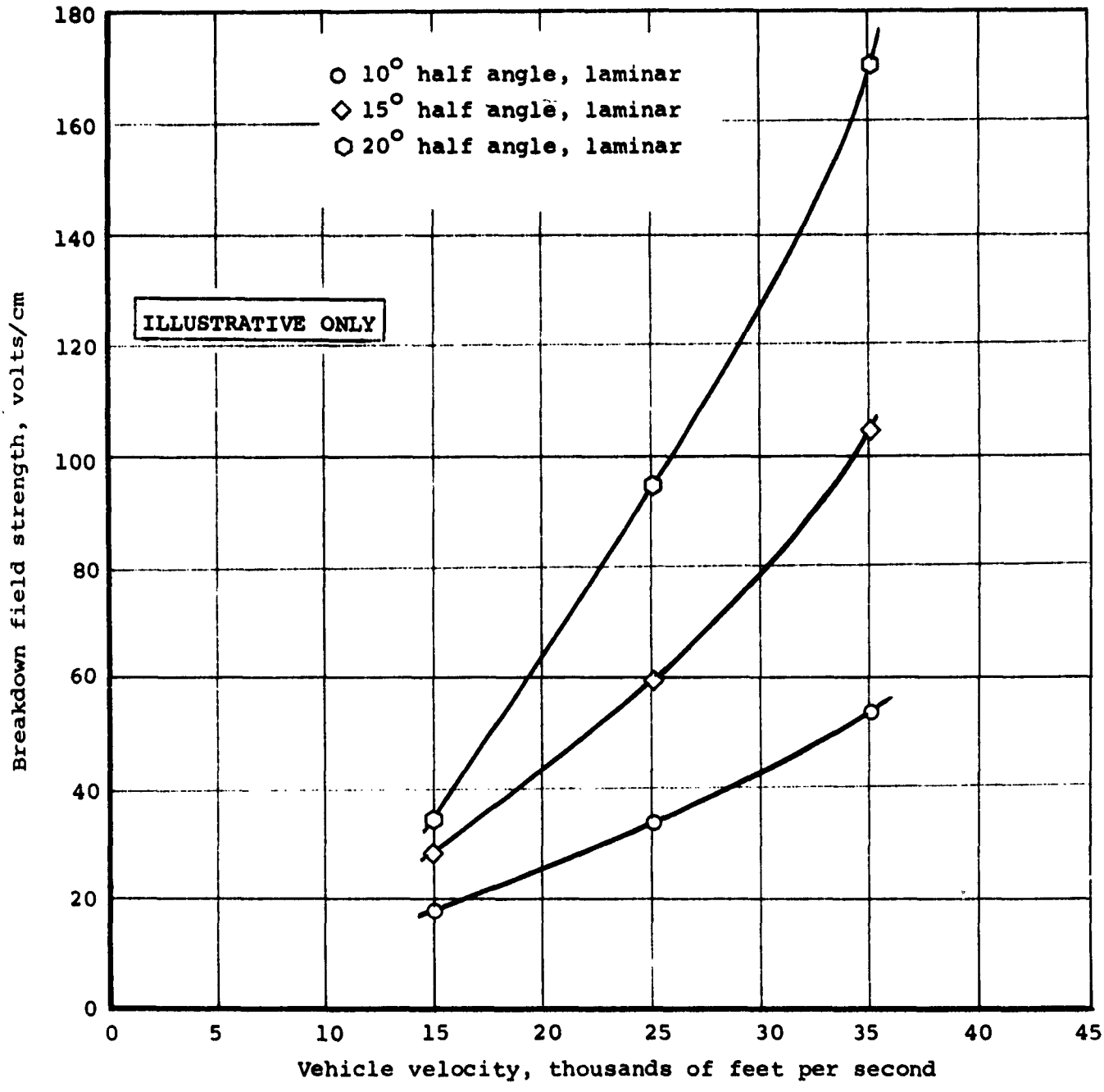

Figure 7.4.- Aperture breakdown field strength versus vehicle velocity for a wedge of 250,000-foot altitude at zero angle of attack. For purposes of illustration only. (Improper ionization frequency used. See Section 7.1.)

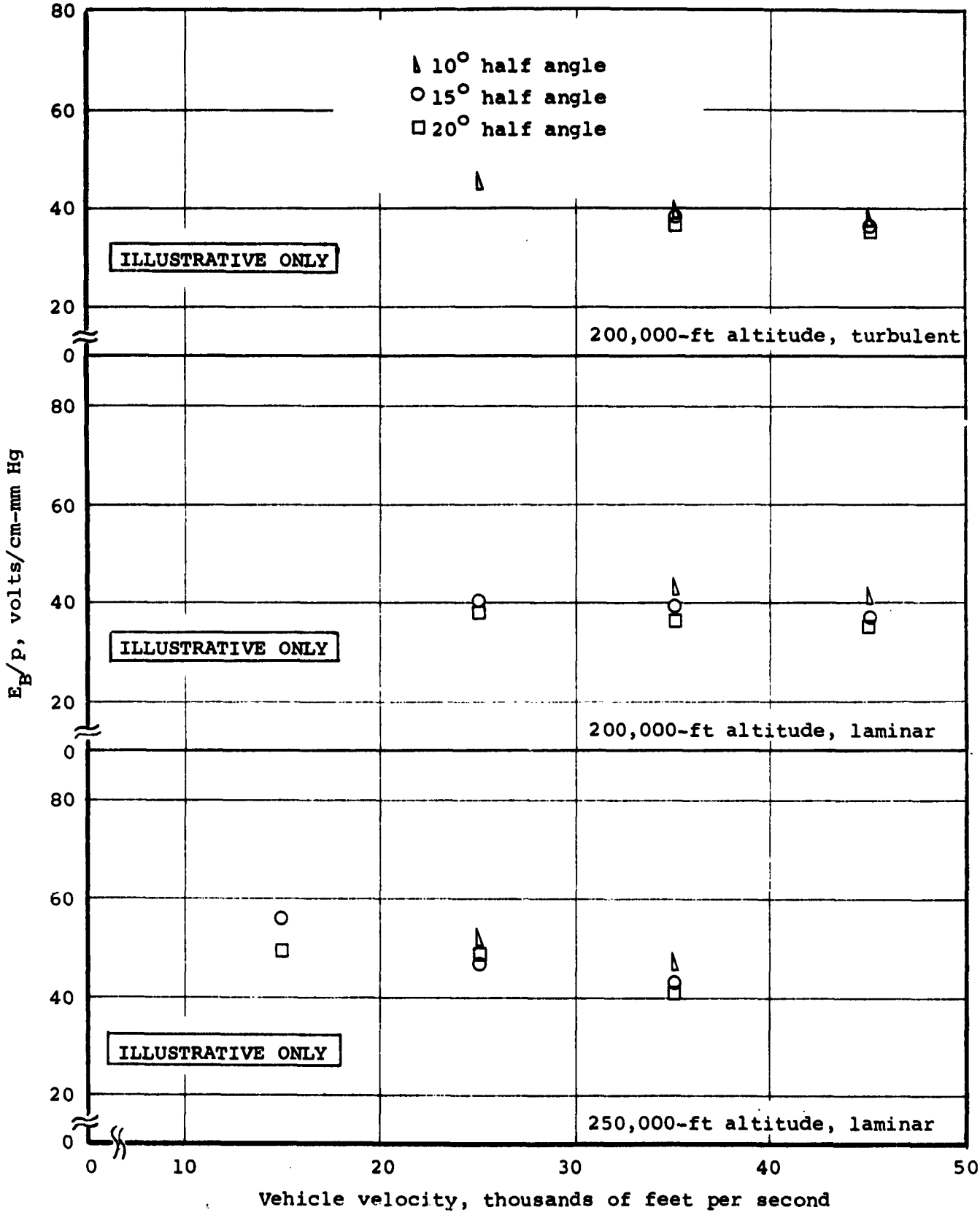

Figure 7.5.- Plots of E_B/p versus vehicle velocity for cones at zero angle of attack. For purposes of illustration only. (Improper ionization frequency used. See Section 7.1.)

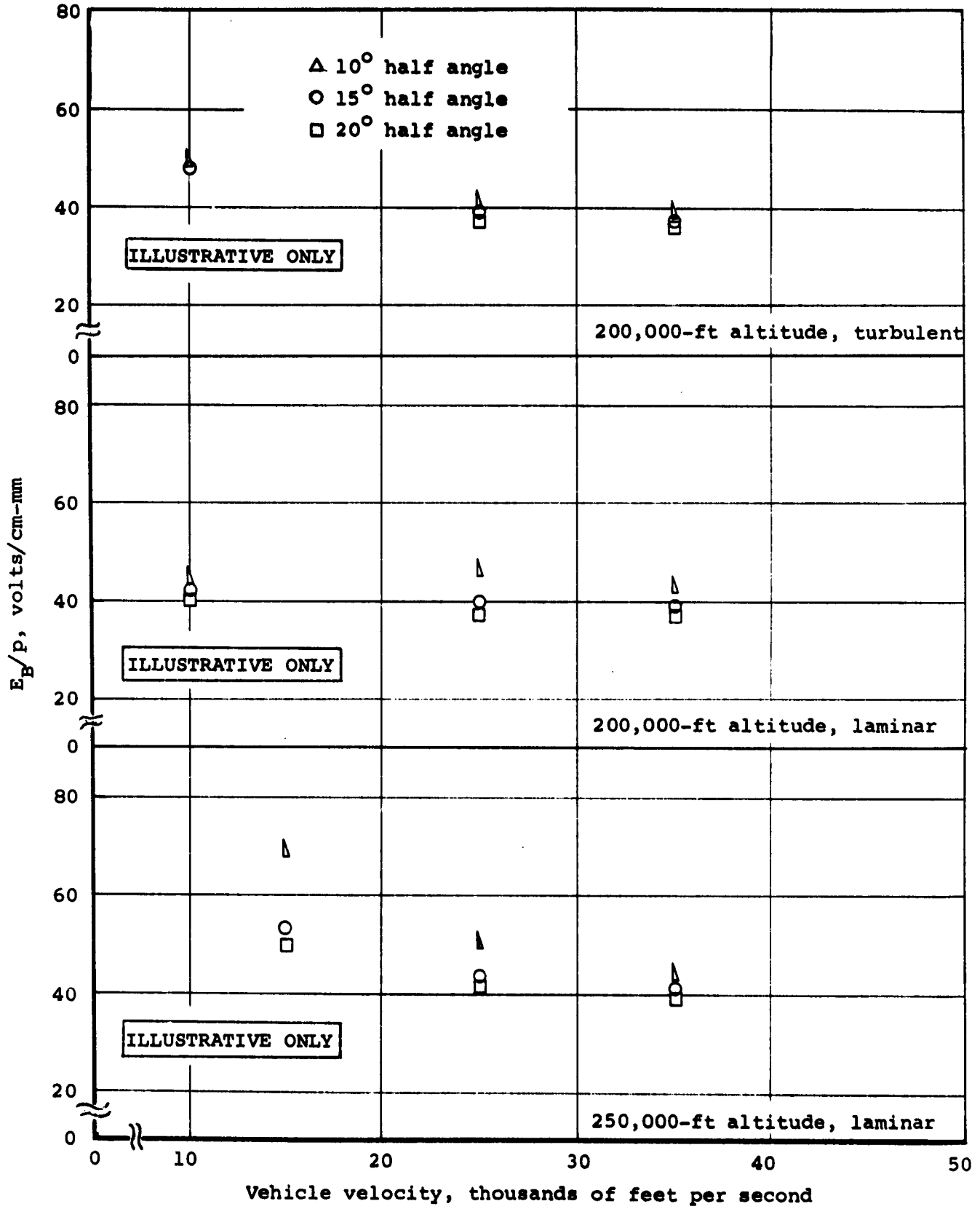

Figure 7.6.- Plots of E_B/p versus vehicle velocity for wedges at zero angle of attack. For purposes of illustration only. (Improper ionization frequency used. See Section 7.1.)

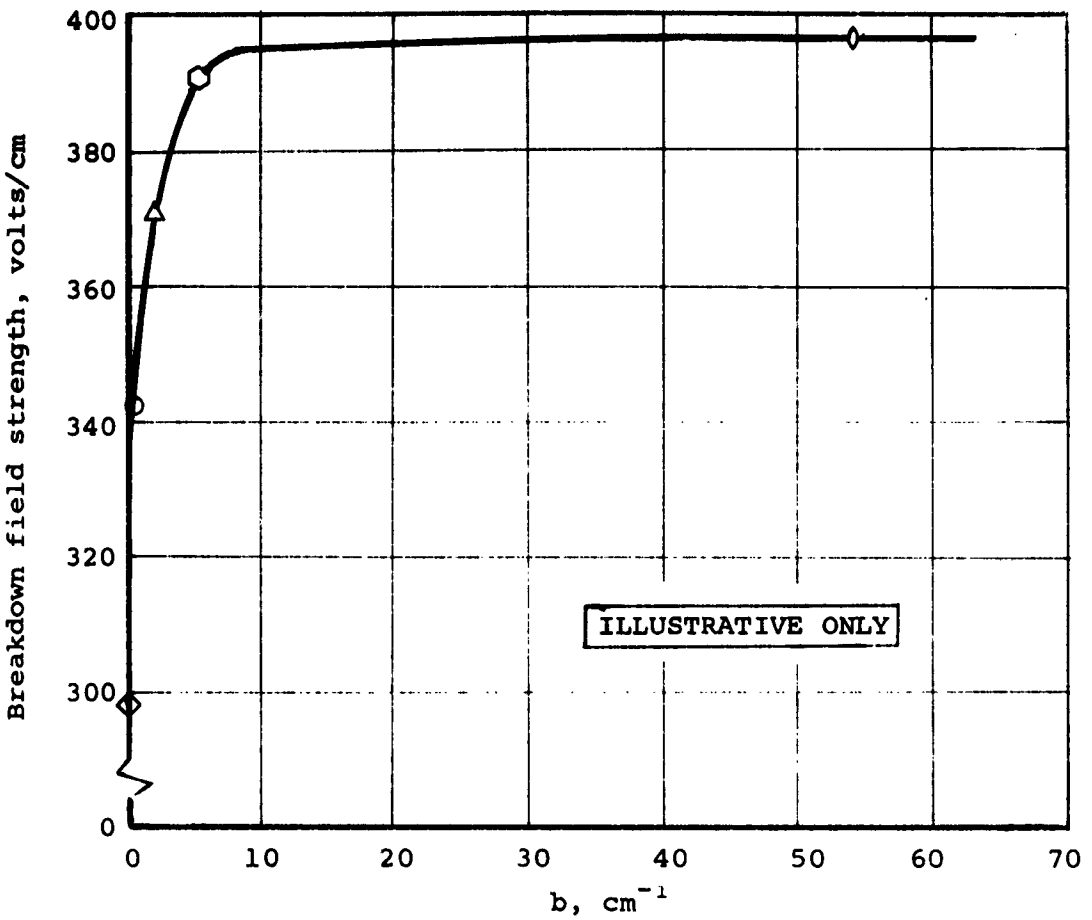

$$V = V_o\,(1 - e^{-by}) \qquad E = E_s e^{-\epsilon_1 y}$$

◇ b = 0 corresponds to infinite boundary-layer thickness or, equivalently, no-flow breakdown

○ b = 1.86 cm^{-1} is the actual value of b for the boundary layer at these conditions

△ b = ϵ_1 = 0.54 cm^{-1}

⬡ b = $10\epsilon_1$

◊ b = $100\epsilon_1$

Figure 7.7.- Effect of varying velocity profile thickness with velocity outside boundary layer and all other parameters held constant. At conditions of the flow field of a 10^0 half-angle cone at 200,000-foot altitude, zero angle of attack, and 35,000-ft/sec velocity at a point 5.73 feet downstream of the vertex. For purposes of illustration only. (Improper ionization frequency used. See Section 7.1.)

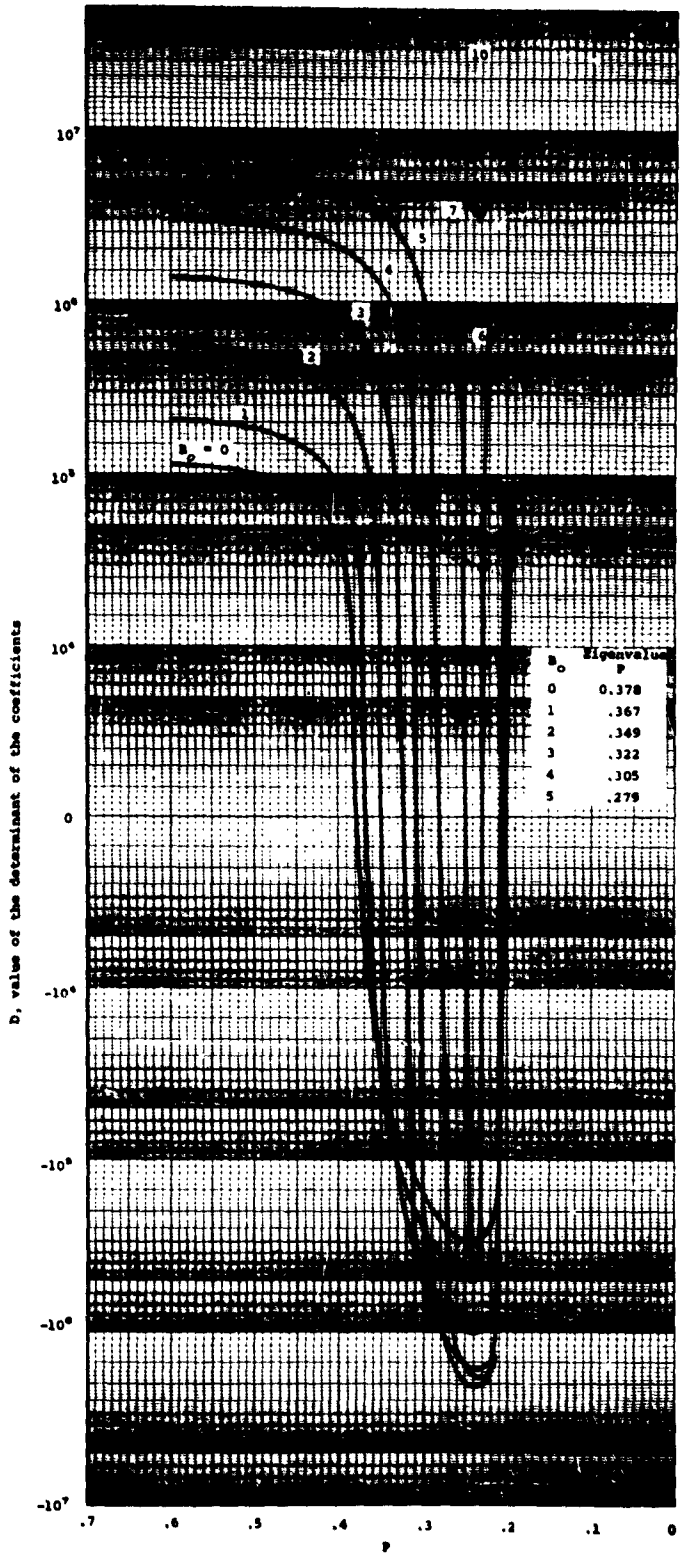

Figure 7.8.- The value of the determinant for Case 6 (see Table 4.3) with varying B_o and 2×2 term representation. Note the hybrid scale for D.

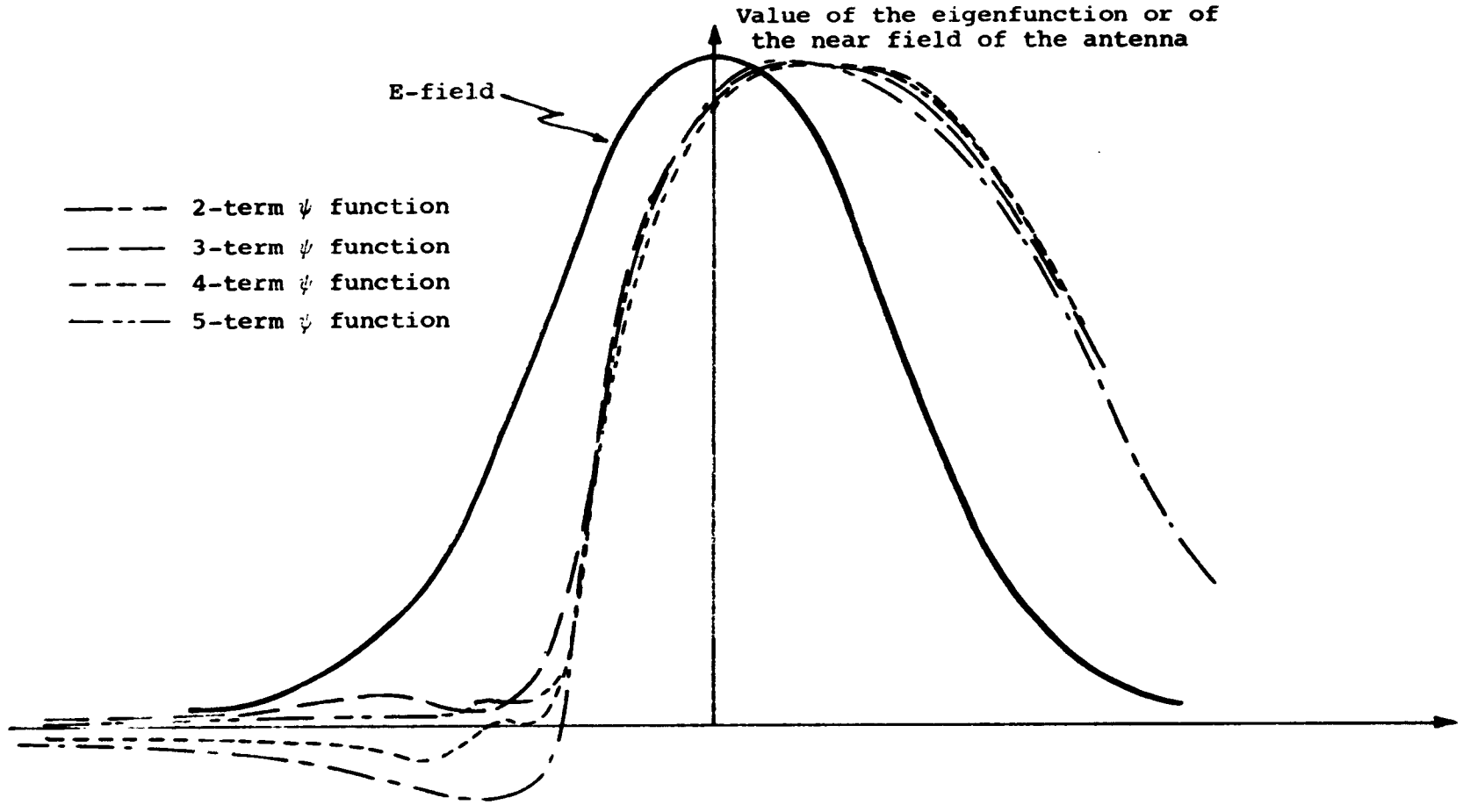

All the eigenfunctions except the five-term one contain loops with negative slope before the actual maximum. If this occurs at a point where E/p^* is greater than 30 volt/cm-mm Hg, then only a breakdown solution can result. The more terms, the less chance that such loops will occur at a given B_o.

Figure 7.9.- Schematic of probable behavior of the trial function with two, three, four, and five terms for z-dependence at constant y.

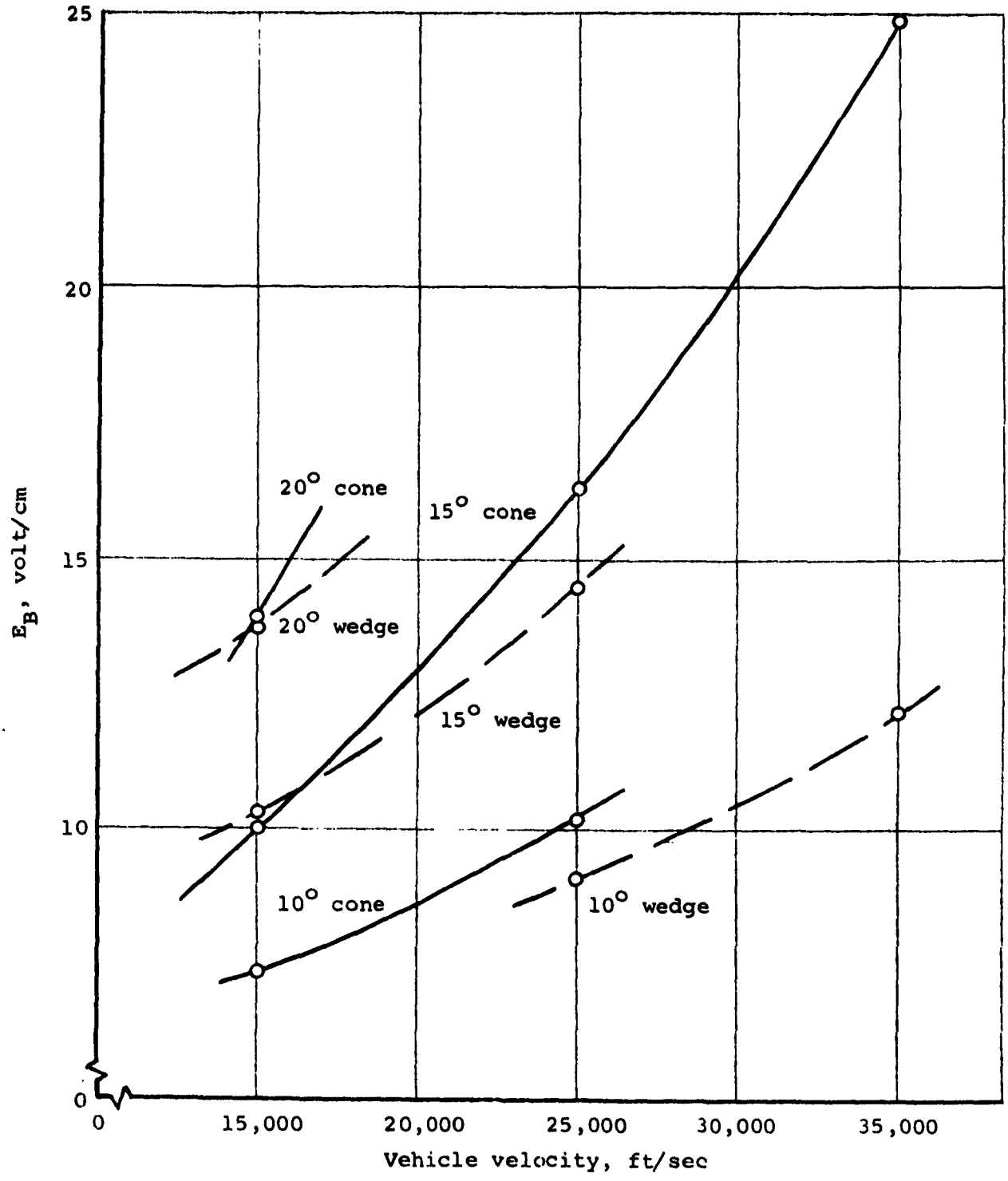

Figure 7.10.- Aperture breakdown field strength versus vehicle velocity at 250,000-foot altitude for wedges and cones for varying half angle at zero angle of attack. The field intensity, E_B, is the field in the antenna aperture at which breakdown will occur.

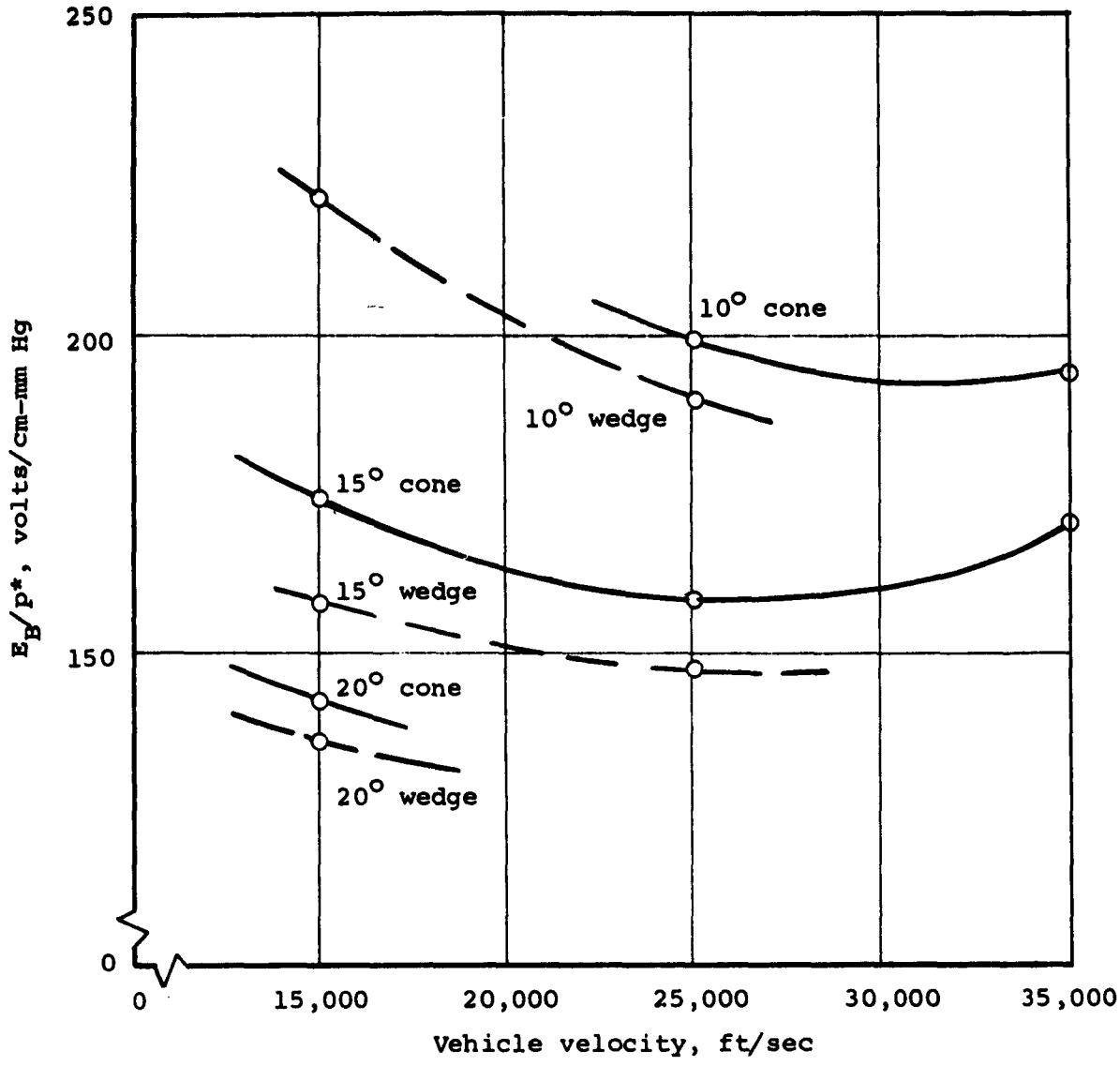

Figure 7.11.- Aperture breakdown field strength divided by p^* versus vehicle velocity at 250,000-foot altitude for wedges and cones of varying half angle at zero angle of attack. The field strength E_B is the field in the antenna aperture at which breakdown occurs. The expression $p^* = (\rho/\rho_o)Z(760)$ is a measure of the particle density in the boundary layer.

8. SUMMARY, CONCLUSIONS, AND RECOMMENDATIONS

8.1 Summary of Work Accomplished

(1) A numerical technique was formulated for obtaining a solution for the antenna breakdown equation giving the field strength at breakdown for any generalized shape of electric field or flow-field condition. We have compared this formulation with existing experimental data for nonflow conditions.

(2) Breakdown conditions were computed for a typical slot antenna mounted on either a wedge- or cone-shaped vehicle under typical high-velocity flight conditions.

(3) A critical examination was performed of the electron conservation equation and the concept of breakdown for c-w, multiple-pulse and single-pulse conditions.

(4) Estimates were derived for the material properties of the gases flowing over the antennas for the range of environmental conditions expected in typical flight situations.

(5) The inviscid and viscous flow fields about the antenna were calculated for several vehicle geometries of interest and over a range of vehicle velocities and altitudes. These results were used in the previously discussed calculations.

8.2 Conclusions

(1) The effect of the vehicle velocity and associated shock wave and boundary layer on the breakdown field strength is not straightforward. It may increase or decrease the breakdown field as follows:

(A) The vehicle velocity tends to <u>increase</u> the breakdown field strength over static breakdown by (a) increasing the density of the gas near the antenna and (b) sweeping out electrons from the critical region near the antenna. The second effect is usually smaller than the first.

(B) The vehicle velocity tends to <u>decrease</u> the breakdown field strength over static breakdown by inducing ionization in the gases above the antenna, changing the diffusion from free to ambipolar and possibly increasing the conductivity of the gas to the point where appreciable absorption of the energy in the electric field results.

(C) The vehicle velocity may either increase or decrease the breakdown field strength due to the induced presence of ablation products or the formation of new air species, each of which may have different ionization and attachment rates than the original air species and which may alter the effective diffusion and ionization coefficients of the air.

In the presence of a low ionization density such that ambipolar diffusion exists already, increasing the vehicle velocity usually tends to increase the breakdown field strength.

Before the relative merits of placing the antenna in the high-pressure upstream regions or downstream on the body can be properly assessed, one must take note of the possible downstream effect of turbulence on electron diffusion. If turbulence increases the electron diffusion sufficiently, a downstream turbulent position may well be best for the antenna. We see that gas density and pointing of the antenna pattern favor the forward position, whereas turbulent diffusion, high flow velocity, and lower background ionization favor the downstream turbulent position. Further extensive calculations using the methods developed in this report would be necessary to assess relative merits at various altitudes and velocities, or for a given trajectory.[13]

---

[13] Note that this discussion concerns only antenna breakdown. The weak-field plasma interaction usually considered may introduce other considerations for antenna placement.

(2) The near-field zone of the antenna is the important region in determining breakdown and the near zone field strength decreases rapidly with distance from the antenna. Therefore, any scheme by which the effective field strength at the edge of the flow field is reduced, such as withdrawing an antenna below the vehicle surface and using a large dielectric cover, will greatly increase the breakdown field strength, allowing large increases in transmitted power without breakdown.

(3) As pointed out in Section 2 the breakdown field strength level may be increased by using pulses rather than c-w and reducing the pulse widths as much as possible. The use of pulsed systems is thus to be desired if other considerations permit.

(4) The necessary macroscopic data for hot air and for hot air with impurities is almost completely unknown and the absolute reliability of estimates of these data is unknown although the data used in this report are believed to be reasonable.

8.3 Recommendations

(1) Additional cases should be computed for the conditions considered in this report as well as others, using more terms for the expansions in the z-direction.

(2) Controlled experiments similar to those suggested in Reference 12 should be performed in order to better fix the macroscopic coefficients necessary to compute the breakdown phenomenon.

(3) Controlled experiments on reentry vehicles should be performed in order to measure breakdown field strengths (power levels) as a function of vehicle shape, altitude, velocity, r.f. frequency, etc. Data available from past flights should be collected and compared with computations performed using the techniques described in this report.

REFERENCES

1. Brown, S. C.: Breakdown in Gases. Alternating and High Frequency Fields. Handbuch d. Physik, vol. XXII, part II, Springer, 1956, p. 531.

2a. Brown, S. C.: Basic Data of Plasma Physics. John Wiley & Sons, 1959.

2b. Brown, S. C. and Allis, W. P.: Basic Data of Electrical Discharges. MIT Res. Lab. of Electronics. Tech. Rep. 283, Fourth Edition, June 9, 1958. (AD 203 458)

3. Gould, L. and Roberts, L. W.: Breakdown at Microwave Frequencies. Jour. Appl. Phys., vol. 27, 1956, p. 1162.

4. Scharfman, W. and Morita, T.: Voltage Breakdown of Antennas at High Altitudes. SRI Tech. Rep. 69, AFCRC TN-60-750, April 1960.

5. Platzman, P. M. and Solt, E. H.: Microwave Breakdown of Air in Nonuniform Electric Fields. Phys. Rev., vol. 119, 1960, p. 1143.

6. Marlotte, G. and Demetriades, A.: Electrical Discharges in Hypersonic Flows. Phys. Fluids, vol. 3, 1960, p. 1028.

7a. Huber, P. W. and Gooderum, P. B.: Experiments with Plasmas Produced by Potassium Seeded Cyanogen-Oxygen Flames for Study of Radio Transmission at Simulated Reentry Vehicle Condition. NASA TN D-627, Jan. 1961.

7b. Ellis, M. C. and Huber, P. W.: Radio Transmission Through the Plasma Sheath Surrounding a Lifting Reentry Vehicle. NASA TN D-507, Jan. 1961.

7c. Chown, J. G.: Study of Plasma Induced Voltage Breakdown at Low Pressure. Final Rep. SRI Proj. No. 3369, July 1961.

8. Romig, M. F.: Steady State Solutions of the Radio Frequency Discharge with Flow. Phys. Fluids, vol. 3, 1960, p. 129.

9. MacDonald, A. D.: High Frequency Breakdown in Air at High Altitudes. Proc. IRE, vol. 47, 1959, p. 456.

10. Whitmer, R. F. and MacDonald, A. D.: RF Antenna Breakdown Conditions in the Presence of a Plasma Sheath. Electromagnetic Effects of Re-entry. Ed. by Rotman and Meltz. Pergamon Press, London, 1961, pp. 149-154.

11. Kelly, D. and Margenau, H.: High Frequency Breakdown of Air. Jour. Appl. Phys., vol. 31, 1960, p. 1617.

12. Ragent, B. and Rudin, M.: Study of Electrical Breakdown Conditions in the Aerodynamic Flow Field of a Hypersonic Vehicle. Semiannual Tech. Rep., Vidya Project No. 64/C, Jan. 30, 1962. Contract No. Nonr 3581(00) under ARPA, Order No. 207-62.

13. Allis, W. P.: Motion of Ions and Electrons. Handbuch d. Physik, vol. XXI, Part I, Springer, 1956, p. 383.

14. Delcroix, J. L.: Introduction to the Theory of Ionized Gases. Interscience, 1960.

15. Shkarofsky, I. P., Bachinski, M. P., and Johnston, T. W.: Collision Frequency Associated with High Temperature Air and Scattering Cross Sections of the Constituents. Electromagnetic Effects of Re-entry. Ed. by Rotman and Meltz. Pergamon Press, London, 1961, p. 24.

16. Spitzer, L.: Physics of Fully Ionized Gases. Interscience, 1956.

17. Ginzburg, V. L. and Gurevich, A. V.: Nonlinear Phenomena in a Plasma Located in an Alternating Electromagnetic Field. Sov. Phys. Uspekhii, vol. 3, 1961, p. 115.

18. Gurevich, A. Y.: Sov. Phys. JETP, vol. 10, 1960, p. 215.

19. Desloge, E. A. and Matthyse, S. W.: Collision Term in the Boltzmann Transport Equation. Amer. Jour. Phys., vol. 28, 1960, p. 1.

20. MacDonald, A. D. and Brown, S. C.: Phys. Rev., vol. 76, 1949, p. 1634; and vol. 75, 1949, p. 411.

21. Smit, J. A.: Physica, vol. 3, 1936, p. 543.

22. Margenau, H.: Phys. Rev., vol. 69, 1946, p. 508.

23. Druyvestein, M. J. and Penning, F. M.: Rev. Mod. Phys., vol. 12, 1940, p. 87.

24. Carleton, N. P. and McGill, L. R.: Electron Energy Distribution in Slightly Ionized Air Under the Influence of Electric and Magnetic Fields. Phys. Rev., vol. 126, 1962, p. 2089.

25. Chapman, S. and Cowling, T. G.: The Mathematical Theory of Non-Uniform Gases. Cambridge Univ. Press, Cambridge, Massachusetts, 1953.

26. Morse, P. M. and Feshbach, H.: Methods of Mathematical Physics. McGraw-Hill Book Co., Inc., 1953, p. 1108.

27. Gröbner, W. and Hofreiter, N.: Integraltafel, Zweite Teil, Bestimmte Integrale. 2nd Improved Edition, Springer, 1957.

28. von Engel, A.: Ionization in Gases by Electrons in Electric Fields. Handbuch d. Physik, vol. XXI, Part I, Springer, 1956, p. 504.

29a. Harrison, M A. and Geballe, R.: Phys. Rev., vol. 91, 1953, p. 1.

29b. Crompton, R. W., Huxley, G. H., and Sutton, D. J.: Proc. Roy. Soc., London, vol. A218, 1953, p. 507.

29c. Healey, R. W. and Reed, J. W.: The Behavior of Slow Electrons in Gases. Analytical Wireless of Australia Ltd., Sydney, 1941.

30. Schulz, G. F.: Phys. Rev., vol. 125, 1962, p. 229.

31. Crompton, R. W. and Sutton, D. J.: Proc. Roy. Soc. A., vol. 215, 1952, p. 467.

32. King, R. W. P.: The Theory of Linear Antennas. Harvard University Press, 1956.

33. Gilmore, F. R.: Equilibrium Composition and Thermodynamic Properties of Air to 24,000° K. RM-1543, The Rand Corporation, 1955.

34. Nielsen, J. N., et al.: Effects of Supersonic and Hypersonic Speed on Aerial Photography. Vidya Rep. No. 37, Jan. 1961, Appendix VIIIA, p. VIII-21. Vidya, Inc., Palo Alto, California, U. S. Army Engineer, Geodesy, Intelligence and Mapping, Res. and Dev. Agency, Fort Belvoir, Viginia, Contract No. DA-44-009-ENG 3990, Proj. No. 8-35-12-420.

35. Kaufman, H. R.: Electron Diffusion in a Turbulent Plasma. NASA TN D-1324, June 1962.

36. McCuen, P. A., Donnelly, P. F., and Tickner, E.: Flow-Field Properties about a Hemisphere Cone Reentry Body with 8.75° Semivertex Angle. Vidya Rep. No. 78, July 6, 1962.

37. Moeckel, W. E.: Oblique-Shock Relations at Hypersonic Speeds for Air in Chemical Equilibrium. NACA TN 3895, Jan. 1957.

38. Minzner, R. A., Champion, K. S. W., and Pond, H. L.: The ARDC Model Atmosphere, 1959. AFCRC-TR-59-267, O.T.S. PB161305, Department of Commerce, Washington, D. C., August 1959.

39. Romig, M.: Conical Flow Parameters for Air in Dissociation Equilibrium. Convair Scientific Research Laboratory, Research Rep. No. 7, May 15, 1960.

APPENDIX A

THE ELECTRON KINETIC EQUATION UNDER FLOW CONDITIONS

In Reference 12, the kinetic equation for electrons, as derived in References 1, 13, 14, 17, 18, or 19, is generalized for the case of a coordinate system in which the gas is flowing. It is found that one effect of the flow is to drag the electrons along with the flow, giving rise to extra collision terms. However, it is pointed out in Reference 12 that one can avoid the consideration of these terms entirely by first adopting a coordinate system that moves with the flow, one for which these extra terms vanish. The equation is then essentially the same as derived by the previously mentioned authors, and we can then make the transformation

$$\vec{r}_{new} = \vec{r}_{old} + \vec{V}\left(t_{old} - t_o\right)$$

$$t_{new} = t_{old} - t_o$$

where $\vec{V} = V(y)\vec{k}$ is the flow velocity. Here we have not changed the electron velocity coordinates so that the electron velocity distribution still describes the electron random velocity, $\vec{c} = \vec{v} - \vec{V}$, but in a stationary coordinate system. The only change in the equation due to the transformation is the appearance of a $V \cdot \nabla F_e$ term.

Let us describe very briefly the derivation of the kinetic equation. It is assumed that the velocity dependence of F_e, the density in phase space of electrons, may be expanded in spherical harmonics about some, as yet arbitrary, polar axis. A good argument that terms higher than the first two may be neglected may be found in Reference 17. Then we include only

$$F_e = F_o + \vec{c} \cdot \vec{F}_1 \qquad (A.1)$$

when in the moving coordinate system. This then is substituted into the kinetic equation. After discarding collision terms of order $(m/M)^2$, the two linearly independent equations of lowest order become

$$\frac{\partial F_o}{\partial t} + \frac{c^2}{3} \nabla \cdot \vec{F}_1 - \frac{e\vec{E}}{3mc^2} \cdot \frac{\partial}{\partial c} \left(c^3 \vec{F}_1 \right) = \frac{m}{Mc^2} \frac{\partial}{\partial c} \left[c^3 \nu_{en} \left(F_o + \frac{kT}{mc} \frac{\partial}{\partial c} F_o \right) \right] - \left(\nu_I + \nu_X + \nu_R + \nu_A - q \right) F_o \tag{A.2}$$

and

$$\frac{\partial}{\partial t} \left(\vec{c} \cdot \vec{F}_1 \right) + \nu_{en} \left(\vec{c} \cdot \vec{F}_1 \right) = - c \cdot \nabla F_o + \frac{e\vec{E}}{m} \cdot \frac{\vec{c}}{c} \frac{\partial}{\partial c} F_o \tag{A.3}$$

where q gives the rate at which electrons appear or reappear at a particular velocity after inelastic collisions.

These equations contain two more assumptions. First, it is evident that charge-charge collisions have been neglected. This assumes

$$\frac{2m}{M} \nu_{en} \gg \nu_{ee} \tag{A.4}$$

since an electron can transfer on the average only $2m/M$ of its energy in a single collision with a heavy particle. This restriction may be lifted and the analysis extended to

$$\nu_{en} \gg \nu_{ee} \tag{A.5a}$$

with the treatment in Reference 17. The results of this extension, which modifies the equations only slightly, are contained in Section 3.1.1.

Another assumption contained in Equations (A.2) and (A.3) is that E is independent of F_e. This assumption precludes the possibility of plasma resonance oscillations. The assumption is valid if the applied frequency satisfies

$$\omega >> \omega_p = 2\pi \left(\frac{n_p e^2}{\pi m}\right)^{1/2} = 2\pi(8.97\times10^3) n_p^{1/2}$$

At $\lambda = 1$ cm, this gives

$$n_p << \left(\frac{10^{14}}{9}\right) cm^{-3} \qquad \text{(A.5b)}$$

This, in practice, is far less restrictive than Equation (A.5a) as expressed in Equation (3.3). However, it does cause some difficulty in treating the single pulse breakdown criteria (see Section 2.3.2).

Let $E = E_o \cos \omega t$ and let F_o be expanded in a Fourier series

$$F_o = \sum_{s=o}^{\infty} F_o^s \cos s\omega t \qquad \text{(A.6)}$$

where the coefficients may be functions of time (i.e., relaxing), but $(\partial F_o^s/\partial t)/F_o^s << \omega/2\pi$. Substitution of this expansion into Equation (A.3) and then solving the resulting equation, gives

$$\vec{F}_1 = -\sum_{s=o}^{\infty} \left\{ \nabla F_o^s \left(\frac{\nu_{en} \cos s\omega t + s\omega \cos s\omega t}{\nu_{en}^2 + s^2\omega^2} \right) \right.$$

$$- \frac{e\vec{E}_o}{2m} \frac{1}{c} \frac{\partial}{\partial c} F_o^s \left[\frac{\nu_{en} \cos(s+1)\omega t + (s+1)\omega \sin(s+1)\omega t}{\nu_{en}^2 + (s+1)^2\omega^2} \right.$$

$$\left. \left. + \frac{\nu_{en} \cos(s-1)\omega t + (s-1)\omega \sin(s-1)\omega t}{\nu_{en}^2 + (s-1)^2\omega^2} \right] \right\} \qquad \text{(A.7)}$$

Here we have neglected transients in the solution for $\vec{F}_1$, which behave as $\exp(-\nu_{en} t)$. This assumes then, that $(\partial F_o^s/\partial t)/F_o^s << \nu_{en}$

(if it were not, one could neglect the time dependence entirely as relaxation would occur quickly) and that $1/\nu_{en}$ is a negligible time. Instead, one could assume that $\vec{F}_1 = 0$ at $t = 0$.

Substitution of Equations (A.7), (A.6), and $E = E_o \cos \omega t$ into Equation (A.2), and separation of linearly independent terms gives for the equation governing F_o^o

$$\frac{\partial}{\partial t} F_o^o - \frac{c}{3} \nabla \cdot \left[\frac{1}{\nu_{en}} \left(\nabla F_o^o - \frac{e\vec{E}_o}{2m} \frac{1}{c} \frac{\partial}{\partial c} F_o^1 \right) \right]$$

$$- \frac{e\vec{E}_o}{6mc^2} \cdot \frac{\partial}{\partial c} \left[c^3 \left(\frac{\nu_{en}}{\nu_{en}^2+\omega^2} \right) \nabla F_o^1 \right] - \frac{e^2 E_o^2}{6m^2c^2} \frac{\partial}{\partial c} \left[\frac{\nu_{en}}{\nu_{en}^2+\omega^2} c^2 \frac{\partial}{\partial c} \left(F_o^o + \frac{1}{2} F_o^2 \right) \right]$$

$$= \frac{m}{Mc^2} \frac{\partial}{\partial c} \left[c^3 \nu_{en} \left(F_o^o + \frac{kT}{mc} \frac{\partial}{\partial c} F_o^o \right) \right] - \left(\nu_I + \nu_X + \nu_A + \nu_R - q \right) F_o^o$$

(A.8)

The terms involving F_o^1 are generally very small compared to the similar terms in F_o^o and are usually neglected.[1] These terms are due to pushing the alternating component of the electron density back and forth and the diffusion away from this alternating component. This alternating component should be negligible compared to the average electron density, except near plasma resonance (i.e., where Eq. (A.5b) is not satisfied).

The term in F_o^2 is a heating term due to second harmonic oscillations. Phenomenological attempts to estimate the effect of this term seem to indicate that it is equivalent, at most, to increasing the E_{eff}/p by 6 volts/cm-mm Hg. This largest correction occurs at $p\lambda \geq 5000$ cm-mm Hg and is negligible for $p\lambda \sim 1$ cm-mm Hg or less (see, e.g., Section 3.2.4).

---

[1] Regarding the neglect of F_o^1, see also Reference 13, bottom half of page 407.

With neglect of these terms and the subsequent transformation of the position and time variables, as mentioned above, Equation (A.8) becomes Equation (3.3). Also, substitution of Equation (A.7) into (A.1) gives Equation (3.1), if only first terms are retained.

For the d.c. case under the same approximations (which includes $(\partial F_1/\partial t)/F_1 \ll \nu_{en}$), Equation (A.3) has the solution

$$\vec{F}_1 = \frac{1}{\nu_{en}} \left(- \nabla F_o + \frac{e\vec{E}}{m} \frac{1}{c} \frac{\partial}{\partial c} F_o \right)$$

Substitution of this into Equation (A.2) gives the same equation as in the a.c. case with E_{dc}^2 replacing $E_{rms}^2/(1 + \omega^2/\nu_{en}^2)$ where $\vec{E} = \sqrt{2}\, \vec{E}_{rms} \cos \omega t$.

APPENDIX B

A VARIATIONAL PRINCIPLE FOR EIGENVALUES

In Reference 26, page 1109, it is pointed out that if Γ, Ω, $\tilde{\Gamma}$, and $\tilde{\Omega}$ are linear differential operators such that they satisfy

$$\int \phi \Gamma \psi \, d\tau = \int \psi \tilde{\Gamma} \phi \, d\tau \tag{B.1}$$

and

$$\int \phi \Omega \psi \, d\tau = \int \psi \tilde{\Omega} \phi \, d\tau \tag{B.2}$$

Then the condition that, for a definite pair of functions ϕ and ψ,

$$k^2 = \frac{\int \phi \Gamma \psi \, d\tau}{\int \phi \Omega \psi \, d\tau} \tag{B.3}$$

does not change with first-order changes in ψ and ϕ demands that ψ satisfy

$$\Gamma \psi = k^2 \Omega \psi \tag{B.4}$$

and ϕ satisfy

$$\tilde{\Gamma} \phi = k^2 \tilde{\Omega} \phi \tag{B.5}$$

so long as the functions ψ and ϕ (and thus the first-order changes in ψ and ϕ as well) satisfy Equations (B.1) and (B.2). Such a function ϕ is generally written $\tilde{\psi}$ and called the adjoint of ψ. Also, $\tilde{\Gamma}$ is the adjoint operator of Γ and $\tilde{\Omega}$ is the adjoint operator of Ω.

Let us apply these facts to our particular problem. Consider Equation (5.1)

$$-k^2 = \frac{\int \tilde{\psi}\left[\nabla^2 - \nabla\cdot\left(\vec{B}\right]\psi\, d\tau\right.}{\int \tilde{\psi} G\psi\, d\tau} \tag{B.6}$$

Let us take the first-order variation

$$\delta(k^2) \equiv k^2(\psi + \delta\psi,\ \tilde{\psi} + \delta\tilde{\psi}) - k^2(\psi,\ \tilde{\psi})$$

where ψ, $\tilde{\psi}$, $\delta\psi$, and $\delta\tilde{\psi}$ all vanish on the boundaries of the region,[1] then

$$-\delta(k^2) = \frac{\delta\int \tilde{\psi}\left[\nabla^2 - \nabla\cdot\left(\vec{B}\right]\psi\, d\tau\right.}{\int \tilde{\psi} G\psi\, d\tau} - \frac{\int \tilde{\psi}\left[\nabla^2 - \nabla\cdot\left(\vec{B}\right]\psi\, d\tau\right.}{\left(\int \tilde{\psi} G\psi\, d\tau\right)^2}\,\delta\int \tilde{\psi} G\psi\, d\tau \tag{B.7}$$

Note that

$$\delta\int \tilde{\psi}\left[\nabla^2 - \nabla\cdot\left(\vec{B}\right]\right.\psi\, d\tau = \int\left\{\delta\tilde{\psi}\left[\nabla^2 - \nabla\cdot\left(\vec{B}\right]\right.\psi + \tilde{\psi}\left[\nabla^2 - \nabla\cdot\left(\vec{B}\right]\right.\delta\psi\right\} d\tau$$

$$= \left\{\delta\tilde{\psi}\left[\nabla^2 - \nabla\cdot\left(\vec{B}\right]\right.\psi + \delta\psi\left(\nabla^2 + \vec{B}\cdot\nabla\right)\tilde{\psi}\right\} d\tau$$

$$+ \int_S \left(\tilde{\psi}\nabla\,\delta\psi - \delta\psi\,\nabla\tilde{\psi} + \vec{B}\tilde{\psi}\,\delta\psi\right)\cdot\hat{n}\, da \tag{B.8}$$

where vector identities and Gauss' integral theorem have been used. This surface integral vanishes because $\tilde{\psi}$ and δ both vanish on the boundaries. Then by substituting Equation (B.8) into (B.7), using (B.6) again, and setting $\delta(k^2)$ equal to zero, one obtains

---

[1]The boundaries here are $y = 0$, $y = \infty$, $z = \pm\infty$, $x = \pm\infty$.

$$\int \delta\tilde{\psi} \left\{ \left[\nabla^2 - \nabla\cdot\left(\mathbf{B}\right] + Gk^2 \right\} \psi \, d\tau + \int \delta\psi \left[\left(\nabla^2 + \mathbf{B}\cdot\nabla \right) + Gk^2 \right] \tilde{\psi} \, d\tau = 0$$

If this expression is to vanish for all possible changes in $\tilde{\psi}$ and ψ, the two integrands must vanish. This gives Equations (2.9) and (5.2).

APPENDIX C

DEVELOPMENT OF k^2 WITH ORTHOGONAL POLYNOMIALS

For development of $\iint \psi(\partial^2/\partial y^2 + \partial^2/\partial z^2)\psi \, dy \, dz$ we will need some identities. From Reference 27, entries 177.4a, b, and c, we have

$$\frac{dH_n^\gamma}{dz} = 2n\gamma H_{n-1}^\gamma \tag{C.1a}$$

$$H_{n+2}^\gamma - 2\gamma z H_{n+1}^\gamma + 2(n+1)\gamma H_n^\gamma = 0 \tag{C.1b}$$

$$\frac{d^2H_n^\gamma}{dz^2} - 2\gamma z \frac{dH_n^\gamma}{dz} + 2n\gamma H_n^\gamma = 0 \tag{C.1c}$$

In addition, one can derive from Equations (C.1a) and (C.1b)

$$\frac{d}{dz}\left(e^{-\gamma z^2} H_n^\gamma\right) = - e^{-\gamma z^2} H_{n+1}^\gamma \tag{C.1d}$$

For the Laguerre polynomials we will need the identities 176.4a and b of Reference 27, namely,[1]

$$L_{n+2}^{\alpha,2} + (\alpha y - 2n - 5) L_{n+1}^{\alpha,2} + (n+1)(n+3) L_n^{\alpha,2} = 0 \tag{C.2a}$$

$$y \frac{d^2}{dy^2} L_n^{\alpha,2} + (3 - \alpha y) \frac{d}{dy} L_n^{\alpha,2} + n\alpha L_n^{\alpha,2} = 0 \tag{C.2b}$$

---

[1] Recall $L_n^{\alpha,2}$ here is $L_n(y, \alpha, 3)$ in Reference 27.

In addition one can derive[2] from Equation (5.10a)

$$y \frac{d}{dy} L_n^{\alpha,2} = (\alpha y - n - 3) L_n^{\alpha,2} + L_{n+1}^{\alpha,2} \tag{C.2c}$$

Using Equations (C.1b) and (C.1c) there follows:

$$\frac{\partial^2}{\partial z^2}\left(e^{-\frac{\gamma z^2}{2}} H_n^{\gamma}\right) = \left[\frac{1}{4} H_{n+2}^{\gamma} - \left(\frac{1}{2} + n\right) \gamma H_n^{\gamma} + n(n-1)\gamma^2 H_{n-2}^{\gamma}\right] e^{-\frac{\gamma z^2}{2}} \tag{C.3}$$

Similarly by use of Equations (C.2b) and (C.2c) there follows:

$$\frac{\partial^2}{\partial y^2}\left(e^{-\frac{\alpha y}{2}} y L_n^{\alpha,2}\right) = \left\{\left[\frac{n+3}{y} - \alpha(n+2) + \frac{\alpha^2}{4} y\right] L_n^{\alpha,2} - \frac{1}{y} L_{n+1}^{\alpha,2}\right\} e^{-\frac{\alpha y}{2}} \tag{C.4}$$

From Equations (C.3), (C.4), and (5.9) there follows immediately:

$$\iint \tilde{\psi}_{m',n'} \left(\frac{\partial^2}{\partial y^2} + \frac{\partial^2}{\partial z^2}\right) \psi_{m,n} \, dy \, dz = (-1)^{n'} Q_{m',n'}^{m,n}$$

---

[2]Using Equation (5.10a)

$$y\left(\frac{d}{dy}\right) L_n^{\alpha,2} = y\left(\alpha - \frac{2}{y}\right) e^{\alpha y} y^{-2}\left(\frac{d^n}{dy^n}\right)\left(e^{-\alpha y} y^{n+2}\right) + y^{-2} e^{\alpha y} y \left(\frac{d^{n+1}}{dy^{n+1}}\right)\left(y^{n+2} e^{-\alpha y}\right)$$

but

$$y \frac{d^{n+1}}{dy^{n+1}}\left(y^{n+2} e^{-\alpha y}\right) = \frac{d}{dy}\left[y \frac{d^n}{dy^n}\left(y^{n+2} e^{-\alpha y}\right)\right] - \frac{d^n}{dy^n}\left(y^{n+2} e^{-\alpha y}\right)$$

$$= \frac{d^2}{dy^2}\left[y \frac{d^{n-1}}{dy^{n-1}}\left(y^{n+2} e^{-\alpha y}\right)\right] - 2 \frac{d^n}{dy^n}\left(y^{n+2} e^{-\alpha y}\right)$$

$$= \cdots$$

$$= \left(\frac{d^{n+1}}{dy^{n+1}}\right)\left(y^{n+3} e^{-\alpha y}\right) - (n+1) \frac{d^n}{dy^n}\left(y^{n+2} e^{-\alpha y}\right)$$

from these two results Equation (C.2c) follows.

where $Q^{m,n}_{m',n'}$ is defined by Equations (5.12), (5.15), and (5.16). Thus with Equation (5.8)

$$\iint \tilde{\psi}\, \nabla^2_{2-D}\, \psi \, dy\, dz = \sum_{m',n'} \sum_{m,n} (-1)^{n'}\, Q^{m,n}_{m',n'}\, A_{m',n'}\, A_{m,n}$$

For evaluation of

$$\iint \tilde{\psi}\, B \cdot \nabla\psi \, dz\, dy = \iint \tilde{\psi}\, B_o \left(1 - e^{-by}\right) \frac{\partial}{\partial z} \psi \, dy\, dz$$

use of Equation (C.1a) and (C.1b) gives immediately

$$\int \tilde{\psi}_{m',n'}\, B \cdot \nabla\psi_{m,n} \, dy\, dz = (-1)^{n'}\, N^{m,n}_{m',n'}$$

where $N^{m,n}_{m',n'}$ is defined by Equations (5.13), (5.15), and (5.16). Thus

$$\iint \tilde{\psi}\, B \cdot \nabla\psi \, dy\, dz = \sum_{m,n} \sum_{m',n'} (-1)^{n'}\, N^{m,n}_{m',n'}\, A_{m',n'}\, A_{m,n}$$

Similarly, it immediately follows (without any of the identities of Eqs. (C.1) or (C.2)) that

$$\iint \tilde{\psi} G \psi \, dy\, dz = \sum_{m,n} \sum_{m',n'} (-1)^{n'}\, M^{m,n}_{m',n'}\, A_{m',n'}\, A_{m,n}$$

APPENDIX D

REDUCTION RELATIONS FOR THE $I^{\gamma,\eta}_{m,n}$

By use of Equation (C.1b) we have

$$I^{\gamma,\eta}_{m,n} = \int_{-\infty}^{\infty} e^{-(\gamma+\eta)z^2} H^{\gamma}_{m} H^{\gamma}_{n}\, dz = \int_{-\infty}^{\infty} e^{-(\gamma+\eta)z^2} H^{\gamma}_{m} \left[\frac{2\gamma z H^{\gamma}_{n+1} - H^{\gamma}_{n+2}}{2(n+1)\gamma}\right] dz$$

$$= -\frac{1}{2(n+1)\gamma} I^{\gamma,\eta}_{m,n+2} + \int_{-\infty}^{\infty} \frac{z}{n+1} e^{-(\gamma+\eta)z^2} H^{\gamma}_{m} H^{\gamma}_{n+1}\, dz$$

or integrating the last term by parts and using Equation (C.1a)

$$I^{\gamma,\eta}_{m,n} = -\frac{1}{2(n+1)\gamma} I^{\gamma,\eta}_{m,n+2} + \frac{1}{2(n+1)(\eta+\gamma)} \left[2m\gamma I^{\gamma,\eta}_{m-1,n+1} + 2(n+1)\gamma I^{\gamma,\eta}_{m,n}\right] \quad (D.1)$$

From this, form the following three expressions: one by taking $m = n + 2$; another by taking $m = n + 2$ and then increasing n by one $(n \to n + 1)$; a third by taking $m = n$ and then increasing n by one. From these three expressions eliminate $I^{\gamma,\eta}_{n+3,n+1}$ and $I^{\gamma,\eta}_{n+2,n}$ obtaining

$$I_{n+3,n+3} = 2(2n+5)\frac{\gamma^2}{\gamma+\eta} I_{n+2,n+2} - 4(n+2)^2 \gamma^2 \frac{\gamma-\eta}{\gamma+\eta} I_{n+1,n+1} \quad (D.2)$$

If now n is decreased by three $(n \to n - 3)$ one obtains Equation (5.17). To obtain Equation (5.18) take $m = n + 2\nu$ in Equation (D.1).

APPENDIX E

REDUCTION RELATION FOR THE $J^{c\ \alpha,\eta}_{m,n}$

By use of Equation (C.2a) we have

$$J^{c\ \alpha,\eta}_{m,n} \equiv \int_0^\infty y^c e^{-(\alpha+\eta)y}\, L_m^{\alpha,2}\, L_n^{\alpha,2}\, dy = -\alpha\ J^{c+1\ \alpha,\eta}_{m,n-1} + (2n+1)\ J^{c\ \alpha,\eta}_{m,n-1}$$

$$- (n^2 - 1)\ J^{c\ \alpha,\eta}_{m,n-2} \qquad (E.1)$$

To obtain an expression with which we can eliminate J^{c+1} from Equation (E.1), we use Equation (C.2c) twice - first with $yL_m^{\alpha,2}$ and then instead with $yL_n^{\alpha,2}$ - add the results and divide by two to obtain

$$\alpha\ J^{c+1\ \alpha,\eta}_{m,n} \equiv \alpha \int_0^\infty y^{c+1} e^{-(\alpha+\eta)y}\, L_m^{\alpha,2}\, dy$$

$$= \frac{1}{2} \int_0^\infty y^{c+1} e^{-(\alpha+\eta)y}\, \frac{\partial}{\partial y} \left(L_m^{\alpha,2}\, L_n^{\alpha,2} \right) dy$$

$$+ \left(\frac{n+m+6}{2} \right) J^{c\ \alpha,\eta}_{m,n} - \frac{1}{2} \left(J^{c\ \alpha,\eta}_{m,n+1} + J^{c\ \alpha,\eta}_{m+1,n} \right)$$

or integrating the first term on the right by parts one finds

$$\alpha\ J^{c+1\ \alpha,\eta}_{m,n} = \left(\frac{\alpha+\eta}{2} \right) \int_0^\infty y^{c+1} e^{-(\alpha+\eta)y}\, L_m^{\alpha,2}\, L_n^{\alpha,2}\, dy$$

$$+ \left(\frac{m+m+5-c}{2} \right) J^{c\ \alpha,\eta}_{m,n} - \frac{1}{2} \left(J^{c\ \alpha,\eta}_{m+1,n} + J^{c\ \alpha,\eta}_{m,n+1} \right)$$

then solving for $J^{c+1}_{m,n}$

$$\left(\frac{\alpha - \eta}{2}\right) J^{c+1}_{m,n} = \left(\frac{m + n + 5 - c}{2}\right) J^{c}_{m,n} - \frac{1}{2}\left(J^{c}_{m+1,n} + J^{c}_{m,n+1}\right) \quad (E.2)$$

Substitution from Equation (E.2) for $J^{c+1}_{m,n-1}$ into Equation (E.1) gives

$$-\eta\, J^{c}_{m,n} = \alpha\, J^{c}_{m+1,n-1} - \alpha(m + n + 4 - c)\, J^{c}_{m,n-1}$$

$$+ (2n + 1)(\alpha - \eta)\, J^{c}_{m,n-1} + (n^2 - 1)(\alpha - \eta)\, J^{c}_{m,n-2} \quad (E.3)$$

Examination shows that this reduction relation is still not adequate. It can be further developed by use of Equation (C.2a). Note that

$$L^{\alpha,2}_m L^{\alpha,2}_n = L^{\alpha,2}\left[(-\alpha y + 2n + 1)\, L^{\alpha,2}_{n-1} + (n - 1)(n + 1)\, L^{\alpha,2}_n\right]$$

$$= L_{m+1}L_{n-1} + (2n + 1)\, L_m L_{n-1} - (n^2 - 1)\, L_m L_{n-2}$$

$$- (2m + 3)\, L_m L_{n-1} + m(m + 2)\, L_{m-1}L_{n-1}$$

Then solving for $L_{m+1}L_{n-1}$, multiplying by $e^{-(\alpha+\eta)y}\, y^c$ and integrating, one finds from this last expression

$$J^{c}_{m+1,n-1} = J^{c}_{m,n} + 2(m - n + 1)\, J^{c}_{m,n-1} + (n^2 - 1)\, J^{c}_{m,n-2}$$

$$- m(m + 2)\, J^{c}_{m-1,n-1} \quad (E.4)$$

Then use this to eliminate $J_{m+1,n-1}$ from Equation (C.3) and gather like terms. This results in Equation (5.19).

TECHNICAL REPORTS ISSUED UNDER CONTRACT Nonr 3581(00), TASK NR 061-124

Chief of Naval Research
Department of the Navy
Washington 25, D. C.
Attn: Code 438 (3)
419 (1)
421 (1)
461 (1)

Commanding Officer
Office of Naval Research
Branch Office
495 Summer Street
Boston 10, Massachusetts (1)

Commanding Officer
Office of Naval Research
Branch Office
The John Crerar Library Building
86 East Randolph Street
Chicago 1, Illinois (1)

Commanding Officer
Office of Naval Research
Branch Office
346 Broadway
New York 13, New York (1)

Commanding Officer
Office of Naval Research
Branch Office
Navy #100, Box 39
Fleet Post Office
New York, New York (15)

Commanding Officer
Office of Naval Research
Branch Office
1030 East Green Street
Pasadena 1, California (1)

Commanding Officer
Office of Naval Research
Branch Office
1000 Geary Street
San Francisco 9, California (1)

Director
Naval Research Laboratory
Washington 25, D. C.
Attn: Code 2000 (6)
2020 (1)
7611 (Dr. A.C.Kolb) (1)

Commanding Officer and Director
David Taylor Model Basin
Washington 7, D. C.
Attn: Dr. F.H.Frankiel(Code 108a)(1)
Aerodynamics Laboratory (1)
Library (1)

Chief, Bureau of Naval Weapons
Department of the Navy
Washington 25, D.C.
Attn: Code RMGA-61 (1)
RAAD-34 (1)
RAAE-4 (1)

Commander
U.S. Naval Weapons Laboratory
Dahlgren, Virginia
Attn: Technical Library (1)

Commander
Naval Ordnance Test Station
China Lake, California
Attn: Code 5006 (1)
753 (1)

Commander
Naval Ordnance Laboratory
White Oak, Maryland
Attn: Aeroballistics Division (1)
Aerophysics Division (1)
Ballistics Department
(Dr.A.E.Seigel) (1)
Gas Dynamics Division (1)
Library (1)

Chief, Bureau of Yards and Docks
Department of the Navy
Washington 25, D. C.
Attn: Code 70 (1)
72 (1)

Commanding Officer and Director
U.S.Naval Civil Engineering Lab
Port Hueneme, California
Attn: Code L54 (1)

Superintendent
Naval Postgraduate School
Monterey, California
Attn: Technical Reports Librarian (1)

Commander
U.S. Naval Missile Center
Point Mugu, California
Attn: Technical Library (1)

Commanding Officer
NROTC & Naval Administrative Unit
Massachusetts Institute of Technology
Cambridge 39, Massachusetts (1)

Commander
Air Force Missile Test Center
APMTC Technical Library (MU 135)
Patrick Air Force Base, Florida (1)

Executive Director
Air Force Office of Scientific Research
Washington 25, D. C.
Attn: Mechanics Division (3)

Headquarters
USAF (AFRD)
Attn: DCS/LNT-USC
Air Force Unit Post Office
Los Angeles 45, California (1)

J.L.Potter, Manager
Research Branch, VKF
ARO, Incorporated
Arnold Air Force Station
Tennessee (2)

ARO, Incorporated
ARDC Library
Arnold Air Force Station
Tennessee (1)

Mr. Lukasiewicz, Chief
Gas Dynamics Facility
ARO, Incorporated
Arnold Air Force Station
Tennessee (1)

WADC (WCOSSI)
Wright-Patterson Air Force Base
Ohio (1)

Commander
Wright Air Development Command
Wright-Patterson Air Force Base
Ohio
Attn: Library (1)

ASD (ASRDF-1)
Wright-Patterson Air Force Base
Ohio (1)

ARL (ARB)
Building 450
Wright-Patterson Air Force Base
Ohio (1)

Elmer G. Johnson, Chief
Fluid Dynamics Facilities Branch
Aeronautical Research Laboratory
Wright-Patterson Air Force Base
Ohio (1)

United States Army Research Office
(Durham)
Box CM, Duke Station
Durham, North Carolina (1)

Commanding General
Aberdeen Proving Ground, Maryland
Attn: Technical Library (BRL) (1)

Dr. J. H. Fraser
Internal Ballistics Laboratory
Aberdeen Proving Ground, Maryland (1)

Dr. C. W. Lampson
Technical Director
Ballistic Research Laboratories
Aberdeen Proving Ground, Maryland (1)

Dr. J. Sternberg
Ballistics Research Laboratory
Aberdeen Proving Ground, Maryland (1)

Dr. F. D. Bennett
Exterior Ballistics Laboratory
BRL
Aberdeen Proving Ground, Maryland (1)

Army Rocket and Guided Missile Agency
Research Laboratory, RSD Operations
Attn: ORDXR-RR
Redstone Arsenal, Alabama (1)

Chief
Defense Atomic Support Agency
Washington 25, D. C. (1)

Executive Secretary
Weapons System Evaluation Group
Office of the Secretary of Defense
The Pentagon
Washington 25, D. C. (1)

Ames Research Center
National Aeronautics and Space
Administration
Moffett Field, California
Attn: Library (1)

Langley Research Center
National Aeronautics and Space
Administration
Langley Field, Virginia
Attn: Library (1)

Lewis Research Center
National Aeronautics and Space
Administration
21000 Brookpark Road
Cleveland 35, Ohio
Attn: Library (1)

National Aeronautics and Space
Administration
150 Pico Boulevard
Santa Monica, California (1)

Director
National Bureau of Standards
Washington 25, D. C.
Attn: Electron Physics Section (1)
Equation of State Section (1)
Fluid Mechanics Section (1)
Mathematical Physics Sect. (1)
Library (1)
Dr. D. H. Tsai (1)

Dr. Lewis M. Branscomb
Chief, Atomic Physics Division
National Bureau of Standards
Washington 25, D. C. (1)

Dr R. N. Thomas
National Bureau of Standards
Boulder Laboratories
Boulder, Colorado (1)

U.S. Atomic Energy Commission
Office of Technical Information
Extension
P.O. Box 62
Oak Ridge, Tennessee (1)

U.S. Atomic Energy Commission
Technical Information Service
Washington 25, D. C.
Attn: Technical Librarian (1)

National Science Foundation
Division of Mathematical, Physical,
and Engineering Sciences
Washington 25, D. C.
Attn: Engineering Sciences Program
Office (1)

Armed Services Technical Information
Agency
Arlington Hall Station
Arlington, Virginia (10)

Dr. M. Abele
General Applied Science Lab, Inc.
Westbury, Long Island, New York (1)

Professor J. O. Akerman
Institute of Technology
University of Minnesota
Minneapolis 14, Minnesota (1)

Professor A. Bleakney
Palmer Physical Laboratory
Princeton University
Princeton, New Jersey (1)

Mr. Wallace F. Davis, President
VIDYA, Incorporated
2626 Hanover Street
Palo Alto, California (1)

Mr. R. L. Deming, Jr.
Assistant Head, Engineering
and Sciences Extension
University of California
2451 Bancroft Way
Berkeley 4, California (1)

Professor G. L. Von Rosenberg
Department of Aeronautical and
Astronautical Engineering
Ohio State University
2036 Neil Avenue
Columbus 10, Ohio (1)

Professor Antonio Ferri
Aerodynamics Laboratory
Polytechnic Institute of Brooklyn
527 Atlantic Avenue
Freeport, New York (1)

Professor R. G. Fowler
Physics Department
University of Oklahoma
Norman, Oklahoma (1)

Dr. I. E. Glass
Institute of Aerophysics
University of Toronto
Toronto 5, Ontario (1)

Dr. Meredith C. Gourdine
Electro & Magneto Fluid Dynamics Lab.
Plasmadyne Corporation
3839 S. Main Street
Santa Ana, California (1)

Professor P. P. Hsieh, Chairman
Chemistry Department
Princeton University
Princeton, New Jersey (1)

Dr. Arthur Kantrowitz, Director
AVCO-Everett Research Laboratory
2385 Revere Beach Parkway
Everett 49, Massachusetts (1)

Professor Otto Laporte
University of Michigan
Physics Department
Ann Arbor, Michigan (1)

Professor H. Liepmann
Department of Aeronautics
California Institute of Technology
Pasadena 4, California (1)

Professor G. S. S. Ludford
Department of Mechanics
Cornell University
Ithaca, New York (1)

Dr. L. Marton
Electron Physics
National Bureau of Standards
Washington, D. C. (1)

Dr. F. K. Moore, Director
Aero-Sciences Division
Cornell Aeronautical Laboratory, Inc.
P. O. Box 235
Buffalo 21, New York (1)

Dr. Boris Regent
VIDYA, Incorporated
2626 Hanover Street
Palo Alto, California (1)

Professor E. L. Resler
Graduate School of Aeronautical
Engineering
Cornell University
Ithaca, New York

Dr. S. A. Schaaf
University of California
Department of Engineering
Berkeley, California (1)

Professor A. H. Shapiro
Department of Mechanical Engineering
Massachusetts Institute of Technology
Cambridge 39, Massachusetts (1)

Professor F. Sherman
Aeronautical Engineering Department
University of Michigan
Ann Arbor, Michigan (1)

Professor K. Stewartson
Department of Mathematics
University of Durham
Science Laboratories
South Road
Durham, England (1)

Professor G. H. Thomas
Research Professor
New Mexico State University
Research Center, Box 756
University Park, New Mexico (1)

Professor A. B. Arons
Department of Physics
Amherst University
Amherst, Massachusetts (1)

Division of Applied Mathematics
Brown University
Providence 12, Rhode Island (1)

Professor Bostin
Division of Engineering
Brown University
Providence 12, Rhode Island (1)

Professor Hoefer
Division of Engineering
Brown University
Providence 12, Rhode Island (1)

Professor Probstein
Division of Engineering
Brown University
Providence 12, Rhode Island (1)

Professor S. S. Penner
Engineering Division
California Institute of Technology
Pasadena 4, California (1)

Jet Propulsion Laboratory
4800 Oak Grove Drive
Pasadena, California
Attn: Library (1)

Professor H. S. Pleasant
Engineering Division
California Institute of Technology
Pasadena 4, California (1)

Professor C. B. Millikan, Director
Guggenheim Aeronautical Laboratory
California Institute of Technology
Pasadena 4, California (1)

Professor L. Lees
Guggenheim Aeronautical Laboratory
California Institute of Technology
Pasadena 4, California (1)

Professor F. Zwicky
Department of Physics
California Institute of Technology
Pasadena 4, California (1)

Professor G. Kuerti
Department of Mechanical Engineering
Case Institute of Technology
10900 Euclid Avenue
Cleveland 6, Ohio (1)

Professor P. Roach
Columbia University
New York, New York (1)

Professor W. Sears
Graduate School of Aeronautical
Engineering
Cornell University
Ithaca, New York (1)

Dr. A. Hertzberg
Cornell Aeronautical Laboratory
4455 Genesee Street
Buffalo, New York (1)

Dr. G. Miller
Denver Research Institute
University Park Campus
Denver University
Denver 10, Colorado (1)

Professor C. F. Carrier
Pierce Hall
Harvard University
Cambridge 38, Massachusetts (1)

Professor H. Emmons
Department of Engineering Sciences
Harvard University
Cambridge 38, Massachusetts (1)

Professor L. Goldberg
Harvard College Observatory
Cambridge 38, Massachusetts (1)

Dr. Fred L. Whipple
60 Garden Street
Cambridge 38, Massachusetts (1)

Dr. T. Paul Torda, Director
Fluid Dynamics and Propulsion Research
Armour Research Foundation
10 West 35th Street
Chicago 16, Illinois (1)

School for Applied Mathematics
Indiana University
Bloomington, Indiana (1)

Professor F. H. Clauser
Department of Aeronautics
Johns Hopkins University
Baltimore 18, Maryland (1)

Professor R. J. Emrich
Department of Physics
Lehigh University
Bethlehem, Pennsylvania (1)

Professor John R. Markham
Room 33-107
Department of Aeronautics and
Astronautics
Massachusetts Institute of Technology
Cambridge, Massachusetts (1)

Professor I. Amdur
Massachusetts Institute of Technology
Cambridge, Massachusetts (1)

Professor George A. Brown
Massachusetts Institute of Technology
3-164
77 Massachusetts Avenue
Cambridge 39, Massachusetts (1)

Professor H. C. Hottel
Department of Chemical Engineering
Massachusetts Institute of Technology
Cambridge 39, Massachusetts (1)

Professor C. C. Lin
Department of Mathematics
Massachusetts Institute of Technology
Cambridge 39, Massachusetts (1)

Department of Mechanical Engineering
Massachusetts Institute of Technology
Cambridge 39, Massachusetts (1)

Professor B. Bederson
Physics Department
New York University
University Heights
New York 53, New York (1)

Professor J. J. Stoker
Institute of Mathematical Sciences
4 Washington Place
New York 3, New York (1)

Professor J. F. Ludloff
Guggenheim School of Aeronautics
New York University
New York 53, New York (1)

Professor Ali Bulent Cambel
Department of Mechanical Engineering
Northwestern University
Evanston, Illinois (1)

Dr. Loren E. Bollinger
The Ohio State University
Rocket Research Laboratory
2240 [illegible] Road
Columbus 10, Ohio (1)

Professor [illegible]
Department of Physics [illegible]
Pennsylvania State University
University Park, Pennsylvania (1)

Professor [illegible]
Forrestal Research Center
Princeton, New Jersey (1)

Professor [illegible]
Department of Aeronautical Engineering
Princeton University
Princeton, New Jersey (1)

Professor L. Spitzer, Jr.
Princeton University Observatory
Princeton, New Jersey (1)

Professor [illegible]
Department of Aeronautical Engineering
Rensselaer Polytechnic Institute
Troy, New York (1)

Dr. C. [illegible]
Stanford Research Institute
Menlo Park, California (1)

Professor [illegible]
Applied Mathematics and Statistics Laboratory
Stanford University
Stanford, California (1)

Department of Aeronautical Engineering
Stanford University
Stanford, California (1)

Professor [illegible]
Department of Aeronautical Engineering
Stanford University
Stanford, California (1)

Professor [illegible]
Mechanical Engineering Department
William M. Rice Institute
Box 1892
Houston 1, Texas (1)

Professor [illegible]
Division of Aeronautical Sciences
University of California
Berkeley 4, California (1)

Professor [illegible]
University of California
Berkeley, California (1)

Professor [illegible]
Division of Mechanical Engineering
University of California
Berkeley 4, California (1)

Dr. [illegible]
Radiation Laboratory
University of California
Livermore, California (1)

Dr. [illegible]
Radiation Laboratory
University of California
Livermore, California (1)

Dr. [illegible]
Los Alamos Scientific Laboratory
University of California
Los Alamos, New Mexico (1)

Dr. [illegible]
Physics Division
Los Alamos Scientific Laboratory
University of California
Los Alamos, New Mexico (1)

Dr. [illegible]
[illegible] Street
Midland, Michigan (1)

Professor [illegible]
Department of Engineering
University of California
Los Angeles 24, California (1)

Dean L.M.K. Boelter
College of Engineering
U.C.L.A.
Los Angeles, California (1)

Dr. [illegible]
Engineering Center
University of Southern California
University Park
Los Angeles 7, California (1)

Professor [illegible]
Department of Physics
U.C.L.A.
Los Angeles, California (1)

Aeronautical Sciences Laboratory
University of California
Richmond Field Station
1301 South 46th Street
Richmond, California (1)

Professor [illegible]
Institute for the Study of Metals
University of Chicago
5640 Ellis Avenue
Chicago 37, Illinois (1)

Professor [illegible], Head
Department of Aeronautical Engineering
University of Cincinnati
Cincinnati 21, Ohio (1)

Professor [illegible]
Department of Physics
University of Florida
Gainesville, Florida (1)

Dr. [illegible]
Physics Department
University of Houston
3801 Cullen Boulevard
Houston, Texas (1)

Professor [illegible]
116 Digital Computer Laboratory
University of Illinois
Urbana, Illinois (1)

Professor [illegible], Chairman
Department of Aeronautical and Astronautical Engineering
University of Illinois
Urbana, Illinois (1)

Professor [illegible]
University of Maryland
College Park, Maryland (1)

Professor Burgers
Institute for Fluid Mechanics and Applied Mathematics
University of Maryland
College Park, Maryland (1)

Professor [illegible]
The Rockefeller Institute
New York 21, New York (1)

Professor [illegible]
Department of Aeronautical Engineering
University of Michigan
Ann Arbor, Michigan (1)

Professor [illegible]
Department of Aeronautical Engineering
University of Michigan
Ann Arbor, Michigan (1)

Professor [illegible]
Radiation Laboratory
The University of Michigan
[illegible] Street
Ann Arbor, Michigan (1)

[illegible]
[illegible]
University of Oklahoma
Norman, Oklahoma (1)

Dr. [illegible]
Physics Department
University of Pittsburgh
Pittsburgh, Pennsylvania (1)

Professor [illegible]
University of Pittsburgh
Pittsburgh, Pennsylvania (1)

[illegible]
Defense Research Laboratory
University of Texas
P. O. Box 8029
Austin, Texas (1)

The Library
Institute of Aerophysics
University of Toronto
Toronto 5, Ontario (1)

Professor [illegible], Director
Experimental Research Group
University of Utah
Salt Lake City, Utah (1)

[illegible], Director
Research Laboratories for the Engineering Sciences
Thornton Hall
University of Virginia
Charlottesville, Virginia (1)

Department Librarian
Department of Aeronautical Engineering
University of Washington
Seattle 5, Washington (1)

Professor J. O. Hirschfelder
Theoretical Chemistry Laboratory
University of Wisconsin
Post Office Box 2127
Madison 5, Wisconsin (1)

Aerojet-General Corporation
Attn: [illegible], Librarian
6352 N. Irwindale Avenue
Azusa, California (1)

William [illegible], Head
Aero-analysis Department
2400 East El Segundo Boulevard
El Segundo, California (1)

American Machine and Foundry Company
Attn: Mechanics Research Department
[illegible]
Niles, Illinois (1)

Australian Weapons Research Establishment
c/o Defence Research and Development
Australian Joint Service Staff
P.O. Box 4837
Washington 8, D. C. (1)

Dr. [illegible]
AVCO-Everett Research Laboratory
2385 Revere Beach Parkway
Everett 49, Massachusetts (1)

AVCO-Everett Research Laboratory
Attn: Library
2385 Revere Beach Parkway
Everett 49, Massachusetts (1)

Mr. [illegible]
Chief of Flight Technology
The Boeing Company
[illegible] Division
P.O. Box 3707
Seattle 24, Washington (1)

Technical Information Center
Chance Vought Corporation
P.O. Box 5907
Dallas 22, Texas (1)

Dr. [illegible]
Chief of Physics
General Dynamics-Convair
Mail Zone [illegible]
San Diego 12, California (1)

[illegible]
Douglas Aircraft Company, Inc.
3000 Ocean Park Boulevard
Santa Monica, California (1)

Fairchild Engine and Airplane Company
Guided Missiles Division
Wyandanch, Long Island, New York (1)

Dr. [illegible]
[illegible]
Flight Sciences Laboratory
1901 Sheridan Drive
Buffalo 21, New York (1)

Dr. [illegible]
General [illegible]
[illegible]
San Diego 12, California

Dr. [illegible]
MSVD Library
General Electric Company
3198 Chestnut Street
Philadelphia 4, Pennsylvania (1)

Dr. [illegible]
General Electric Company
3198 Chestnut Street
Philadelphia 4, Pennsylvania (1)

Dr. [illegible]
General Electric Company
Research Laboratory
P.O. Box 1088
Schenectady, New York (1)

Dr. [illegible]
General Electric Company
Research Laboratory
P.O. Box 1088
Schenectady, New York (1)

Dr. [illegible]
General Electric Company
Research Laboratory
P.O. Box 1088
Schenectady, New York (1)

Dr. [illegible]
General Mills, Inc.
[illegible]
2003 E. [illegible] Avenue
Minneapolis 13, Minnesota (1)

[illegible]
Research Laboratories
General Motors Corporation
12 Mile and Mound Road
Warren, Michigan (1)

Engineering Library
Grumman Aircraft Engineering Corp.
Bethpage, Long Island, New York (1)

Mr. [illegible]
Hughes Aircraft Company
Building [illegible] Station [illegible]
Culver City, California (1)

Mr. Phillip [illegible]
Hydronautics, Inc.
200 Monroe Street
Rockville, Maryland (1)

Mr. Marshall P. Tulin
Hydronautics, Inc.
200 Monroe Street
Rockville, Maryland (1)

Dr. [illegible]
IBM Research Center
P.O. Box 218
Yorktown Heights, New York (1)

Mr. [illegible]
Chief Scientist
Lockheed Missiles and Space Company
P.O. Box 504
Sunnyvale, California (1)

Engineering Library
The Marquardt Corporation
16555 Saticoy
Van Nuys, California (1)

Mr. [illegible] Cooper
The Martin Company
[illegible], Research Library, A-52
P.O. Box 179
Denver 1, Colorado (1)

Dr. [illegible]
Midwest Research Institute
Physics and Mathematics Division
425 Volker Boulevard
Kansas City 10, Missouri (1)

Midwest Research Institute
Attn: Library
425 Volker Boulevard
Kansas City 10, Missouri (1)

Dr. [illegible] Freeman
National Physical Laboratory
Teddington, Middlesex, England (1)

Mr. [illegible]
[illegible], Unsteady Aerodynamics
National Aeronautical Establishment
National Research Council
Ottawa 2, Canada (1)

Dr. [illegible]
[illegible] American Aviation, Inc.
Space and Information Systems Division
12214 Lakewood Boulevard
Downey, California (1)

[illegible] Corporation
[illegible] Division
Attn: Technical Information
[illegible]
[illegible], California (1)

[illegible] Corporation
[illegible]
Technical Information Services
[illegible] Avenue
[illegible] Park, California

[illegible]
Rand Corporation
1700 Main Street
Santa Monica, California (1)

[illegible], Chief
[illegible] Simulation Laboratory
[illegible] Research & Development
Republic Aviation Corporation
Farmingdale, New York (1)

Republic Aviation Corporation
Attn: Mr. [illegible]
Space Systems and Research
Farmingdale, Long Island, New York (1)

[illegible]
Ministry of Aviation
Royal Aircraft Establishment
[illegible] Department
Farnborough, Hants, England (1)

Dr. [illegible], Jr. 5112
Sandia Corporation
Sandia Base
Albuquerque, New Mexico (1)

Mr. [illegible]
Sandia Corporation
Sandia Base
Albuquerque, New Mexico (1)

Mr. [illegible], Director
Physics Research
Sandia Corporation
Sandia Base
Albuquerque, New Mexico (1)

Dr. [illegible]
Manager, Gas Dynamics
Space Sciences Laboratory
Space Technology Center
King of Prussia, Pennsylvania (1)

Dr. [illegible]
Therm Advanced Research
Therm, Incorporated
Ithaca, New York (1)

United Aircraft Corporation
Research Laboratories
[illegible] Street
East Hartford 8, Connecticut (1)

Dr. [illegible], Director
Poulter Laboratories
Stanford Research Institute
Menlo Park, California (1)

Dr. [illegible]
Stanford Research Institute
Poulter Laboratories
Menlo Park, California (1)

[illegible], Incorporated
[illegible] Avenue
Cambridge 39, Massachusetts
Attn: [illegible] (1)

AVCO Research & Advanced Development Div.
[illegible] Street
Wilmington, Massachusetts
Attn: Chief of Aerodynamics